PROVENANCE AND SEDIMENT DISPERSAL OF MISSISSIPPIAN SANDSTONES IN THE BLACK WARRIOR BASIN, NE MISSISSIPPI

By

PATRICK MICHAEL O'CONNOR

Bachelor of Science, 2012
Ohio University
Athens, Ohio

Submitted to the Graduate Faculty of
The College of Science and Engineering
Texas Christian University
In partial fulfillment of the requirements for the degree of

MASTER OF SCIENCE

May, 2015

PROVENANCE AND SEDIMENT DISPERSAL OF MISSISSIPPIAN SANDSTONES IN THE BLACK WARRIOR BASIN, NE MISSISSIPPI
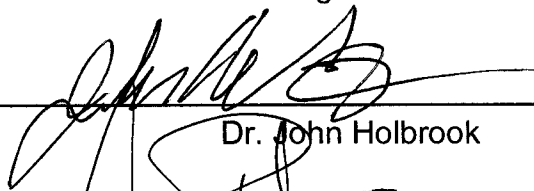
By

Patrick O'Connor

Thesis approved:

Dr. Xiangyang Xie (Major Advisor)

Dr. Helge Alsleben

Dr. John Holbrook

For The College of Science and Engineering

ACKNOWLEDGEMENTS

TABLE OF CONTENTS

VITA

ABSTRACT

LIST OF FIGURES

LIST OF TABLES

1. INTRODUCTION

The Black Warrior basin (BWb) is a triangular shaped foreland basin located in Alabama and Mississippi (Figure 1) (Mellen, 1947; Kugler and Pashin, 1992). From west to east the basin province spans approximately 220 miles (~350 km), from Tallahatchie County, Mississippi, to Cullman County, Alabama. From north to south the basin spans approximately 190 miles (~305 km), from Tishomingo County, Mississippi, to Sumter County, Alabama (Hatch and Pawlewicz, 2007). Historically, the BWb province has been of economic importance due to its reserves in oil, gas, coal, and coal-bed methane gas (Thomas, 1988). The basin contains various pay zones at relatively shallow depth, multiple reservoirs, and stratigraphic and structural traps that contribute to reduced costs in drilling and completions (Bearden, 1985).

Several of the reservoirs are Mississippian sand bodies (Lewis, Evans, Sanders, and Carter sandstones) whose provenance has been widely discussed (Swann, 1964; Thomas 1972, 1974; Welch, 1978; Cleaves and Broussard, 1980; Thomas and Mack, 1982; Cleaves, 1983; Mack et al., 1983; Bearden and Mancini, 1985; Cleaves and Bat, 1988; Thomas, 1988; Stapor and Cleaves, 1992; Ettensohn and Pashin, 1993; Pashin and Rindsberg, 1993; Thomas, 2011). Multiple sources of sediment provenance have been proposed (Figure 2). The first model suggests that clastic sediments were derived from a northern, cratonic source, such as the Ozark Dome or Illinois Basin, northwest of the BWb, and transported through southeastern prograding rivers and deltas to its current location (Swann, 1964; Welch, 1978; Cleaves and Broussard, 1980; Cleaves, 1983; Bearden, 1985; Cleaves and Bat, 1988; Stapor and Cleaves, 1992; Ettensohn and Pashin, 1993; Pashin and Rindsberg, 1993). The second model argues that clastic sediments are from a delta system that prograded in a northeastward direction from an

orogenic source southwest of the Black Warrior basin (Thomas 1972, 1974; Thomas and Mack, 1982; Mack et al., 1983; Nix, 1991; Thomas, 2011). While previous studies have focused on petrography (Sheperd, 1979; Mack et al., 1981; Thomas and Mack, 1982; Cleaves, 1983; Mack et al., 1983; Bat, 1987; Cleaves and Bat, 1988; Hughes and Meylan, 1988) and/or subsurface mapping (Swann, 1964; Thomas, 1972; 1974; Cleaves and Broussard, 1980; Mack et al., 1981; Cleaves, 1983; Cleaves and Bat, 1988; Thomas, 1988) of Mississippian units, this study incorporates sandstone petrography, point counting and U-Pb detrital zircon geochronology to 1) examine petrographic characteristics of the Mississippian age Lewis, Sanders, and Carter formations, to 2) determine sediment provenance of the Lewis, Sanders, and Carter sandstone bodies in northeastern Mississippi and to 3) reconstruct the paleogeography and sediment dispersal patterns in the BWb. Data for this synthesis includes conventional core from 7 wells and 47 thin sections.
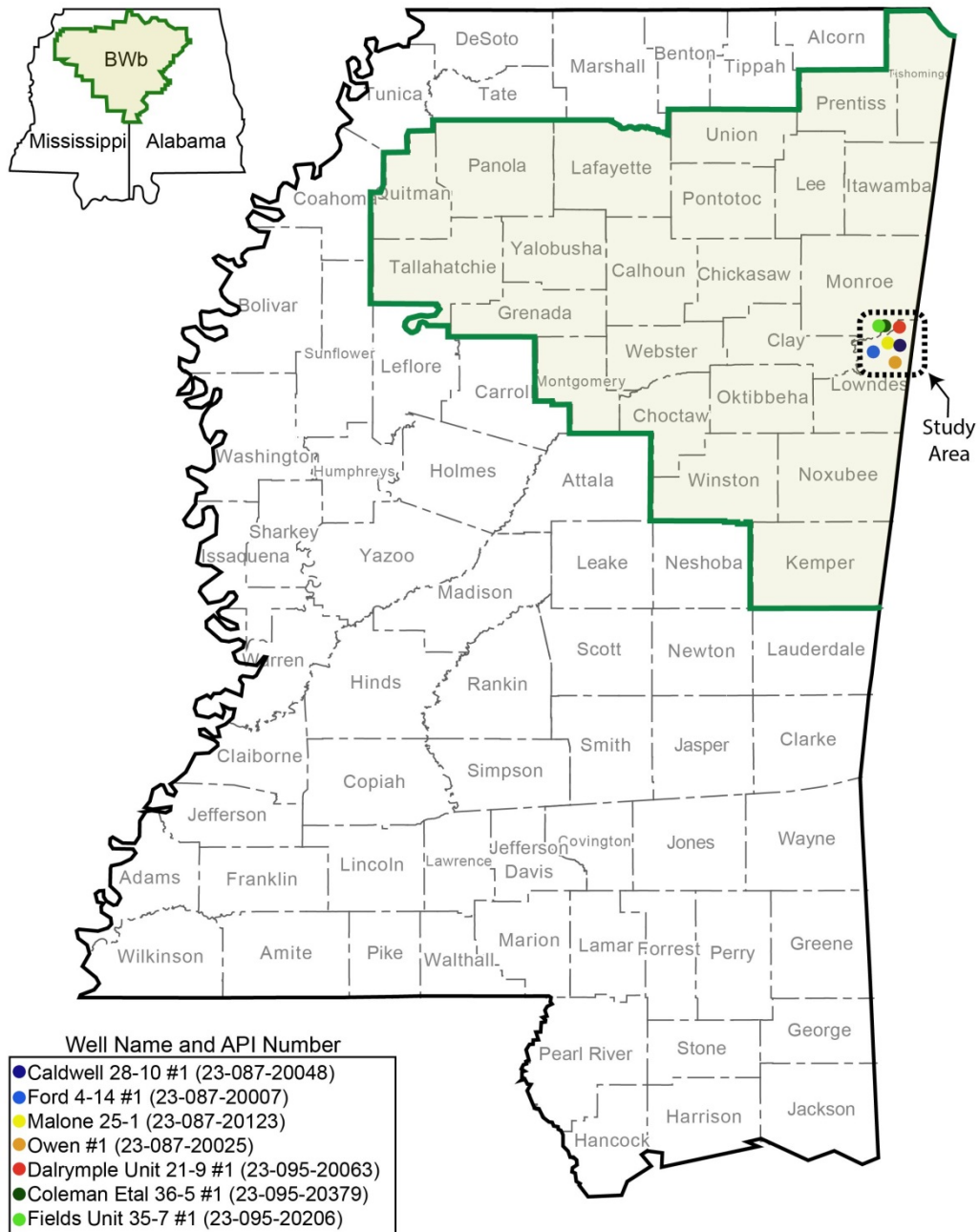
Figure 1. Map of Mississippi with an outline of the Black Warrior Basin (green) and locations of wells with core used for thin sections and detrital zircon geochronology in this study
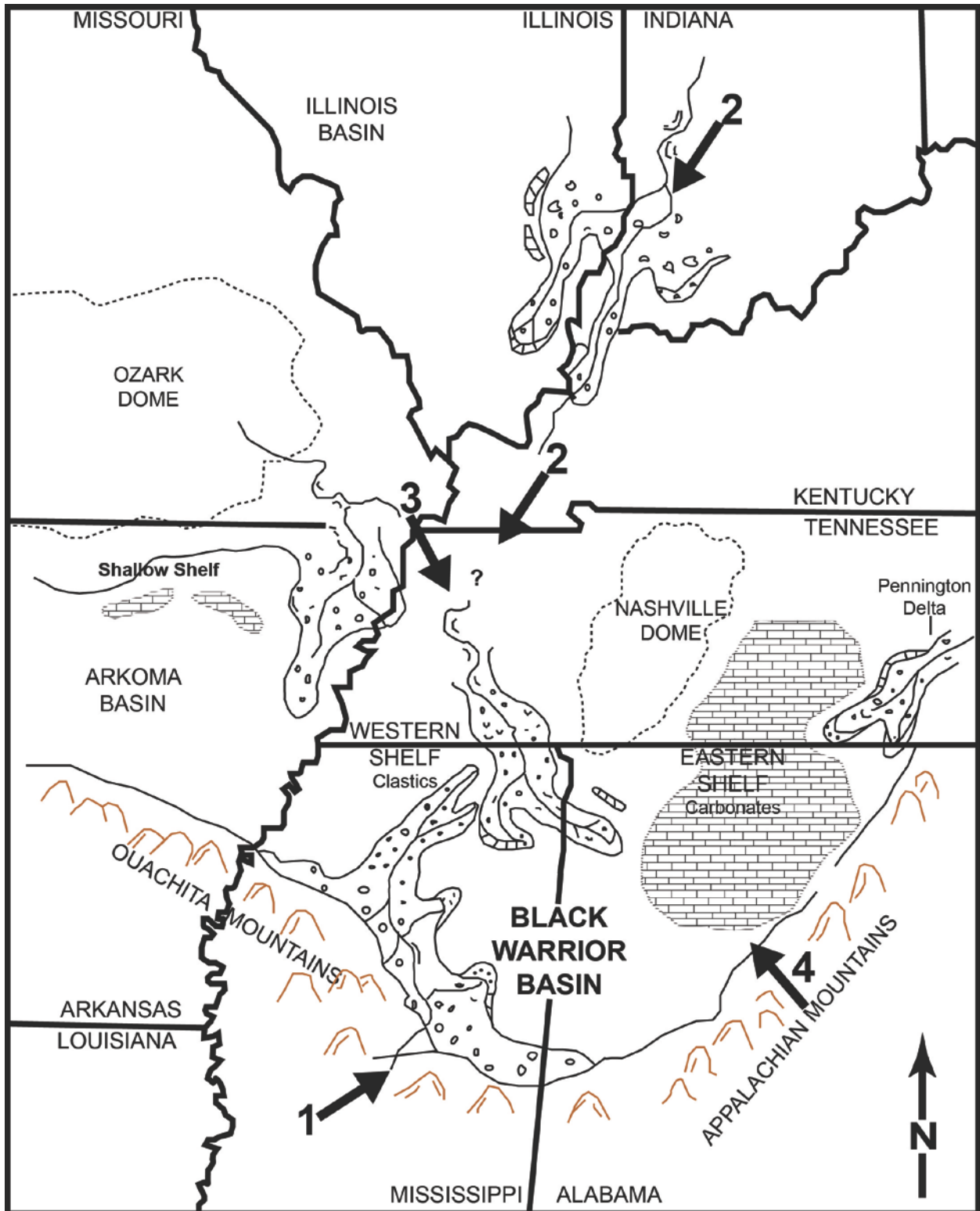
Figure 2. Previously proposed sediment dispersal paths for Chesterian deposition in the BWb: #1 Mack et al., (1981), Thomas and Mack (1982); #2 Swann (1964); #3 Cleaves and Broussard (1980); #4 Ehrlich (1965). Modified from Cleaves and Broussard (1983).

1.1 Geological Setting

The BWb is bounded to the north by the Nashville dome, to the northwest by the Mississippi Valley Graben, to the southwest by the northwesterly-striking Ouachita thrust front, and to the southeast by the Appalachian orogenic belt (Thomas, 1985, 1988, 1989, 2010). The basin consists of Cambrian to Pennsylvanian strata that lie within a structural recess in an orthogonal juncture between the Ouachita and Appalachian thrust belts (Thomas, 1995). A Wilson cycle is responsible for creating the pre-orogenic framework for the Ouachita and Appalachian belts that formed a structural recess for the Black Warrior Basin (Figure 3) (Thomas, 2010). Rifting caused the breakup of Rodinia, opened the Iapetus Ocean, and created Laurentia (the North American craton) during late Precambrian to early Cambrian time (~730-560 Ma) (Thomas, 1991, 2010; Cawood and Nemchin, 2001). The Iapetan rifted margin of southern Laurentia consists of the northwest-southeast Alabama-Oklahoma transform margin and the southwest-northeast Blue Ridge rift margin (Thomas, 1989, 2010). This margin, from the Alabama Promontory up to southern Oklahoma, along the Alabama-Oklahoma transform fault, reflects a passive margin from Cambrian through Devonian, and subsequently evolved into the western limit of a foreland basin after arc-continent collision along the southern margin of the North American craton (Thomas, 1976, 1989; Mack et al., 1981). In the subsurface is a northwesterly-striking system of down to the southwest normal faults that parallel the Ouachita Orogenic Belt (Thomas, 2010). Displacement of these faults affects rocks as young as Middle Pennsylvanian in the BWb but localized stratigraphic irregularities suggest fault movement took place during late Mississippian (Thomas, 1988).

Unconformably on top of the foreland basin units, and adjacent to the orogenic belts, lie southwesterly-dipping Mesozoic-Cenozoic deposits formed during the structural development of the Gulf Coastal Plain (Thomas, 1988). In the subsurface of southeastern Mississippi, Ouachita-derived strata pass below Appalachian derived thrusts, suggesting the BWb is an Ouachita foreland basin, and the Appalachian thrust faults are younger (Viele and Thomas, 1989; Thomas, 2010).
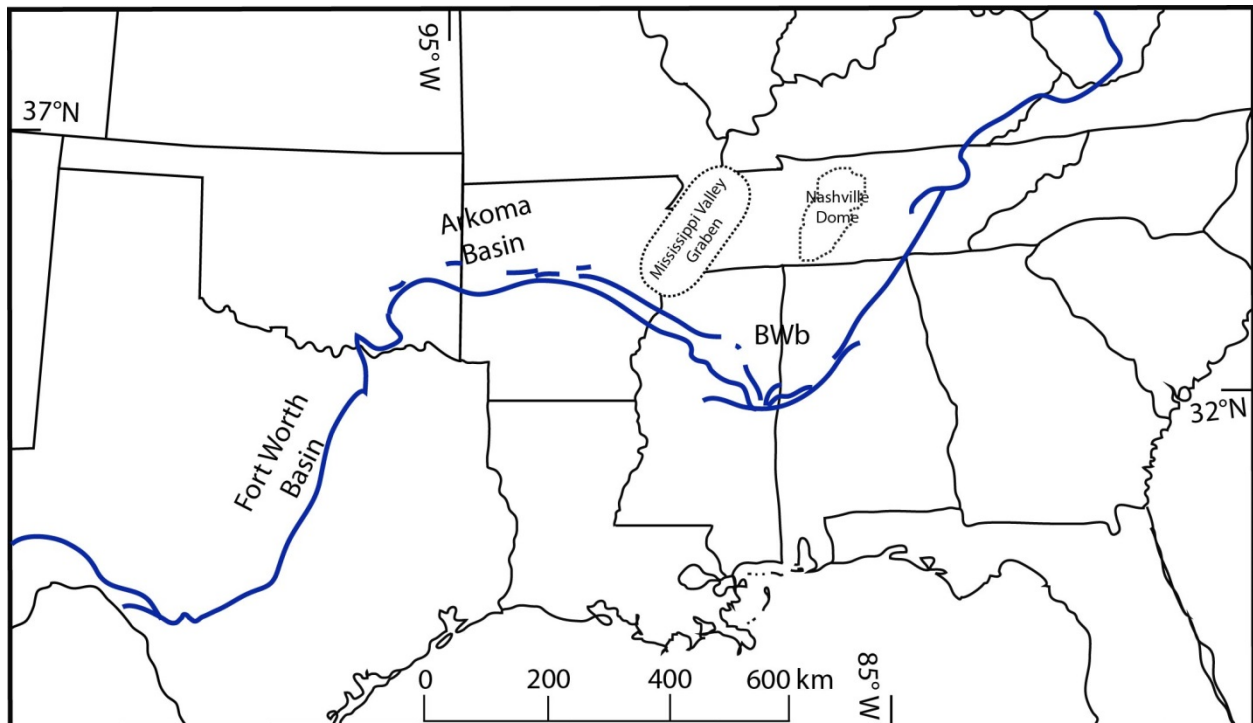
Figure 3. Outline of Ouachita fold/thrust belt (blue), position of other Appalachian-Ouachita belt foreland basins, and position of the Black Warrior Basin (BWb). Map modified from Thomas (2010). Approximate position of Mississippi Valley Graben and Nashville dome are modified from Cleaves and Broussard (1980); Harry and Londono (2004).

1.2 Stratigraphy

The BWb is comprised of passive margin sequences containing shallow-marine carbonate shelf facies from the Cambrian to Mississippian, with an increase of shallow-marine to deltaic-clastic sediments from the Mississippian to Pennsylvanian (Thomas 1985; 2010). The stratigraphy of Paleozoic strata can be divided into four parts including 1) basal clastic Cambrian units, 2) an abundant and laterally extensive Cambrian-Ordovician carbonate shelf facies, 3) a thin, and in places absent Ordovician-lower Mississippian shelf system, and 4) the upper Mississippian-Pennsylvanian synorogenic clastic wedge (Cleaves, 1983; Thomas, 1985; Cleaves and Bat, 1988; Thomas, 1989). The Cambrian-Ordovician carbonate-shelf is indicative of maximum transgression, with locally occurring, thin, sandy limestone. In some areas of what is now north-central Mississippi, thin, shallow marine sandstone, sandy limestone, and shale cover the Ordovician carbonates. Chert, shallow shelf limestone, and mudstone comprise the Silurian age strata, which is overlain by Devonian, shallow shelf chert. In places, the Devonian chert contains thin black shale (Chattanooga) units that are sourced from the east but are rare and discontinuous (Thomas, 1989).

Mississippian to Pennsylvanian strata of the basin are oriented as a southwestwardly-dipping homocline that thickens to the southwest and extends beneath the Ouachita frontal thrust belt with a paleo-dip of approximately 2° (Thomas, 1988). The Mississippian lithology is composed of limestone, shale, and regionally occurring sand bodies (Figure 4). Higginbotham (1986) proposed that tectonic activity had an effect on regulating sediment dispersal because depositional processes could not be responsible for geographic restriction and the geometry of Mississippian sand bodies.
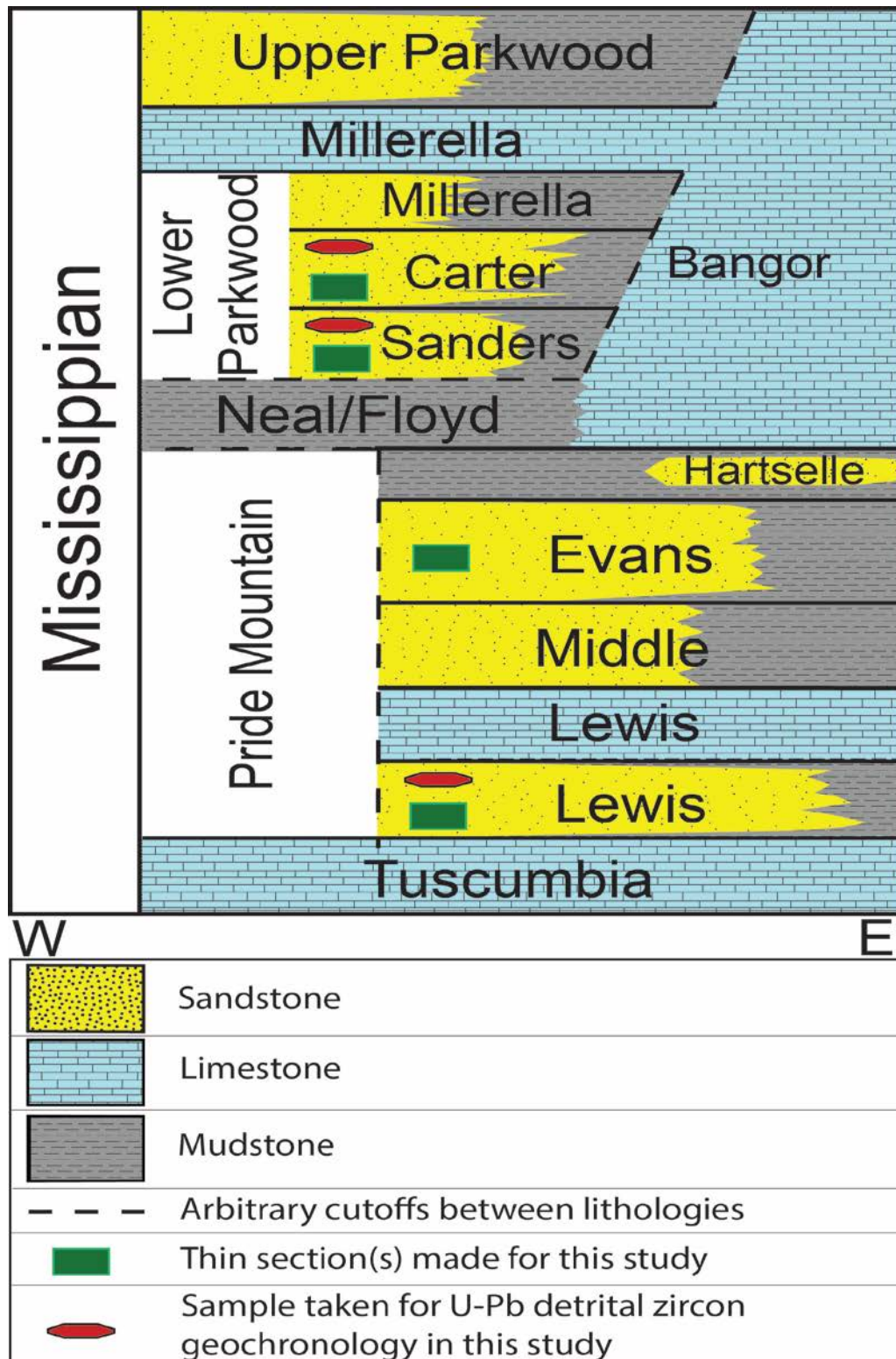
Figure 4. Stratigraphic column of Mississippian age units in the BWb. This stratigraphic column contains units sampled for detrital zircon geochronology and units that were cut for thin sections in this study. Stratigraphic section only shows proposed units within this study area. Interpretation of stratigraphy from Cleaves (1983) and Kidd (2008).

According to Thomas (1985, 1989) a late Mississippian-early Pennsylvanian synorogenic clastic wedge represents the youngest Paleozoic strata and overlies the passive margin facies. The clastic wedge consists of five parts and includes three isolated tongues of upper Mississippian-age clastic sediment. The five sections (in ascending order) include the Pride Mountain-Hartselle (bottom tongue) and corresponding Floyd (also called Neal) Shale, the lower-middle Parkwood (middle tongue) with corresponding upper Floyd Shale, the upper Parkwood (top tongue), the Pennsylvanian lower Pottsville, and the Pennsylvanian upper Pottsville (Thomas, 1972, 1988, 1995).

The clastic wedge, of proposed synorogenic origin, appears to prograde northeastward, away from the Ouachita belt, is thicker southwestward, and consists of clastic gray mudstones and sandstones (Thomas, 1995, 2010; Ettensohn and Pashin, 1993). The wedge displays shallow-marine to deltaic facies, and has a maximum thickness of 10,500 feet (~ 3,200 meters). In the southwestern part of the basin, maximum thickness of Mississippian age strata is approximately 1,640 feet (~500 meters), whereas the remaining 8,860 feet (~2,700 meters) is Pennsylvanian rock (Thomas, 1988).

Cleaves (1983) separated the Mississippian sandstone reservoirs into four Chesterian depositional groups. The oldest in this sequence is the Lewis system, which consists of lobate delta complexes. Above the Lewis are the Evans and Hartselle systems, which are wave-dominated delta systems. The Muldon Complex (Rea, Abernathy, Sanders, and Carter formations) are river-dominated elongate and lobate

deltas, while the youngest, Gilmer, is both a constructional prograding delta, with destructional wave-dominated features (Cleaves, 1983).

According to Thomas (1989), the transition from a passive to active margin is evident in the stratigraphy with the emergence of Middle Mississippian clastics entering the system after the Ouachita thrusting event. This collisional event is responsible for forming the peripheral foreland basin due to subduction along the continental margin and tectonic loading. The geometry of the basin suggests subsidence is greater in eastern Mississippi (Clay, Lowndes, Monroe counties) and accommodation space was filled with sediment from the proposed orogenic event. In the eastern part of the basin, specifically Alabama, slower subsidence is reflected by Mississippian carbonate shelf and less fill (Thomas, 1988).

2. SANDSTONE MODAL MINERAL ANALYSIS

2.1 Point Counting Methods

Samples for this study were obtained from conventional core that was provided by the Mississippi Department of Environmental Quality in Jackson, MS. Locations of the seven wells that penetrated four different Mississippian age formations (Lewis, Evans, Sanders, and Carter) reside in Monroe, and Lowndes Counties of Mississippi. Information about the conventional core cut for thin sections is displayed in the Appendices and details the operator name, lease name, API #, county, depth, formation name, and thin section identification name. Core intervals cut for thin sections were chosen based on visual changes in lithology, color, and grain size.

In total, forty-seven samples were cut for thin sections. All thin sections were cut to a standard 30-micron thickness, treated with blue epoxy to indicate porosity, and stained yellow for potassium feldspar. Following the "Gazzi-Dickinson" point-counting method (Gazzi, 1966; Dickinson, 1970; Gazzi et al., 1973; Ingersoll et al., 1984), eleven categories have been identified (Table 1). Three hundred framework grains were counted for each thin section, providing statistically reliable results that ensure a confidence range or 6% or less (Van Der Plas and Tobi, 1965). The PetrogLite[TM] computer and automatic point counting stage was used to avoid repeated counting of the same grain and prevent bias.

The eleven categories identified in these thin sections include:

1. Monocrystalline Quartz (Q_m)

    Q_m is classified based on the presence of straight to slightly undulose extinction. Grains may have some vacuoles and colors range from gray to white or cream. In general, they have low birefringence, low positive relief, lack cleavage and twinning, and are often subequant and xenomorphic (Figures 5-8).

2. Polycrystalline Quartz (Q_p)
    Q_p is composed of multiple very fine (less than silt sized) grains that are commonly polygonal and make up a single, large quartz grain. In this study, chert was classified under polycrystalline quartz (Figure 5).

3. Potassium Feldspar (F_k)
    F_k can be easily recognized by the presence of low relief and yellow staining (Figure 6).

4. Plagioclase Feldspar (F_p)
    F_p is recognized on the basis of albite twinning, and twin lamellae that are straight and parallel. Interference colors range from gray-white to gray due to visibly lower birefringence than quartz (Figure 7).

5. Volcanic Lithics (L_v)
    These grains are often sand-sized fragments of aphanitic mass or lava flow, or volcanic ejecta. Lath-like feldspar crystals and ferromagnesian rich minerals make up the majority of the feldspathic mass.

6. Metamorphic/Sedimentary Lithics (L_{m+s})
    These grains contain a combination of fine-grained quartz, mica, and in places clays within single grains. These grains are fragments of sedimentary bodies, limestone, slate, phyllite, schist, metaquartzite, or gneiss. These grains often contain more polygonal and less elongate sub grains than volcanic lithics (Figure 7).

7. Phyllosilicates
    These grains are hydrous potassium aluminum silicates, most notably muscovite and biotite. They are flaky with parallel extinction, high birefringence, and a slightly speckled texture (Figure 8).

8. Heavy Minerals
    These minerals are noticed on their very high positive relief, high birefringence, small size, and bright interference colors. These included ultra-stable group minerals such as zircon, tourmaline, and rutile (Figure 8).

9. Cement/Matrix

Cement and matrix is classified based on lack of grain boundaries. Most common cements in this study are calcite and silica (Figures 5 and 6).

10. Pore Space
    Pore space is characterized by blue staining on all thin sections (Figure 8).

11. Others
    Other constituents in this study are fossils, opaque minerals, and clays.

Table 1. Nomenclature used for identifying point counting constituents and recalculated grain type parameters

ID #	Raw Grain Type	Description
1	Qm	Monocrystalline quartz
2	Qp	Polycrystalline quartz
3	Fk	Potassium feldspar
4	Fp	Plagioclase feldspar
5	L_v	Volcanic lithic fragments
6	L_{m+s}	Metamorphic and sedimentary lithics
7	Phyllosilicates	Mica grains (muscovite and biotite)
8	Heavy Minerals	Zircon, Tourmaline, Rutile
9	Cement/Matrix	Calcitic and silica cement
10	Pore Space	
11	Others	
	Recalculated Grain Type	**Description**
	Q	Total quartzose grains (Q_m+Q_p)
	F	Total feldspar grains (F_k+F_p)
	L	Total lithic fragments (L_v+L_{m+s})
	Lt	Polycrystalline lithics ($L_v+L_{m+s}+Q_p$)
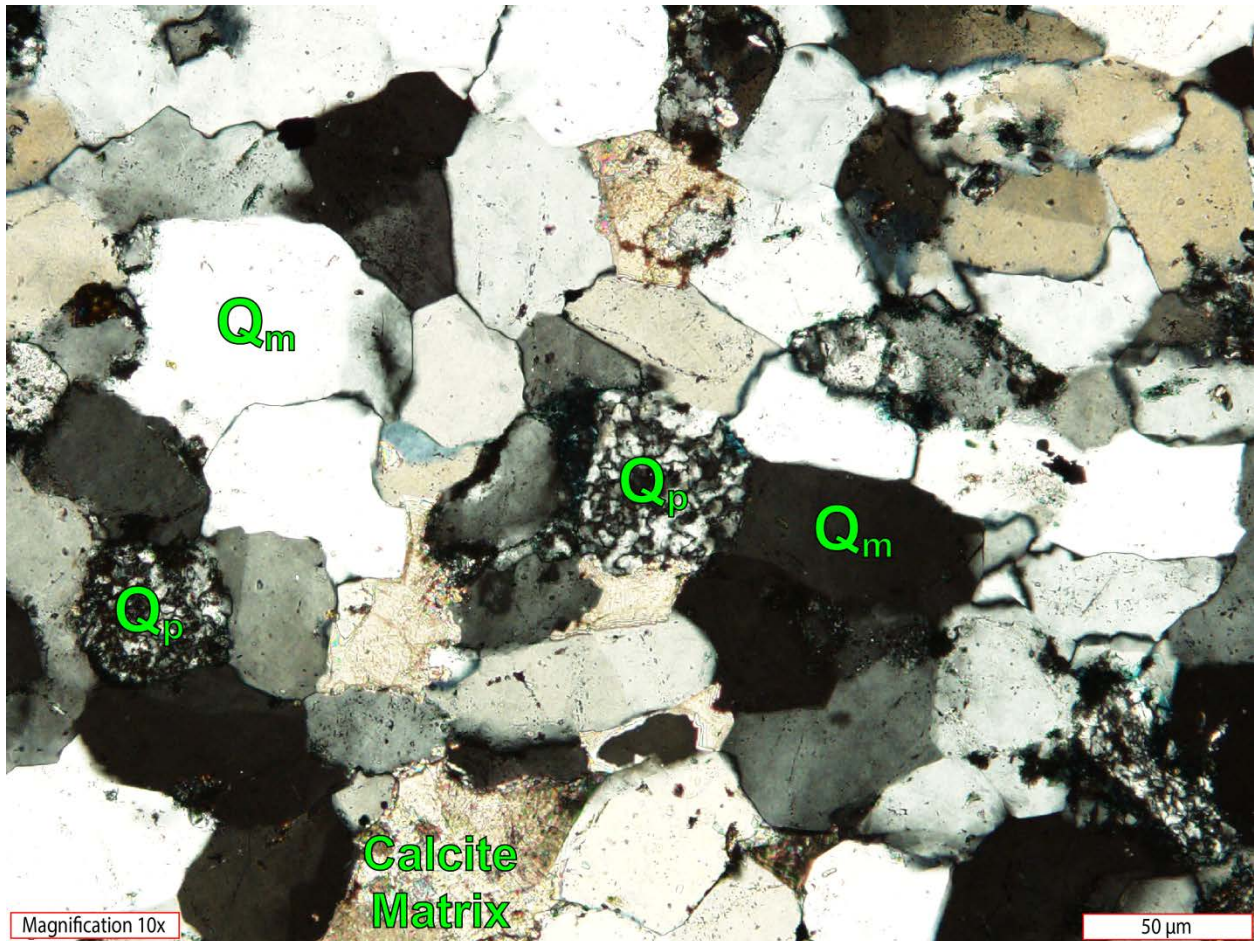
Figure 5. Photomicrograph of a thin section from the Lewis Sandstone displaying monocrystalline quartz (Q_m), polycrystalline quartz (Q_p), and calcite matrix. Constituents are medium to coarse-grained and range from sub-angular to sub rounded.
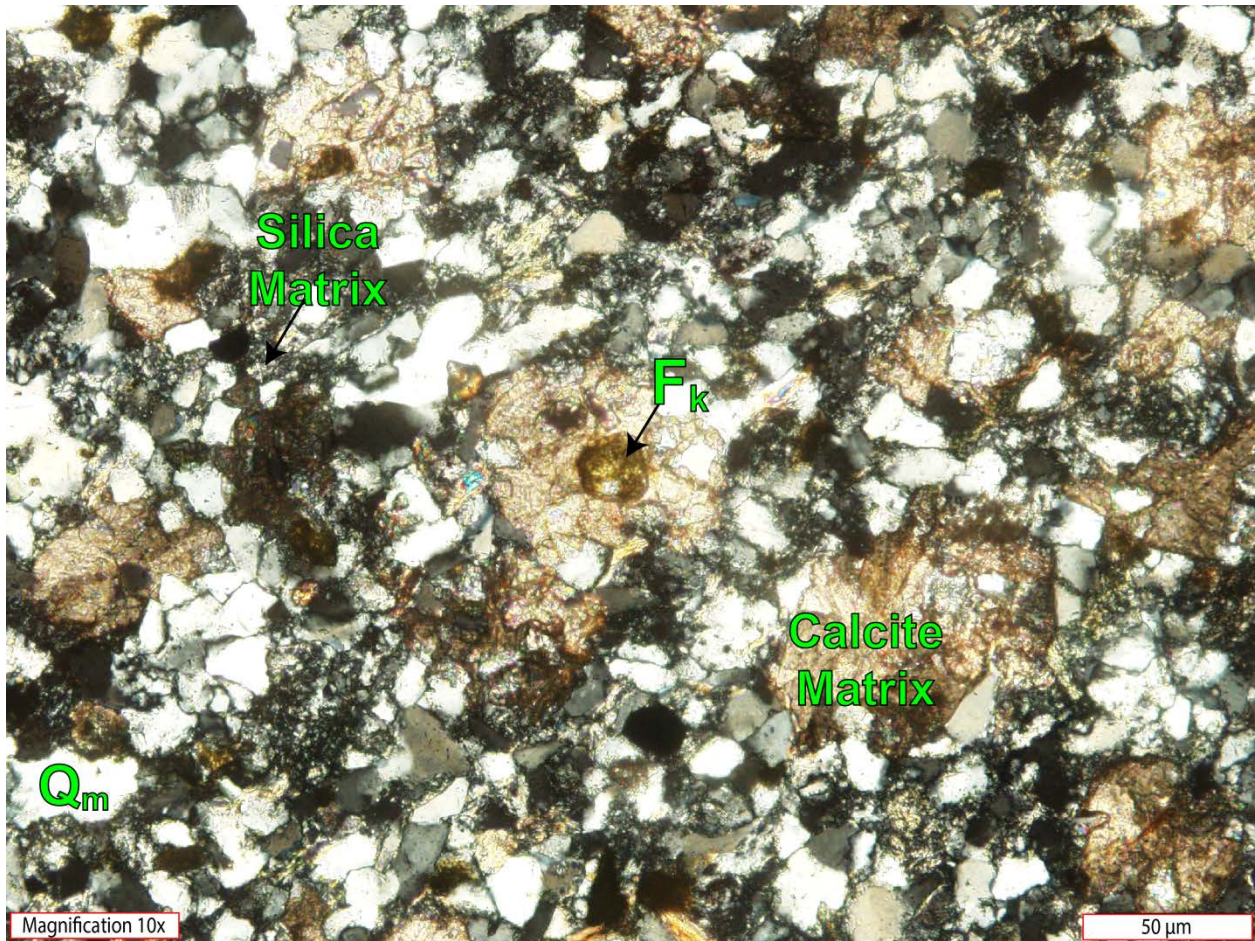
Figure 6. Photomicrograph of a thin section from the Carter Sandstone displaying potassium feldspar (F_k); identified by yellow staining), monocrystalline quartz (Q_m), silica-rich matrix, and calcite matrix. Constituents are fine-grained and range from sub-angular to sub-rounded.
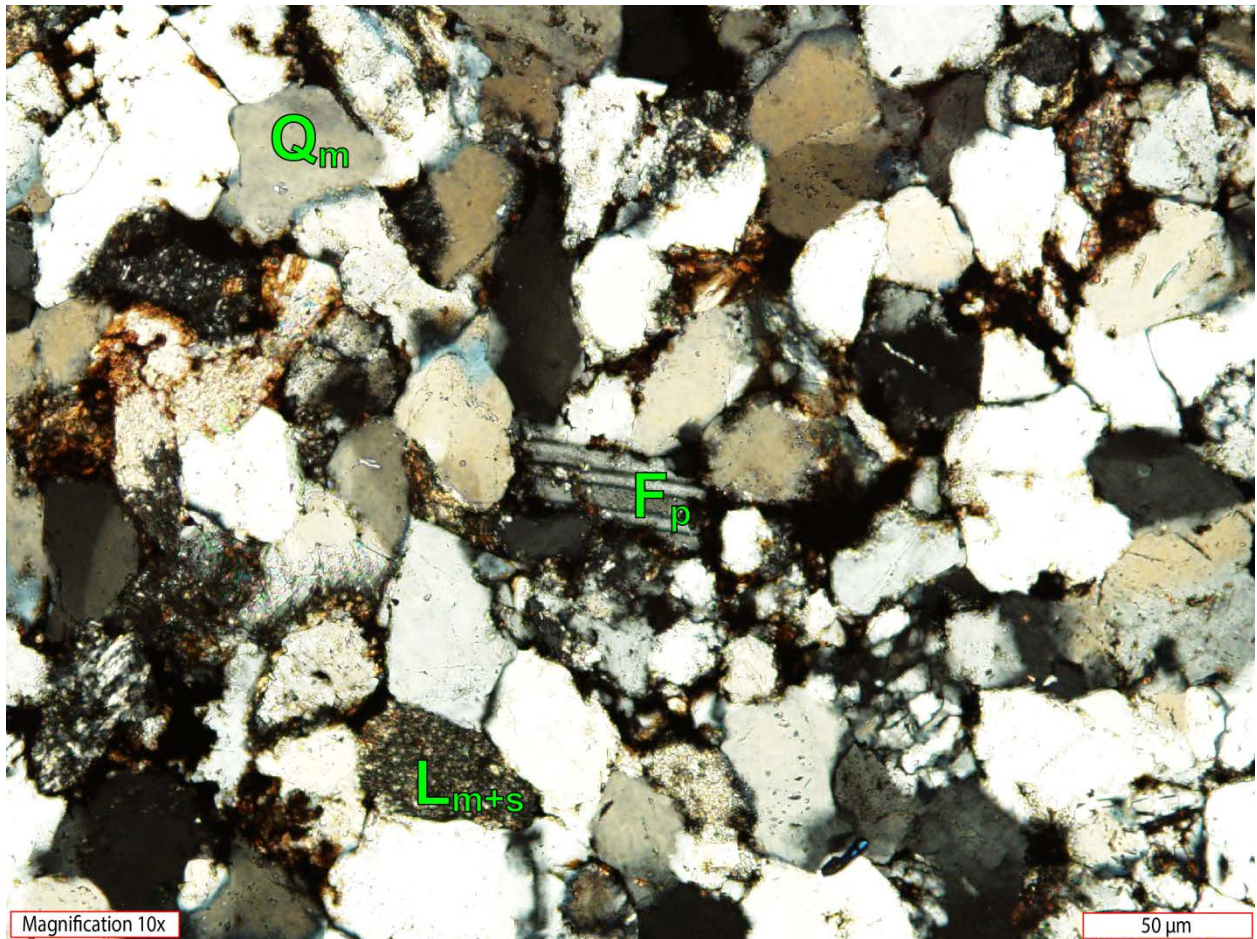
Figure 7. Photomicrograph of a thin section from the Carter Sandstone displaying plagioclase feldspar (F_p; note twinning), lithic fragment (L_{m+s}) from sedimentary or metamorphic parent, and monocrystalline quartz (Q_m). Constituents are medium-grained and range from sub-angular to sub-rounded.
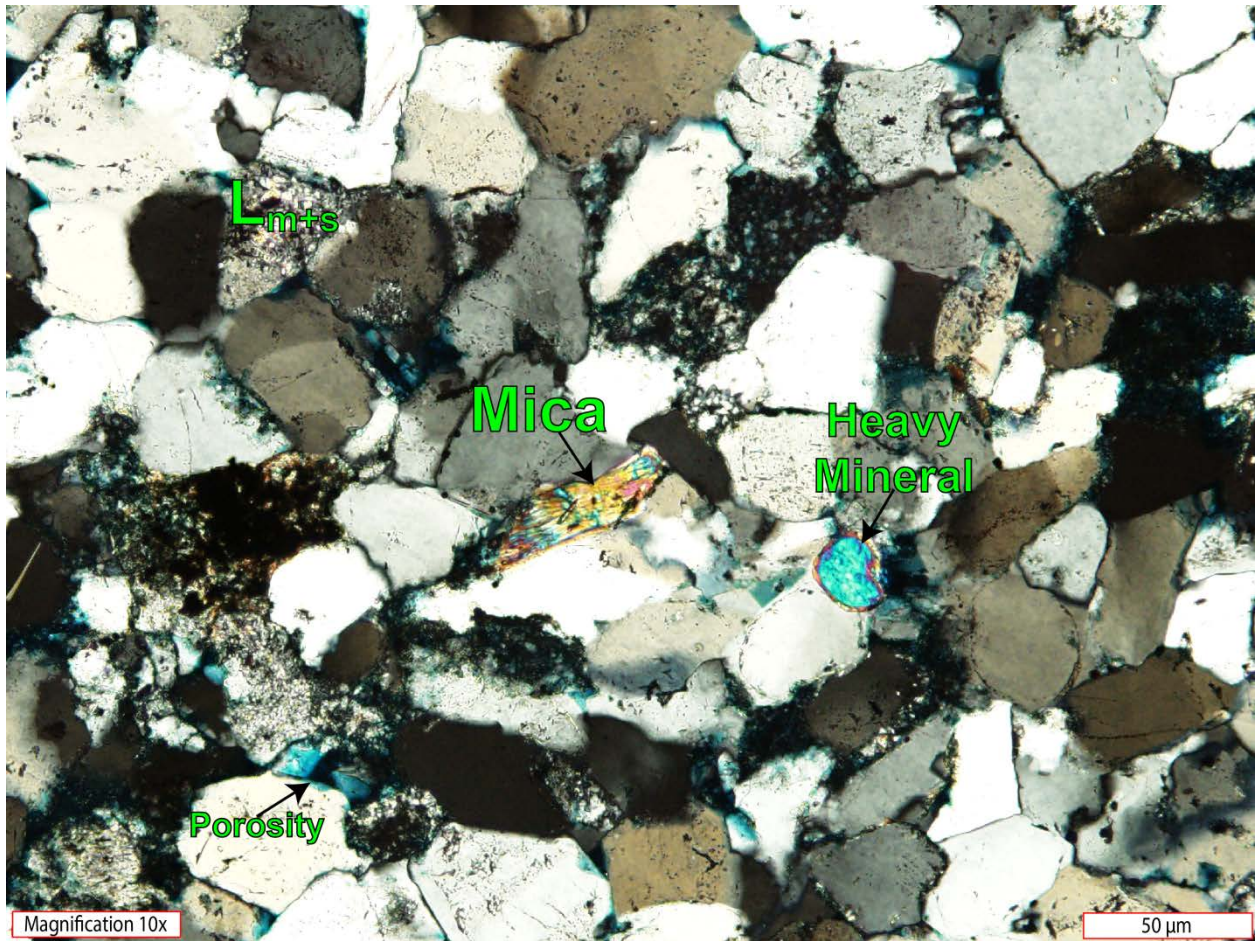
Figure 8. Photomicrograph of a thin section from the Evans Sandstone displaying a mica fragment, heavy mineral, a lithic fragment (L_{m+s}) from a sedimentary or metamorphic parent, and porosity (stained in blue). Constituents are medium to coarse-grained and range from sub-angular to sub-rounded.

2.2 Point Counting Results

The Lewis Sandstone is the oldest Mississippian aged sand body analyzed with the "Gazzi-Dickinson" point counting method. All samples (n=7) from the Lewis Sandstone display obvious concentration within the quartzarenite division (average Q99, F0, L1) of the Folk (1980) nomenclature (Figure 9). Quartz is the dominant framework grain within this sample and ranges from 97 to 100% in the Lewis samples (Table 3). With respect to provenance, based on the Dickinson et al. (1983) classification, the Lewis Sandstone plots close to Q on the QFL (Figure 10) and Qm on the QmFLt ternary diagrams (Figure 11). These fields are suggestive of a cratonic interior provenance on both diagrams. Lewis Sandstone results are distributed as raw (Table 2) and recalculated (Table 3) for analysis.

The Evans Sandstone (n=10) is characterized as a quartzarenite (average Q99, F0, L1) using Folk's (1980) nomenclature (Figure 9). Quartz is again the leading framework grain and ranges from 96 to 100% in the Evans samples (Table 5). When plotted on the Dickinson et al. (1983) QFL ternary diagram, the majority of data from the Evans is considered to be from a cratonic interior province, where one outlier from the group shares a boundary with the recycled orogeny grouping (Figure 10). On the QmFLt (Dickinson et al., 1983) (Figure 11), the Evans Sandstone is distinguished as either a cratonic interior rock, or one composed of sediment from a recycled quartzose. Evans Sandstone data is separated by both raw (Table 4) and recalculated parameters (Table 5).

The Sanders Sandstone (n=15), plots similarly to the Lewis Sandstone with respect to composition (average Q99, F0, L1) and provenance. The principal framework

grain within this sample is once again quartz, which ranges from 97 to 100% in the

Sanders samples (Table 7). The Sanders can be categorized as a quartzarenite (Folk,

1980) (Figure 9), with a cratonic interior provenance origin (Dicksinson, 1983) based on

the QFL (Figure 10) and QmFLt (Figure 11) diagrams. Results are distributed under raw

(Table 6) and recalculated parameters (Table 7) for the Sanders Sandstone.

The youngest examined rocks from the Carter Sandstone (n=15) differ the most

from the other studied rocks with respect to composition (average Q96, F1, L3) and

provenance. The main framework grain within this sample, quartz, ranges from 88 to

99% in the Carter samples (Table 9). The Carter ranges from a quartzarenite to a

sublitharenite on the Folk (1980) diagram (Figure 9). Provenance of the Carter ranges

from craton interior to recycled orogenic on the Dickinson et al. (1983) QFL ternary

diagram (Figure 10). Dickinson's (1983) QmFLt (Figure 11) plots the Carter Sandstone

as cratonic interior to quartzose recycled provenance. Raw (Table 8) and recalculated

(Table 9) parameters are used to display results for the Carter Sandstone.

Table 2. Raw point counting sandstone data

Raw point-count data for sandstone samples from the Lewis Sandstone											
Sample	Qm	Qp	Fk	Fp	Lv	Lm+s	Phyllosilicates	Heavy Minerals	Matrix	Porosity	Others
L (Coleman Etal 36-5 #1) n=6											
L1	269	27		3		2			171		27
L3	293	6		1					9	31	5
L4	287	8		1		4		5	16	29	
L5	290	10							8	18	10
L6	291	9						1	3	21	
L7	282	18							2	59	
A (Fields Unit 35-7 #1) n=1											
A1	286	6				7	1	2	65	1	

Table 3. Recalculated point counting sandstone data

Recalculated point-count ternary percentages from the Lewis Sandstone								
Sample	QFL%				QmFLt%			
	Q%	F%	L%		Qm%	F%	Lt%	
L (Coleman Etal 36-5 #1) n=6								
L1	99	0	1		91	0	9	
L3	100	0	0		97	1	2	
L4	98	0	2		95	1	4	
L5	100	0	0		97	0	3	
L6	100	0	0		97	0	3	
L7	100	0	0		94	0	6	
A (Fields Unit 35-7 #1) n=1								
A1	97	0	3		95	0	5	

Table 4. Raw point counting sandstone data

Raw point-count data for sandstone samples from the Evans Sandstone											
Sample	Qm	Qp	Fk	Fp	Lv	Lm+s	Phyllosilicates	Heavy Minerals	Matrix	Porosity	Others
D (Dalrymple Un 21-9 #1) n=10											
D1	267	33					1		52	27	3
D2	288	8		1		3		5	10	25	
D3	252	37				11			19	17	
D4	292	5	1	1			9		60	32	
D5	263	37							133	24	2
D6	294	5	1					1	54	23	
D7	241	57	1	1					1	10	
D8	288	12					1	3	10	13	
D9	256	44							3	16	
D10	283	10	2	2		2	1	3	29	9	

Table 5. Recalculated point counting sandstone data

Recalculated point-count ternary percentages from the Evans Sandstone							
Sample	QFL%				QmFLt%		
	Q%	F%	L%		Qm%	F%	Lt%
D (Dalrymple Un 21-9 #1) n=10							
D1	100	0	0		89	0	11
D2	99	0	1		95	1	4
D3	96	0	4		84	0	16
D4	100	0	0		97	1	2
D5	100	0	0		88	0	12
D6	100	0	0		97	1	2
D7	99	1	0		80	1	19
D8	100	0	0		96	0	4
D9	100	0	0		85	0	15
D10	97	2	1		94	2	4

Table 6. Raw point counting sandstone data

Sample	Qm	Qp	Fk	Fp	Lv	Lm+s	Phyllosilicates	Heavy Minerals	Matrix	Porosity
Raw point-count data for sandstone samples from the Sanders Sandstone										
O (Owen #1) n=3										
O1	275	20				5			61	25
O2	271	29							55	22
O3	281	19							44	30
M (Malone 25-1) n=12										
M1	275	17				8			5	9
M3	285	14				1		2	13	32
M5	290	9				1			37	9
M7	287	6	2			5		8	40	8
M8	297	3							63	14
M9	287	3	1	2		6			26	18
M10	296	3				1			14	12
M11	288	9	1			1	1	4	33	14
M13	297	3							4	10
M14	293	4	1			1			21	7
M16	298	2						2	17	4
M18	292	4				3		1	14	10

Table 7. Recalculated point counting sandstone data

Recalculated point-count ternary percentages from the Sanders Sandstone						
Sample	**QFL%**				**QmFLt%**	
	Q%	F%	L%		Qm%	F%	Lt%
O (Owen #1) n=3							
O1	98	0	2		93	0	7
O2	100	0	0		90	0	10
O3	100	0	0		94	0	6
M (Malone 25-1) n=12							
M1	97	0	3		92	0	8
M3	100	0	0		95	0	5
M5	100	0	0		97	0	3
M7	97	1	2		95	1	4
M8	100	0	0		99	0	1
M9	97	1	2		96	1	3
M10	100	0	0		99	0	1
M11	100	0	0		95	1	4
M13	100	0	0		99	0	1
M14	100	0	0		97	1	2
M16	100	0	0		99	0	1
M18	99	0	1		97	0	3

Table 8. Raw point counting sandstone data

Raw point-count data for sandstone samples from the Carter Sandstone											
Sample	Qm	Qp	Fk	Fp	Lv	Lm+s	Phyllosilicates	Heavy Minerals	Matrix	Porosity	Others
C (Caldwell 28-10 #1) n=10											
C3	229	46	1	3		21			35		
C5	252	22		3		22	1	3	44		
C7	264	24				11		5	1	7	
C8	281	8		4		7		3	27	6	
C9	263	29				8	1	2	15	6	
C10	287	6		1		6	5	8	16	14	
C11	289	8				3		1	21	3	
C12	288	7	1			3	1		13	6	
C13	272	17				11	1		22	9	
C14	293	6		1			1	1	15	4	
F (Ford 4-14 #1) n=5											
F1	290	6				3	1	4	15	2	
F2	246	19	7	4		25	7	17	74		
F3	284	8				8	8	13	69		
F4	284	10		2		4		3	21	4	
F5	286	7		1		6	1	8	27	3	

Table 9. Recalculated point counting sandstone data

Sample	QFL%				QmFLt%		
	Q%	F%	L%		Qm%	F%	Lt%
C (Caldwell 28-10 #1) n=10							
C3	91	1	7		77	1	22
C5	91	1	7		84	1	15
C7	96	0	4		88	0	12
C8	98	0	2		95	0	5
C9	97	0	3		88	0	12
C10	98	0	2		95	1	4
C11	99	0	1		96	0	4
C12	96	0	4		90	1	9
C13	97	1	2		95	1	4
C14	99	1	0		97	1	2
F (Ford 4-14 #1) n=5							
F1	99	0	1		97	0	3
F2	88	4	8		81	4	15
F3	97	0	3		95	0	5
F4	98	1	1		94	1	5
F5	98	0	2		97	1	2
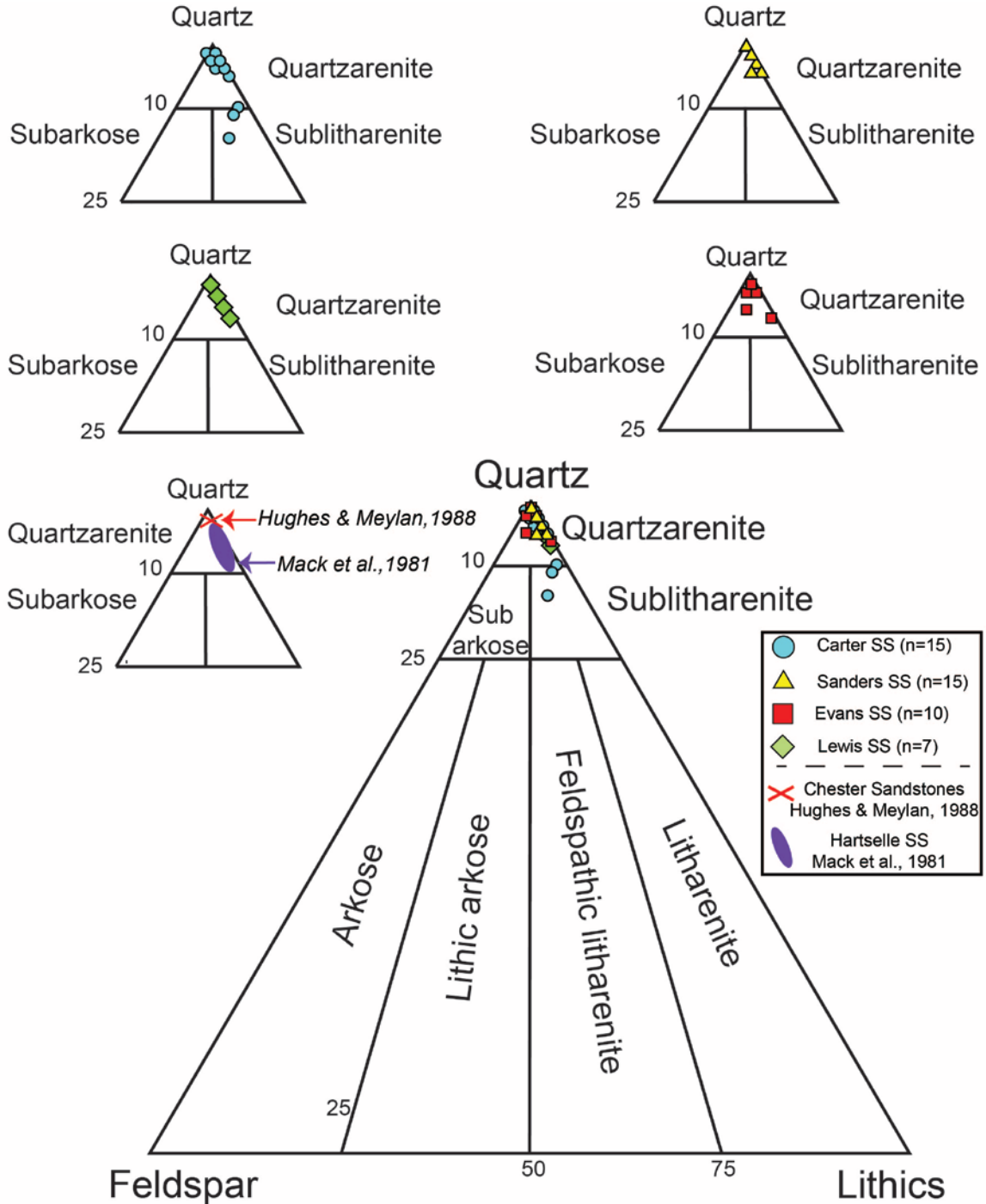
Figure 9. QFL diagrams depicting sandstone nomenclature based on Folk's 1980 classification.
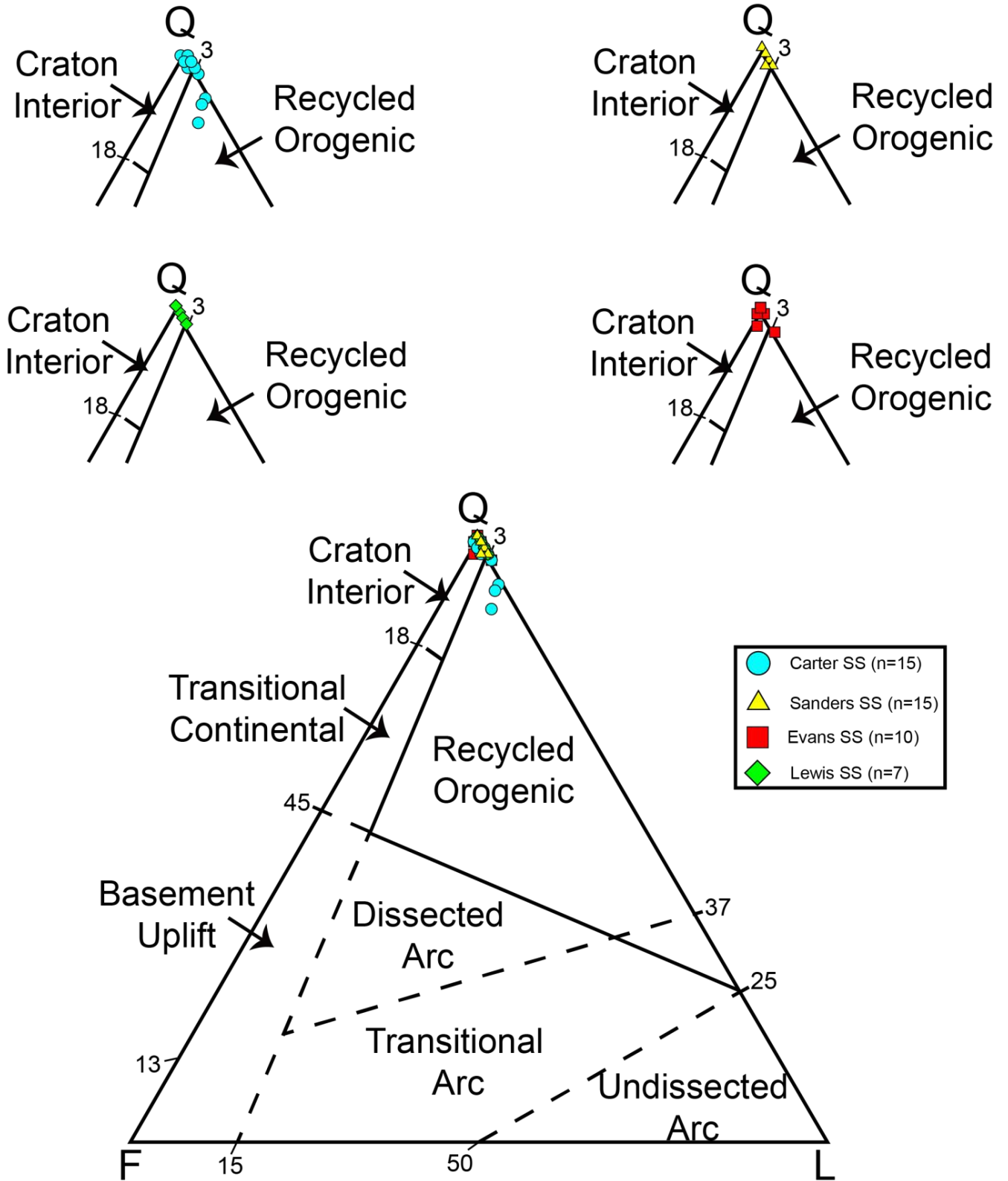
Figure 10. QFL ternary diagram (based on Dickinson et al., 1983) displaying the number of thin sections point counted ("n") and the provenance relationship between the four studied Mississippian-aged sandstones.
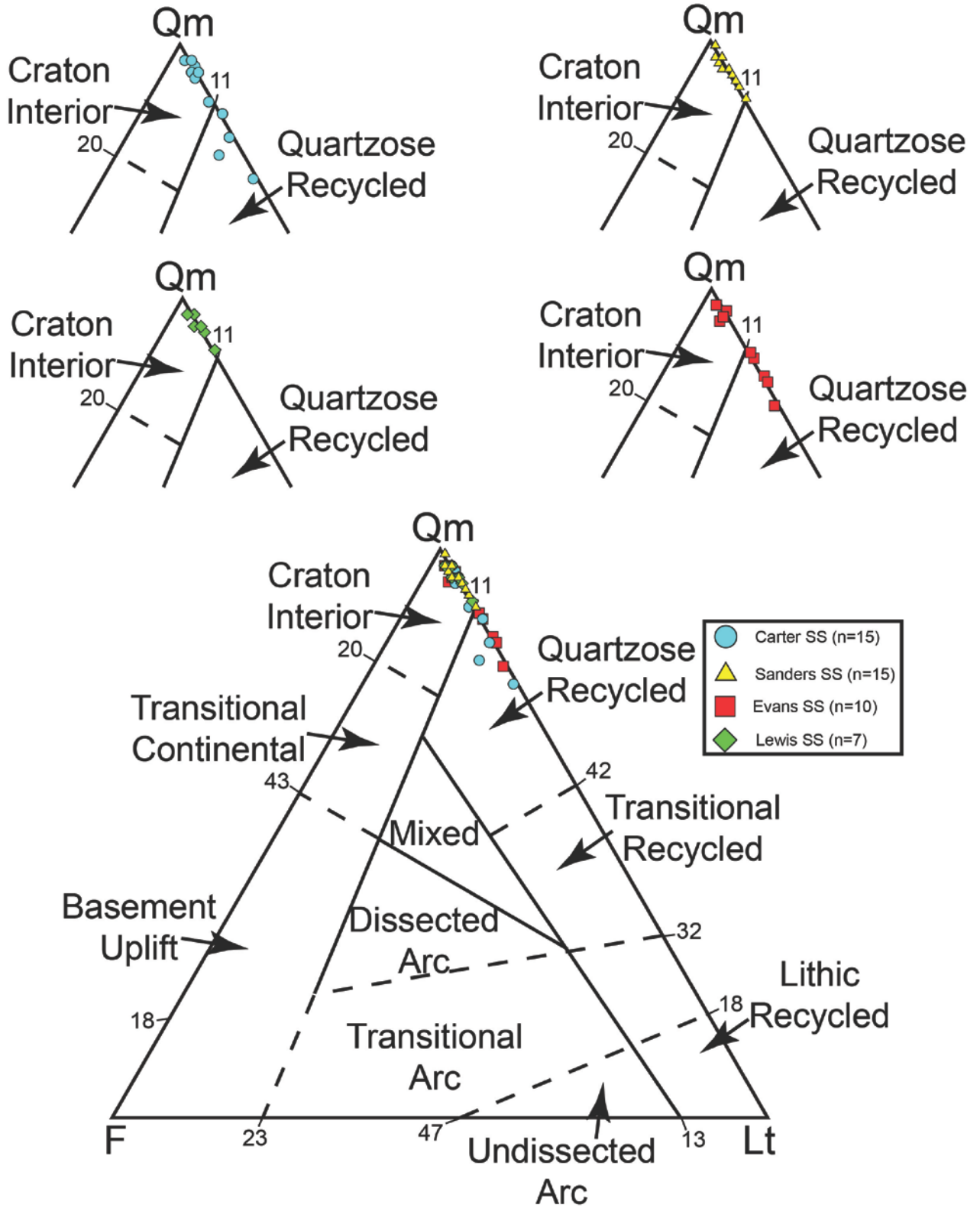
Figure 11. QmFLt ternary diagram (based on Dickinson et al., 1983) displaying the number of thin sections point counted ("n") and the provenance relationship between the four studied Mississippian-aged sandstones.

3. U-PB DETRITAL ZIRCON GEOCHRONOLOGY

3.1 Geochronology Methods

There is risk involved in relying exclusively on sandstone petrography to identify original source rock information. Milliken (1988) noted the common occurrence of processes such as k-feldspar loss, albitization of plagioclase, reduction of heavy minerals, further diagenetic processes and their significance in provenance signal loss. Significant signal loss has been suggested when interpreting provenance of grains that authors have called *diagenetic quartzarenites* (McBride, 1987). To gain a better understanding of the origin of this sediment this study also incorporates detrital zircon geochronology since zircons retain information of parent rock regardless of sedimentary diagenesis and transport. This second method may help with interpretations of inferred source rock terranes. Three samples of core were taken from three different age sandstones; one from the Lewis Sandstone, one from the Sanders Sandstone, and one from the Carter Sandstone. Detrital zircon grains were removed from these cores using standard separation techniques. First, to separate the zircons core was broken by rock hammer, and then shaved into fine-medium grains using a disc-mill at University of Texas at Dallas. Sediment was then rinsed and agitated with water to remove clays. Subsequently, sediment was put into a Frantz magnetic separator, which was operated with a 10° front slope and 20° side slope at 1.0 amps, and then again at 1.5 amps. The next step involved heavy liquid separation at University of Texas at Arlington using Methylene Iodide (ρ>3.3g/cm^3) which was used to isolate zircons from the rest of the sample. Finally, zircons were separated from other heavy minerals in the sample under

a microscope by hand. Once separation was complete, the zircons were taken to the Arizona LaserChron Center for U-Pb detrital zircon geochronology analyses.

Methods used at the University of Arizona LaserChron Center have been frequently documented in similar provenance studies and multiple authors have provided detailed discussions of laser ablation inductively coupled with plasma mass spectrometry (LA-ICPMS) methods being used (e.g., Stacey and Kramers, 1975; Gehrels et al., 2006; Gehrels et al., 2008; Ludwig, 2008). At the University of Arizona, LA-ICPMS was used to analyze zircon grains. Zircon grains were combined with Sri Lanka standard zircons (564 ±4Ma) on a one-inch epoxy mount, sanded to ~20 microns, polished, imaged, and cleaned in preparation for laser ablation. The Sri Lankan zircon grains were used as a standard for comparison and analyzed five times at the beginning of each sample set (after every 5th unknown zircon) and five more times after the sample set. Selected samples of mounted zircon grains analyzed in this study are displayed on backscatter images (Figures 12-14). To summarize the process, a Photo Machines Analyte G2 excimer laser ablates a spot with a diameter of 30 microns. A helium carrier airway transports the ablated matter to a plasma source which contains a flight tube capable of simultaneously measuring U, Th, and Pb isotopes. Faraday detectors containing $3x10^{11}$ ohm resistors detect ^{238}U, ^{232}Th, ^{208}Pb-^{206}Pb, in static mode, and use discrete dynode ion counters for analysis of ^{204}Pb and ^{202}Hg. Per each examination are 15, one-second laser fires, with 30-second delays to purge the previous sample. A ~15 micron depth ablation pit is the result.

Errors for $^{206}Pb/^{238}U$ and $^{206}Pb/^{204}Pb$ can produce ~1-2% (1-sigma level) in $^{206}Pb/^{238}U$ age; ~1-2% (1-sigma level) for $^{206}Pb/^{207}Pb$ and $^{206}Pb/^{204}Pb$ uncertainty age

for >1.0 Ga grains. Generally, accuracy in crossover of ^{206}Pb/^{238}U and ^{206}Pb/^{207}Pb age

grains is ~1.0 Ga. In this study, grains younger than 1.0 Ga were considered to be

concordant if ^{206}Pb/^{238}U was within ±20% of ^{207}Pb/^{235}U. For grains whose age was >1.0

Ga, acceptable species were those within ±20% of concordance calculations based on

^{206}Pb/^{238}U and ^{206}Pb/^{207}Pb (Gehrels et al., 2006, 2008). Analyses that did not lie within

those parameters were rejected from the final dataset. Two grains (~305 Ma) were

younger than the age of the Carter Sandstone were also discarded from the final

dataset. These two grains were likely due to data contamination from other zircon dating

studies. Grains <400 Ma were considered free of U-Pb age discrimination, appeared as

"NA" in data results, and were always used.

Uncertainties in analytical data (See Appendices) are solely measurement errors

and are at the 1-sigma level. Deduced ages are presented on U-Pb concordia diagrams

(see below) and relative age-probability diagrams (see below) using routines in *Isoplot*

from Ludwig (2008). Age-probability diagrams reveal individual ages and their

uncertainties (measurement error only) as a normal distribution display, and sum all

ages from a sample into one curve. Composite age probability plots were constructed

through an University of Arizona Excel program that normalized each curved based on

the number of components; each curve has the same area, and the probability curves

are stacked. To further review the isotope dating, laser ablation methods, and data

analysis processes, please refer to the references (Stacey and Kramers, 1975; Gehrels

et al., 2006, 2008), and see the University of Arizona LaserChron Center website at

http://www.geo.arizona.edu/alc
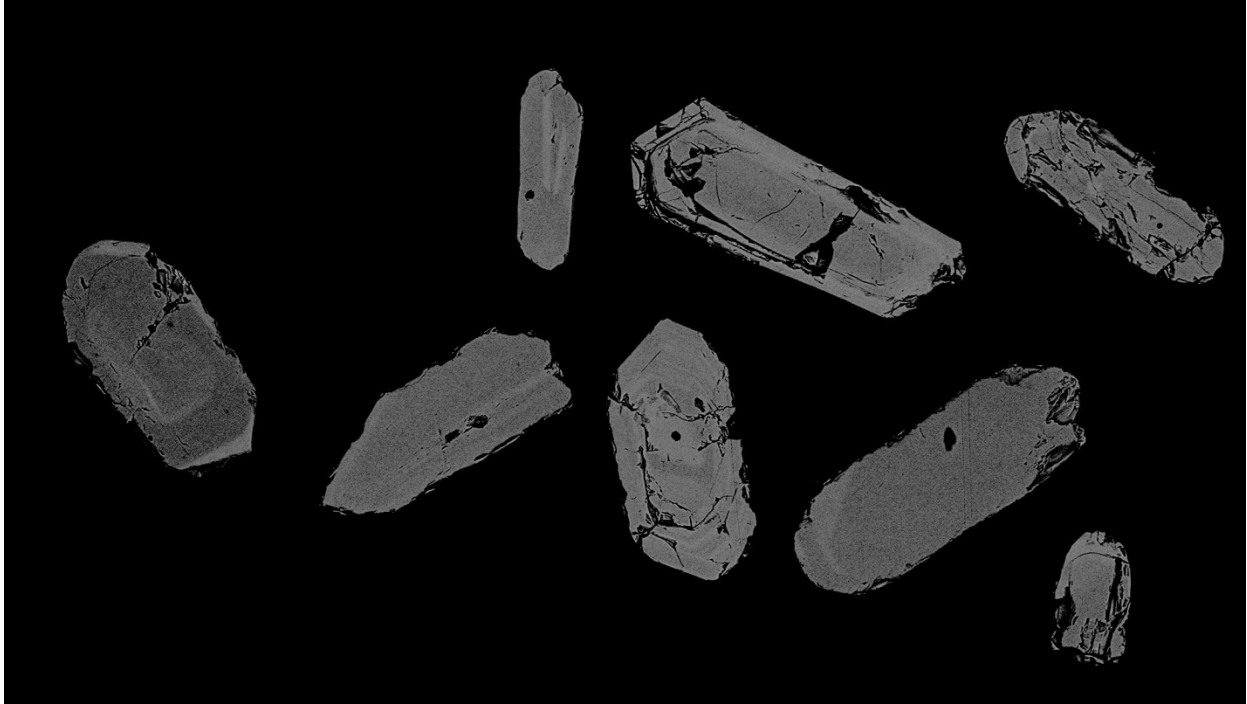
Figure 12. Selected backscattered electron image of zircon concentrations from BW1 (Lewis Sandstone) that was used for detrital zircon geochronology.

Figure 13. Selected backscattered electron image of zircon concentrations from BW2 (Sanders Sandstone) that was used for detrital zircon geochronology.

Figure 14. Selected backscattered electron image of zircon concentrations from BW3 (Carter Sandstone) that was used for detrital zircon geochronology.

3.2.1 Geochronology Results

Results from the Mississippian Lewis, Sanders, and Carter formations will be discussed independently along with corresponding relative age probability plots, U-Pb Concordia plots, and U-Pb Concordia Tera-Wasserburg distribution plots (all at the 1σ confidence interval). Relative age probability plots display the number of grains examined (left y-axis) versus the age in millions of years (x-axis) versus the relative probability (right y-axis). The blue histogram bars report the number of grains examined and coincide with the left y-axis, whereas the red line corresponds to the relative probability on the right y-axis.

U-Pb Concordia diagrams are plotted in both normal distribution and the Tera-Wasserburg distribution. The U-Pb normal distribution plot focuses on highlighting older (>1 Ga) grains by comparing the $^{206}Pb/^{238}U$ ratio with the $^{207}Pb/^{235}U$ ratio. The U-Pb Concordia Tera-Wasserburg diagram focuses on highlighting younger (>1Ga) grains by comparing the $^{207}Pb/^{206}Pb$ ratio with the $^{238}U/^{206}Pb$ ratio. Ovals that lie closer along the red line are closer to being concordant, whereas those that deviate beyond the red line are further from statistically probable. Smaller ovals are those with higher resolution whereas larger ovals depict a larger error potential. All displayed data in this paper lie within ±20% concordance range.

Ages were split into six sections for this study based on potential source terranes, which will be discussed in more detail below. However, for simplicity and as a reference, detrital zircon age results from the Lewis, Sanders, and Carter Sandstones from this study (by raw number and percentage of grains analyzed) are presented with the corresponding age terranes that are most proximal and perhaps most probable

sources (Table 10). Composite age distribution curves for detrital zircon grains in the

Mississippian age sandstones from this study are displayed stacked in a normalized

probability plot (Figure 15). Normalized age probability plots allow visual comparison of

provinces that are most probable sediment sources in relation to other terranes through

geologic time. These curves are normalized so that each sample holds the same area

underneath its curve as the other samples. When referencing the normalized age

probability plots, it is important to understand that a high peak is not indicative of more

data points, but is actually indicating a high resolution event with a low associated error

bar. These normalized age probability plots should be analyzed with caution and

compared to the relative age probability plots (as follows) since the relative age

probability plots show number of data points as well as probability.

Table 10. Interpreted ages of detrital zircons from sandstones in this study

Age Range (Ma)	Interpreted Source Terrane	Lewis Sandstone n=68		Sanders Sandstone n=78		Carter Sandstone n=151	
540 ~ 367	Paleozoic	25	37%	29	37%	31	21%
725 ~515	Neoproterozoic	5	7%	6	8%	1	1%
1350 ~ 900	Grenville	16	24%	21	27%	47	31%
1480 ~1340	Granite-Rhyolite	8	12%	8	10%	18	12%
1800 ~ 1600	Yavapai-Mazatzal	10	14%	10	13%	34	22%
>1800	Paleoproterozoic & Archean	4	6%	4	5%	20	13%
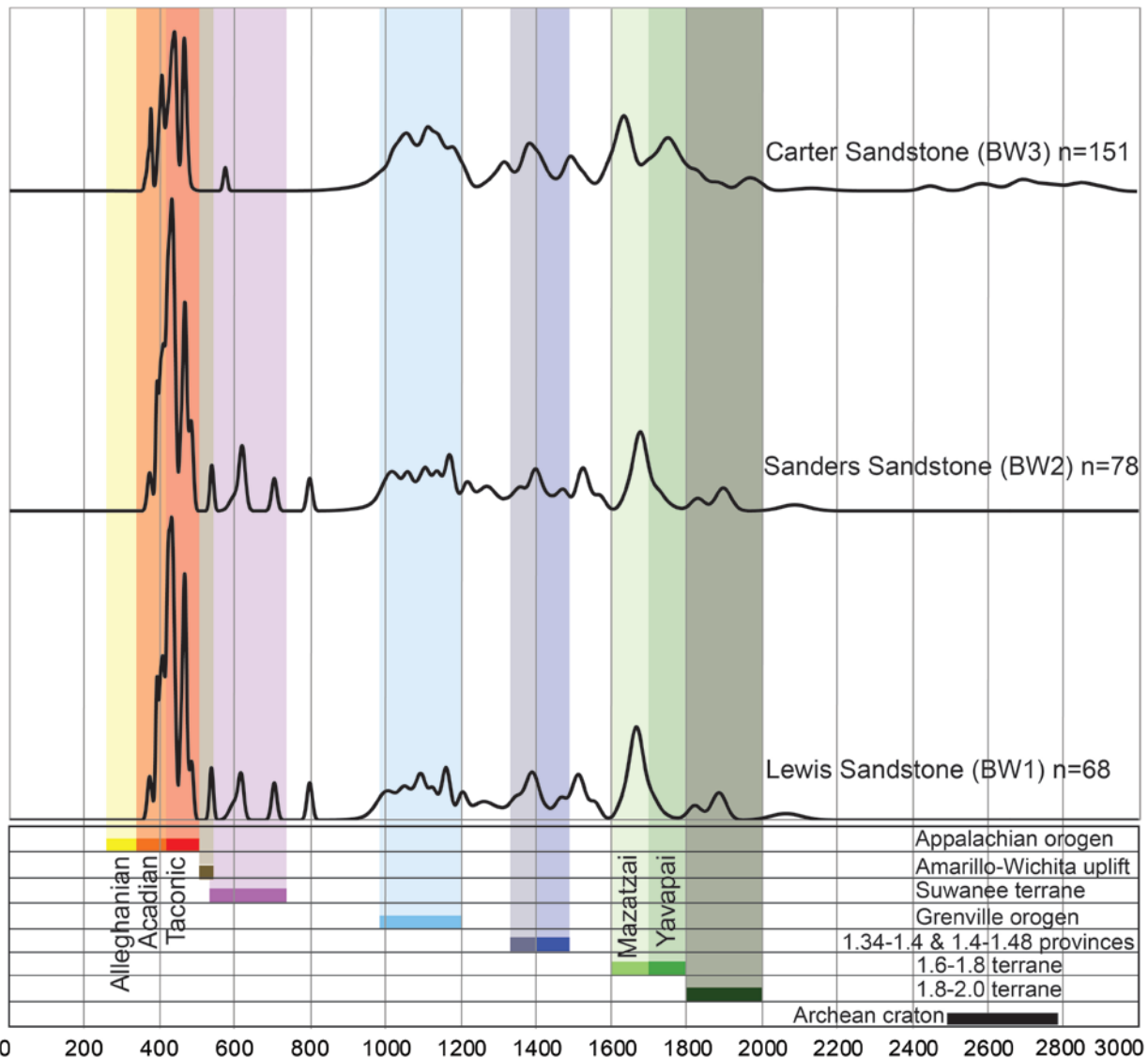
Figure 15. Composite age distribution curves for detrital zircon grains in the Mississippian age sandstone samples from the Black Warrior basin. Ages and terranes modified from Gehrels et al. (2011)

The Lewis Sandstone (n=68)

Of the 100 Lewis Sandstone zircons that were analyzed, the dataset is represented by 68 grains (within ±20% concordance) due to loss of data with discordant or reverse discordant results. The relative age probability plot of the Lewis Sandstone (BW1) is displayed at the 1σ confidence level (Figure 16). Ages of the Lewis Sandstone range from 2064 to 374 Ma. Ages from the raw number of grains follow (presented as

blue histogram peaks in intervals of 125 Ma). Zircons with Archean and

Paleoproterozoic ages (>1800 Ma) represent the smallest proportion of this sample and

are denoted by 4 grains (~6% of the Lewis Sandstone sample). Late Paleoproterozoic

ages (1800-1600 Ma) constitute 10 grains (~15% of the sample). Zircons from the Early

Mesoproterozoic age (1480-1340 Ma) are represented by 8 grains (12%) in the sample.

Mesoproterozoic age (1350-900 Ma) grains make up the second greatest population for

this sample with 16 grains (23%). The Neoproterozoic-Early Paleozoic (725 - 515 Ma)

derived populations were minor, being represented by 5 grains (7%). Zircons from the

Paleozoic (<515 Ma) form the largest population in this sample with 25 grains (37%).
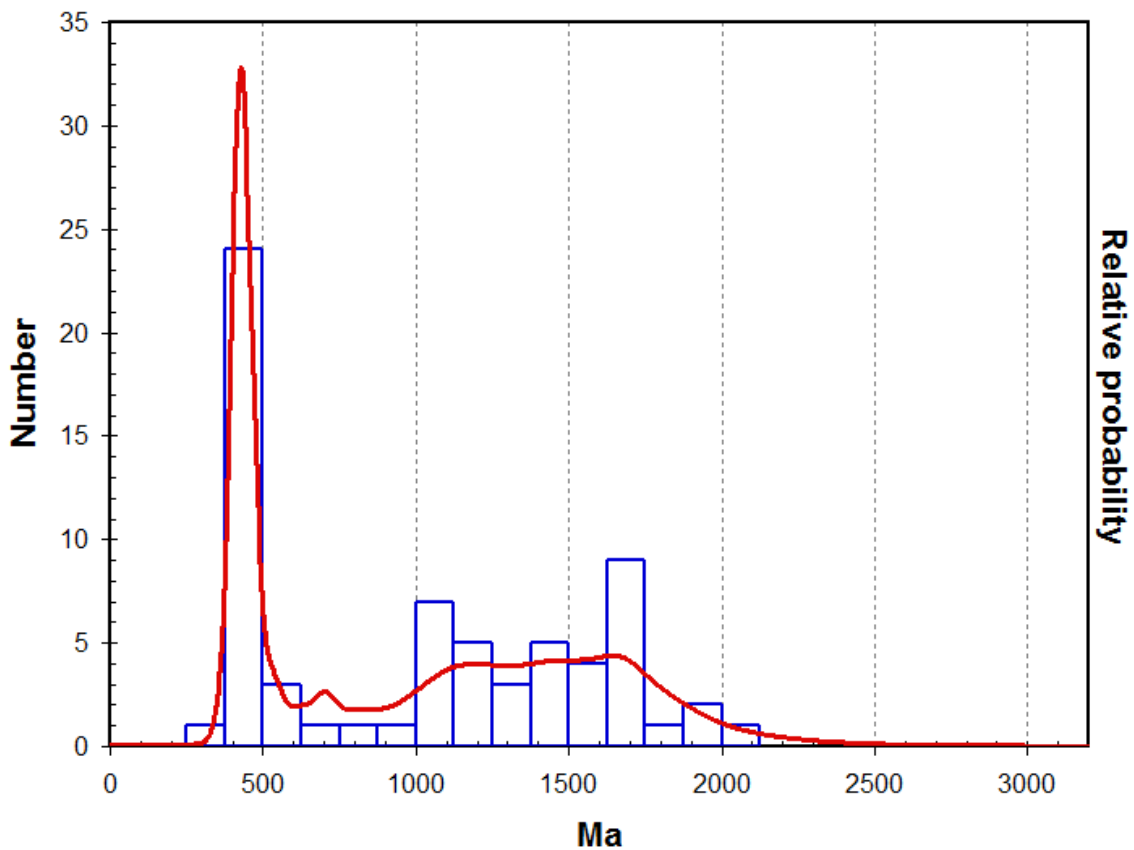
Figure 16. Relative age probability plot (0-3200 Ma) for the Mississippian age Lewis Sandstone (BW1) at the 1σ confidence level.

For analysis of concordant dates, data from the Lewis Sandstone is plotted on U-Pb Concordia normal distribution and Tera-Wasserburg distribution plots (Figures 17 and 18, respectively). All grains displayed (n=68) have ages that are within ±20% discordant. Of the 68 grains 71% (n=48) are <5% discordant, 19% (n=13) are 5-10% discordant, 3% (n=2) are 10-15% discordant, and 3% (n=2) are 15-20% discordant. The remaining 4% of grains (n=3) are valid and reported as being "NA" in the concordance calculations since there is so much error within calculating ages younger than 400 Ma. Zircon ages from 375-500 Ma (35% of the sample; n=24) make up the dominant age group (based on probability) and contain 10 grains within 5% discordant, 9 grains within 10% discordant, 2 grains within 20% discordant, and the remaining 3 grains are "NA" since they are <400 Ma.
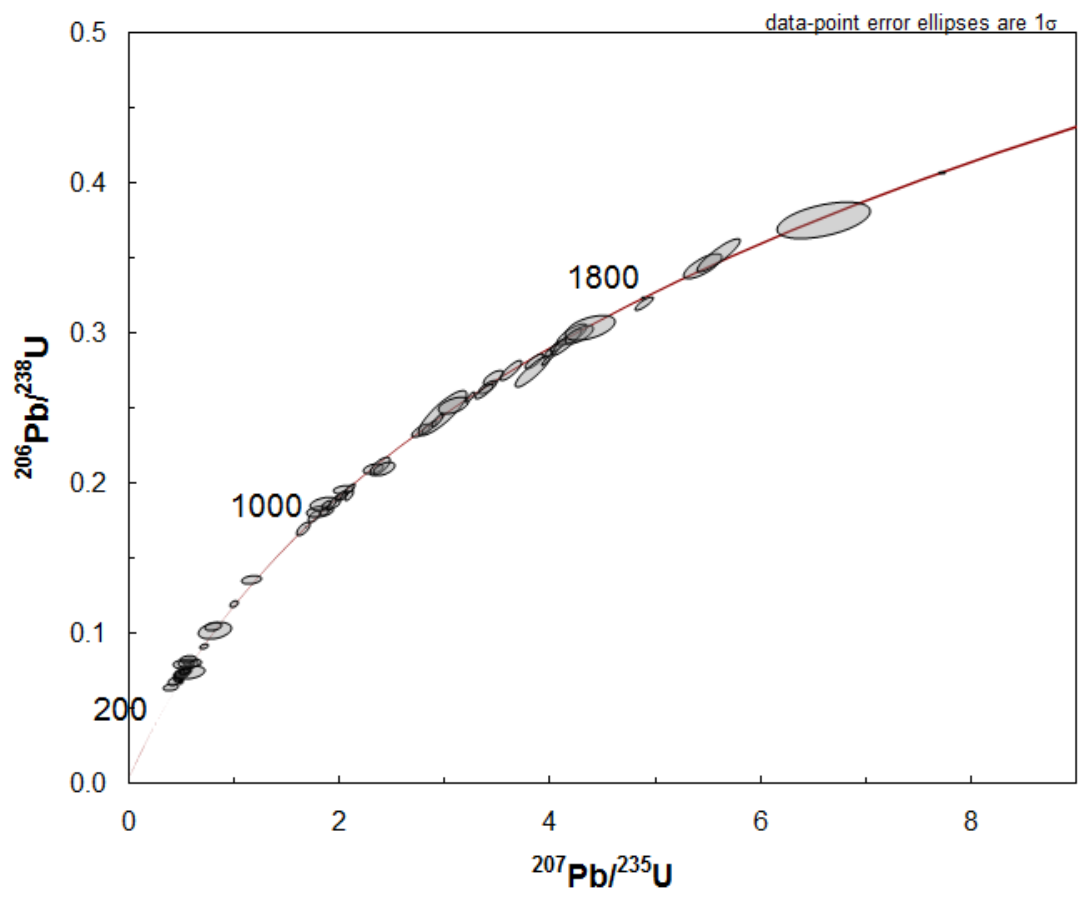
Figure 17. U-Pb Concordia normal distribution plot at the 1σ confidence level for the Mississippian age Lewis Sandstone (BW1)
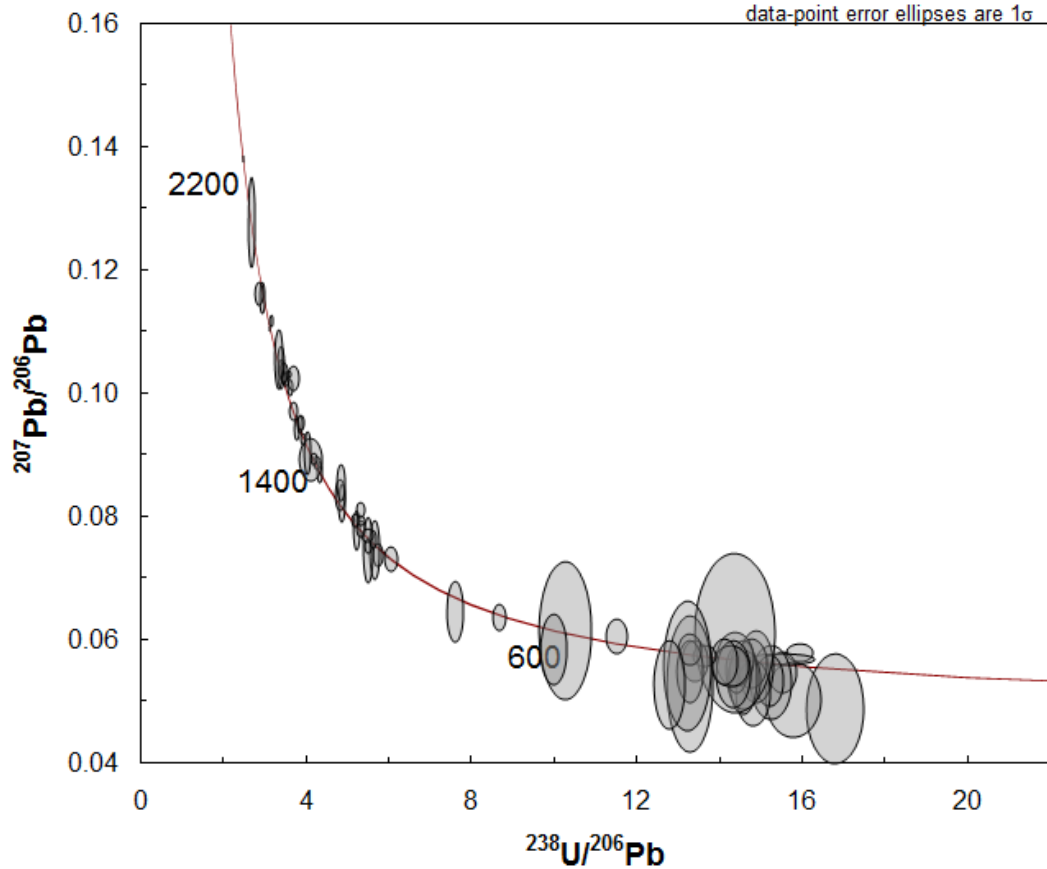
Figure 18. U-Pb Concordia Tera-Wasserburg distribution plot at the 1σ confidence level for the Mississippian age Lewis Sandstone (BW1)

The Sanders Sandstone (n=78)

Of the 100 zircons that were analyzed from the Sanders Sandstone, the dataset is represented by 78 grains (within ±20% concordance) due to loss of data with discordant or reverse discordant results. The relative age probability plot of the Sanders Sandstone (BW2) is presented at the 1σ confidence level (Figure 19). Zircon ages from the Sanders Sandstone range from 2087 to 374 Ma. Results of the Sanders Sandstone display great similarity to the Lewis Sandstone sample. Ages from the raw number of grains (presented as blue histogram bars in intervals of 200 Ma) follow. Four zircon

grains (~5% of the Sanders sample) from the Archean and Paleoproterozoic periods (>1800 Ma) constitute the smallest of any age group within the Sanders Sandstone. Ten zircon grains (~13% of the sample) are late Paleoproterozoic (1800-1600 Ma). Zircons from the Early Mesoproterozoic (1480-1340 Ma) are represented by 8 grains (10% of the sample). The second largest population from the Sanders Sandstone is represented by Mesoproterozoic age grains (1350-900 Ma) (21 grains; 27% of the sample). The Neoproterozoic-Early Paleozoic (725 - 515 Ma) age populations are minor, being represented by 6 grains (8%). Zircons from the Paleozoic (<515 Ma) form the largest population for this sample with 29 grains (37%).
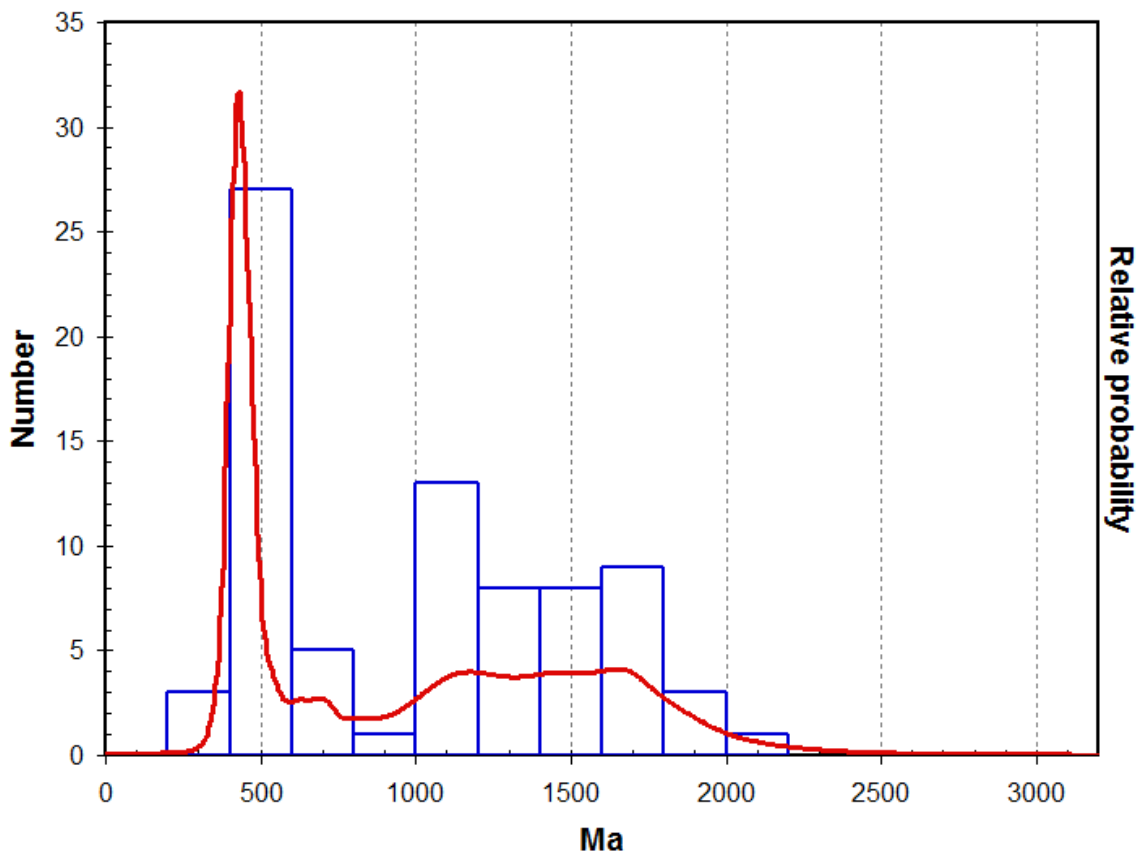
Figure 19. Relative age probability plot (0-3200 Ma) for the Mississippian age Sanders Sandstone (BW2) at the 1σ confidence level.

Age results from the Sanders Sandstone are displayed on U-Pb Concordia

normal distribution and Tera-Wasserburg distribution plots (Figures 20 and 21,

respectively). All grains displayed (n=78) have ages that are less than 20% discordant.

Of the 78 grains 72% (n=56) were <5% discordant, 15% (n=12) were <10% discordant,

3% (n=2) were <15% discordant, and 6% (n=5) were <20% discordant. The remaining

4% of grains (n=3) are valid and reported as being "NA" in the concordance calculations

since there is so much error within calculating ages younger than 400 Ma. The

dominant age group (based on probability) of 400-600 Ma (35% of the sample; n=27)

contains 15 grains within 5% discordant, 7 grains within 10% discordant,1 grain within

15% discordant, and 4 grains within 20% discordant.
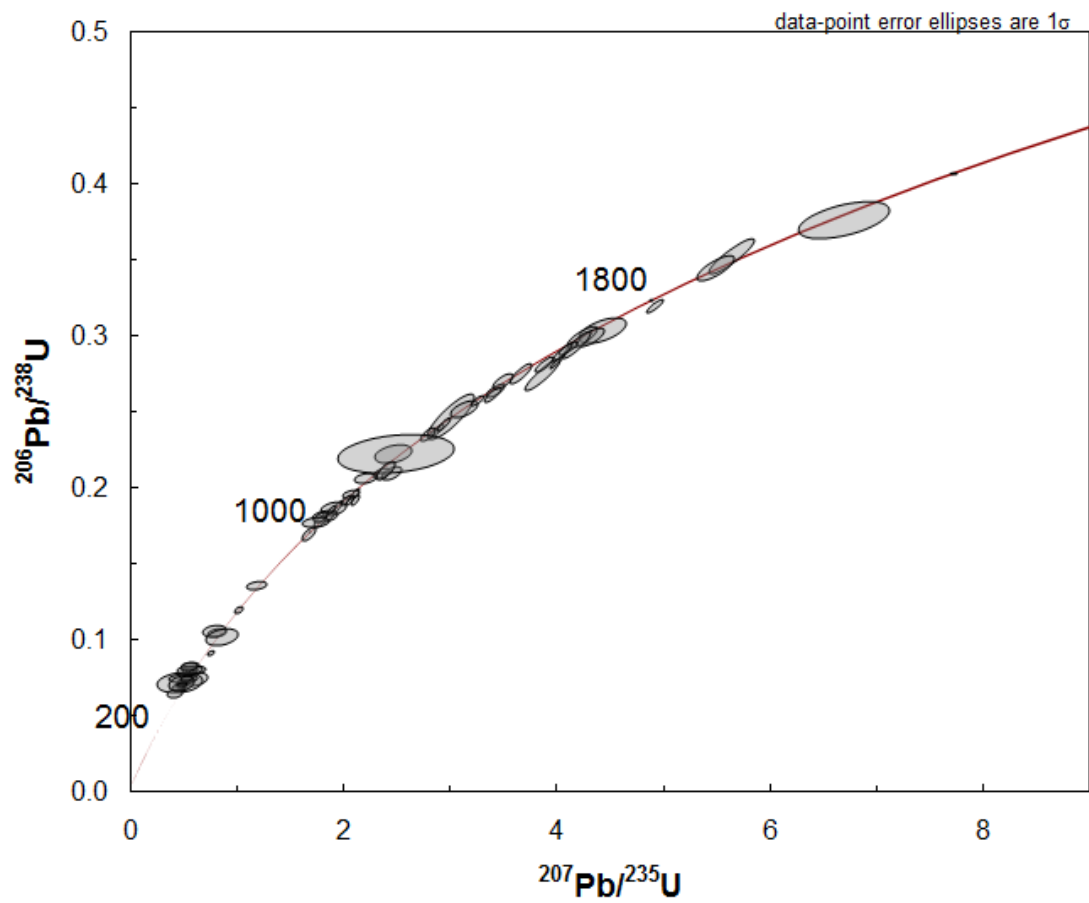
Figure 20. U-Pb Concordia normal distribution plot at the 1σ confidence level for the Mississippian age Sanders Sandstone (BW2)
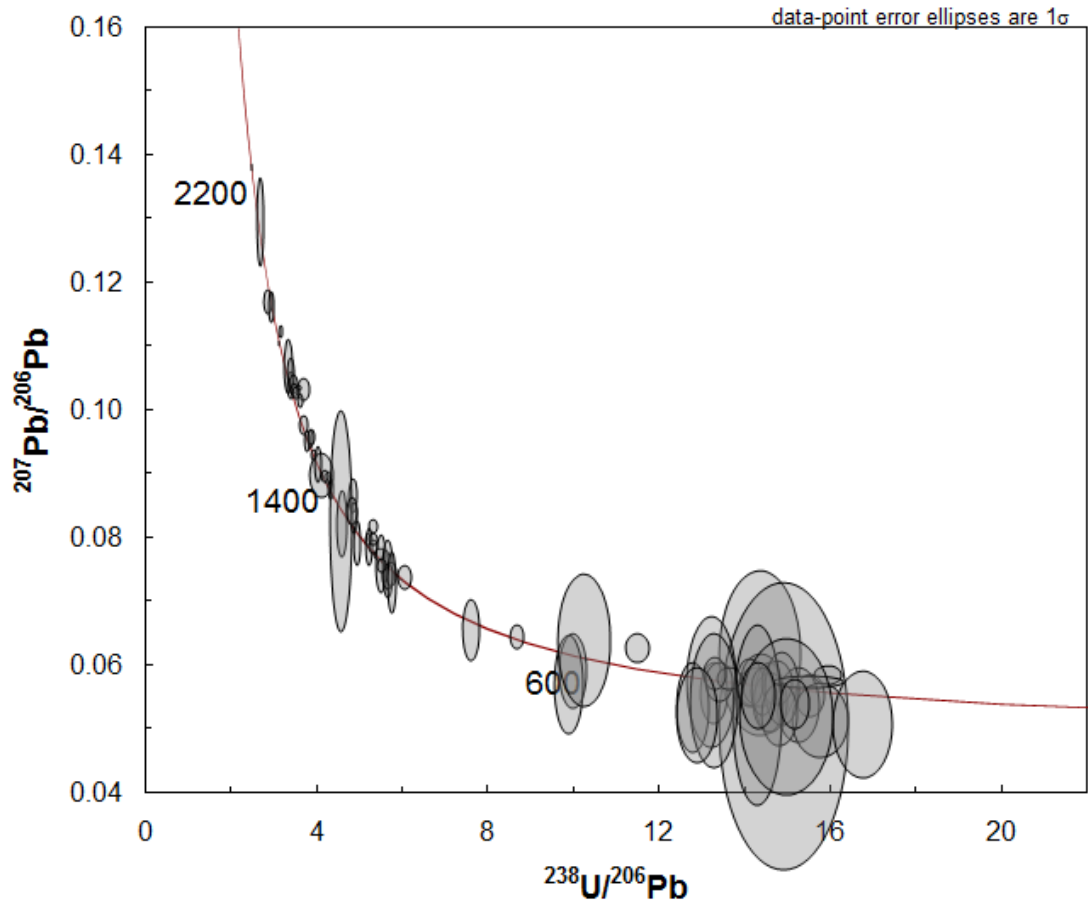
Figure 21. U-Pb Concordia Tera-Wasserburg distribution plot at the 1σ confidence level for the Mississippian age Sanders Sandstone (BW2)

The Carter Sandstone (n=151)

Of the 200 zircons that were analyzed from the Carter Sandstone, 151 grains (within ±20% concordance) represent the dataset due to loss of data with discordant or reverse discordant results. Results from Carter Sandstone (BW3) are represented on a relative age probability plot (Figure 22) at the 1σ confidence level. Ages from the Carter Sandstone range from 2911 to 367 Ma. Ages from the raw number of grains (presented as blue histogram peaks in intervals of 183 Ma) follow. The Carter Sandstone has a greater representation (20 grains; 13% of the Carter sample) of ages from the Archean

and Paleoproterozoic (>1800 Ma) than the Lewis and Sanders samples. Zircons from the late Paleoproterozoic (1800 - 1600 Ma) make up the second largest population in this sample (34 grains; ~22% of the Carter sample). The Early Mesoproterozoic (1480 - 1340 Ma) is represented by 18 grains (12%) of the sample. Mesoproterozoic (1350 - 900 Ma) age zircons make up the greatest population for this sample with 47 grains (31%). The Neoproterozoic-Early Paleozoic (725 - 515 Ma) population is minor and is represented by 1 grain (<1% of sample). The Paleozoic (<515 Ma) age is characterized by 31 grains (21% of the Carter sample).
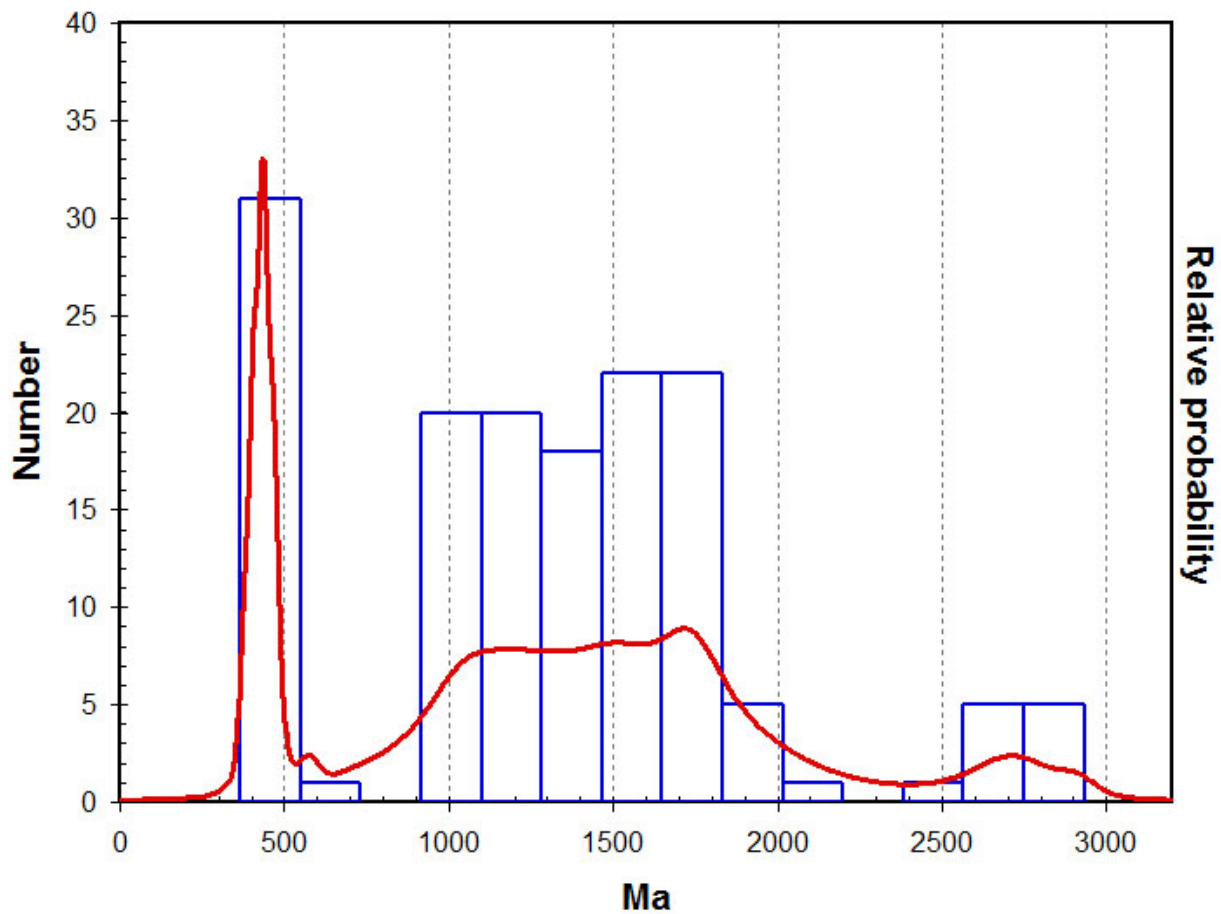
Figure 22. Relative age probability plot (0-3200 Ma) for the Mississippian age Carter Sandstone (BW3) at the 1σ confidence level.

Results for the Carter Sandstone are plotted on U-Pb Concordia normal distribution and Tera-Wasserburg distribution plots (Figures 23 and 24, respectively). All grains displayed (n=151) have ages that are less than 20% discordant. Of the 151 grains 74% (n=113) are <5% discordant, 12% (n=18) are <10% discordant, 9 % (n=13) are <15% discordant, and 2 % (n=3) are <20% discordant. The remaining 3% of grains (n=5) are valid and reported as being "NA" in the concordance calculations since there is so much error within calculating ages younger than 400 Ma. The dominant age group (based on probability) of 412-550 Ma (14% of the sample; n=22) contains 7 grains within 5% discordant, 8 grains within 10% discordant, and 7 grains within 15% discordant.
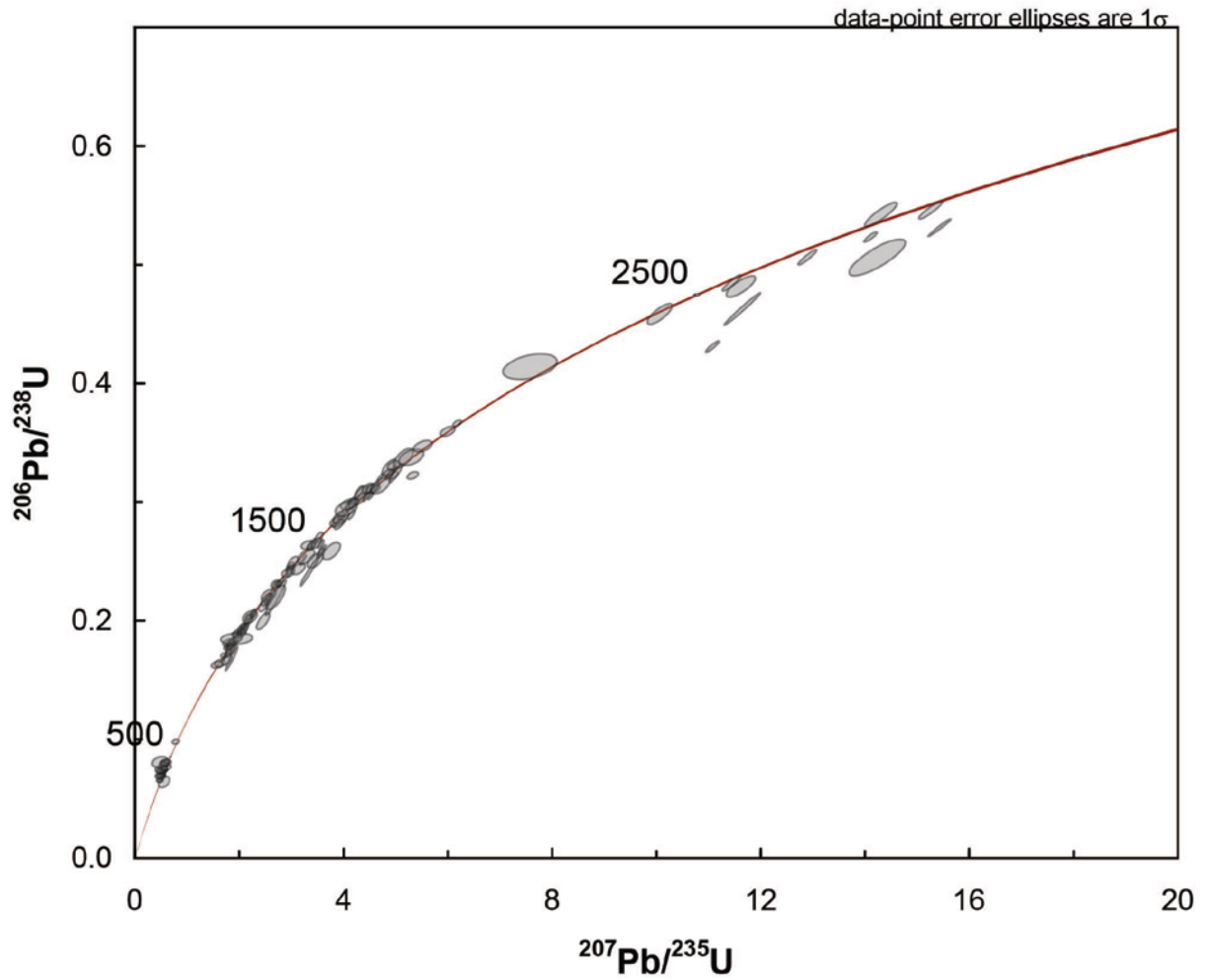
Figure 23. U-Pb Concordia normal distribution plot at the 1σ confidence level for the Mississippian age Carter Sandstone (BW3)
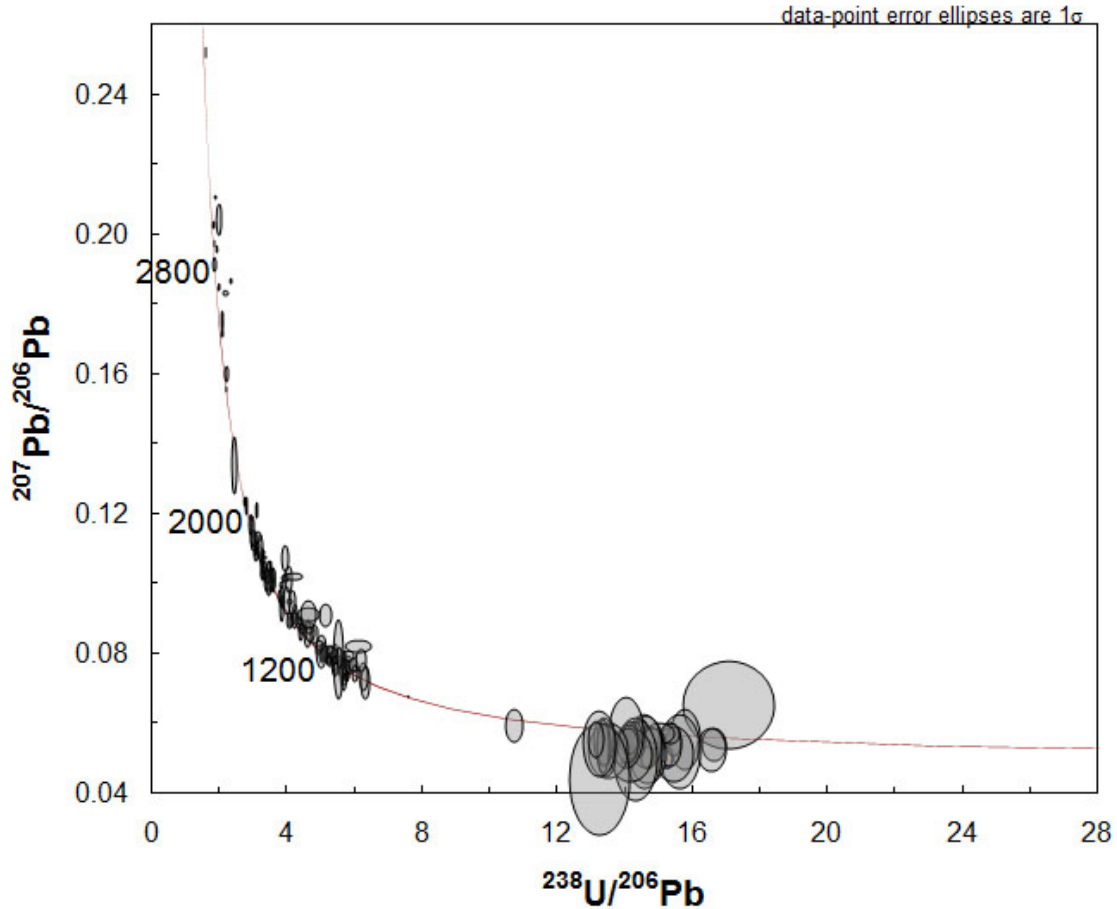
Figure 24. U-Pb Concordia Tera-Wasserburg distribution plot at the 1σ confidence level for the Mississippian age Carter Sandstone (BW3)

3.2.2 K-S similarity analyses

In order to compare detrital zircon age distributions, the Kolmogorov-Smirnoff test (K-S test) was adapted from Press et al. (1986) and utilized in this study. To summarize Guynn and Gehrels (2010), the K-S test mathematically compares two distributions to each other in order to assess the potential that they are statistically different. By comparing the two samples with the K-S test it can be seen whether the two distributions are from different populations; for example, the principle is to test if P is less than a value (~0.05 which may equate to a confidence level >95%). However, the K-S test does not conclude whether the two populations are the same. It is seen here

that the Lewis and Sanders are not from different populations (not necessarily from the

same either) (Table 11). The Lewis and the Sanders are similar enough to pass this

test. However, the Carter Sandstone is different from the other two samples; in each

case, the P value is <0.05.

Table 11. K-S Results for the three sandstones analyzed in this study. Values in yellow pass for the 95% confidence level and are not rejected.

	Lewis	Sanders	Carter
K-S P-values using error in the CDF			
Lewis		**1.000**	0.022
Sanders	**1.000**		0.010
Carter	0.022	0.010	

4. POTENTIAL SOURCE TERRANES

Crystalline basement terranes (central/southern Precambrian and Phanerozoic age belts of North America) and regional orogenic terranes are evaluated for sedimentary provenance (Figure 25). These provinces were evaluated as likely sources for this study due to their proximity to the BWb and their significance in other provenance studies as potential sediment suppliers.

Archean and Paleoproterozoic (>1800 Ma)

Grains with Archean and Paleoproterozoic ages are present in this study. Laurentian cratonic sources include the Penokean-Trans-Hudson (2000 -1800 Ma) and Superior Province (>2500 Ma) (Hoffman, 1989; Van Schmus et al., 1996; Soreghan and Soreghan, 2013). Grains with ages between 2.0-2.3 Ga have been seen in Pennsylvanian rocks in the Appalachian Basin but may reflect a Gondwana source (Thomas et al., 2004).

Late Paleoproterozoic (1800-1600 Ma)

Late Paleoproterozoic ages found proximal to the midcontinent region are likely from the Yavapai-Mazatzal terrane (1800-1600 Ma) (Van Schmus et al., 1996; Gehrels et al., 2011; Thomas, 2011). This terrane consists of metasedimentary and metavolcanic units and spans much of central and southwestern North America (Soreghan and Soreghan, 2013). Runkel and Tipping (1998) postulated that all crystalline basement rocks of the midcontinent region (Penokean-Yavapai-Mazatzal, Archean and Superior, and Midcontinent Rift) are likely first-cycle sources for sediment supply to early Paleozoic quartzarenites. However, other authors (Thiel, 1935; Ostrom, 1970; Ostrom and Odom, 1978) have stated that mature to super-mature quartzarenites

do not have to be composed of sediment purely derived from a first-cycle weathering of

crystalline basement terranes.
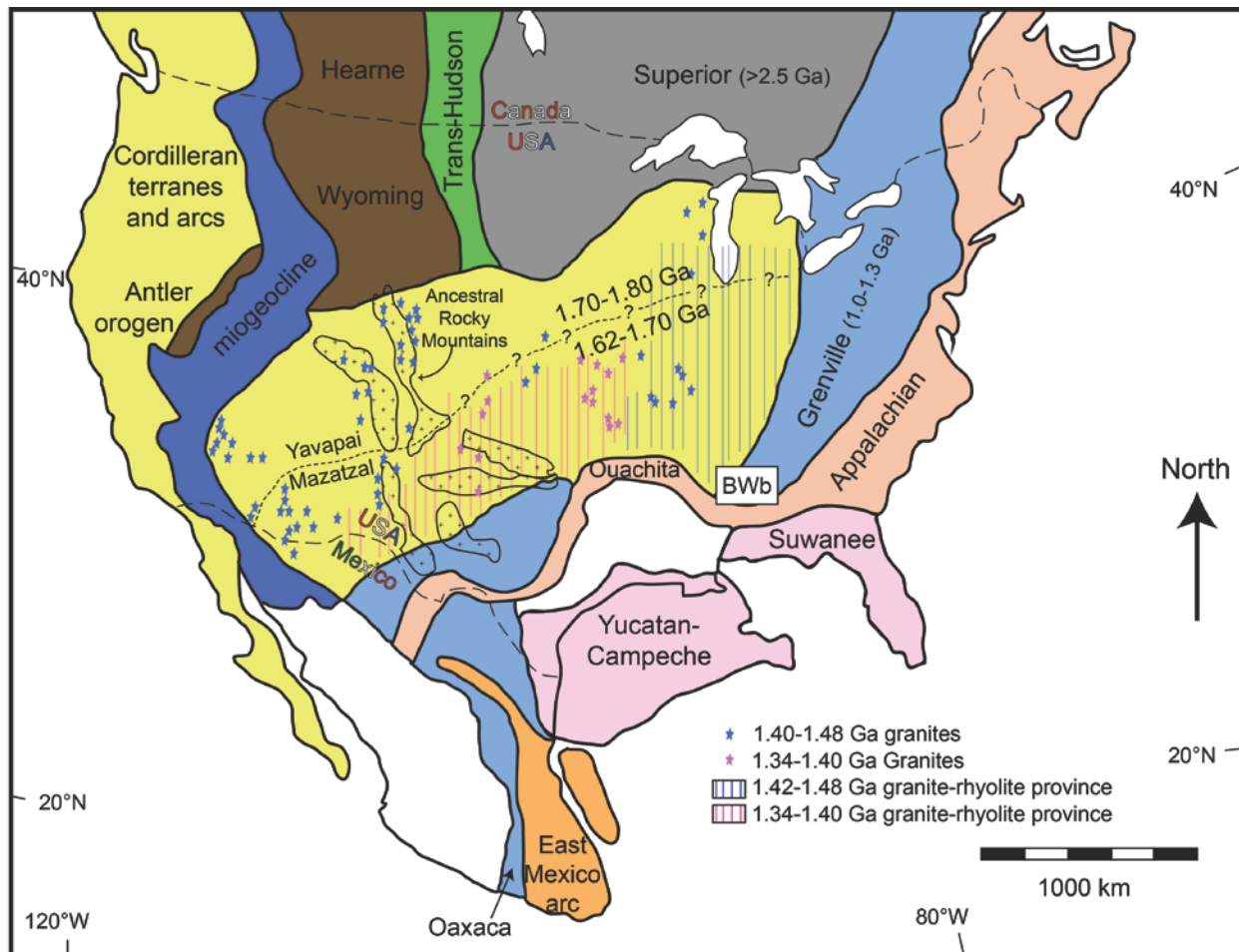
Figure 25. Location of the Black Warrior basin (BWb) relative to Precambrian and Phanerozoic age belts of central and southern North America. Modified from Gehrels et al. (2011) and references listed therein.

Early Mesoproterozoic (1480-1340 Ma)

The Early Mesoproterozoic region relevant for this study is the midcontinent

granite-rhyolite province. This midcontinent province is represented by an anorogenic

magmatic event that resulted in an irregular distribution of plutons (Van Schmus et al.,

1996). In this midcontinent region, a granite-rhyolite province (1400-1340 Ma) covers

the western midcontinent region, while the eastern half is covered by 1480-1420 Ma

granite-rhyolites (Gehrels et al., 2011).

Mesoproterozoic (1350-900 Ma)

In provenance studies, grains derived from the Grenville Orogeny (1350-900 Ma;

Moores, 1991; Dalziel, 1992; Whitmeyer and Karlstrom, 2007) are sometimes

overrepresented (Hietpas et al., 2011). Patchett et al. (1999) discussed the significant

magnitude of transport from Appalachian sediments and thus, Grenville age signatures,

throughout the North American Craton. Patchett et al. (1999) analyzed Phanerozoic

Neodymium (Nd) isotopes and concluded the reason the Grenville signature is so

prevalent in zircon populations is that sedimentary formations that make up the

Appalachian Orogen inherit the age signature from the Grenville crust. Eriksson et al.

(2003) examined Appalachian basin sandstones and stated that the Grenville Orogeny

was the most significant in providing zircons to eastern North America.

Neoproterozoic-Early Paleozoic (725-515 Ma)

Several sources of Neoproterozoic-Early Paleozoic detritus exist in proximity to

the BWb. These include terranes from the northern and southern parts of the

Appalachian Orogeny (Avalon and Carolina, respectively), and the Suwannee

(subsurface of Florida) (Opdyke et al., 1987; Mueller et al., 1994; Nance and

Thompson, 1996; Murphy et al., 2003).

Paleozoic (540-360 Ma)

Delivery of Paleozoic grains could be from the Taconic, Acadian, Alleghanian,

and Ouachita Orogens. An Ordovician signature in the sediment is possibly related to

volcanic structures that make up the Taconic Orogen (490-440). The existence of

volcanic features is evidenced by exposed plutons, which mark the root of a magmatic arc, within the Appalachian Piedmont (Shaw and Wasserburg, 1984; Tucker and Robinson, 1990; Sevigny and Hanson, 1993; Sinha et al., 1997; Karabinos et al., 1998; Coler et al., 2000; McClellan and Miller, 2000; Miller et al., 2000; Aleinikoff et al., 2002). Middle Ordovician to Silurian sediments may represent transport from the Taconic Orogen to the Appalachian foreland basin (Thomas, 1977; Drake et al., 1989). The Acadian Orogen (420-350 Ma) is evidenced by northern Appalachian plutons along the Appalachian Piedmont (Osberg et al., 1989; Eusden et al., 2000; Miller et al., 2000). Similar to sediments from the Taconic Orogen, the Acadian Orogen is represented in the Appalachian Basin, though this time by Devonian to Early Mississippian ages (Thomas, 1977; Osberg et al., 1989).

Numerous authors have extensively discussed the Ouachita belt as a southwestern sediment source for the BWb (Thomas 1972, 1974; Thomas and Mack, 1982; Mack et al., 1981; Mack et al., 1983; Nix, 1991; Thomas, 2011). Additionally, potential source terranes exist north/northwest of the BWb. It was summarized previously by multiple authors (Swann, 1964; Welch, 1978; Cleaves and Broussard, 1980; Cleaves, 1983; Bearden, 1985; Bearden and Mancini, 1985; Cleaves and Bat, 1988) that a northern sediment source (possibly the Illinois Basin, or the Ozark dome) supplied sediment for the Mississippian sands of the BWb. An Ouachita and Illinois Basin source will be analyzed in detail in the Discussion.

5. DISCUSSION

5.1 Comparison of BWb and Appalachian Foreland Geochronology Results

A normalized age probability plot of detrital zircon age data (n=1828) compiled from various authors studying the Appalachian foreland basin (Gray and Zeitler, 1997; McLennan et al., 2001; Eriksson et al., 2004; Thomas, 2004; Becker et al., 2005; Park et al., 2010) allows comparison of similarities and differences in the Lewis, Sanders, and Carter sandstones from the BWb (Figure 26). Populations from the time of the Acadian Orogeny (420-350 Ma) show a high probability on the relative probability plot in Lewis and Sanders samples (peaks at ~ 380, 400, 415, 420 Ma) and Carter sample (peaks at ~380 and 410 Ma) (Figure 26). Signatures from the Taconic orogen (490-440 Ma) are present in the Lewis, Sanders, and Carter dataset (peaks at ~435, 435, 440, and 465 Ma) (Figure 26). Dorsch et al. (1994) explained that weathering and reworking of sediments occurred after isostatic rebound of the Taconic orogen. This process, along with recycling of passive margin sandstones may be responsible for producing such mature sandstones within the Taconic foreland basin (Dorsch et al., 1994), and possibly those quartzarenites in the BWb.
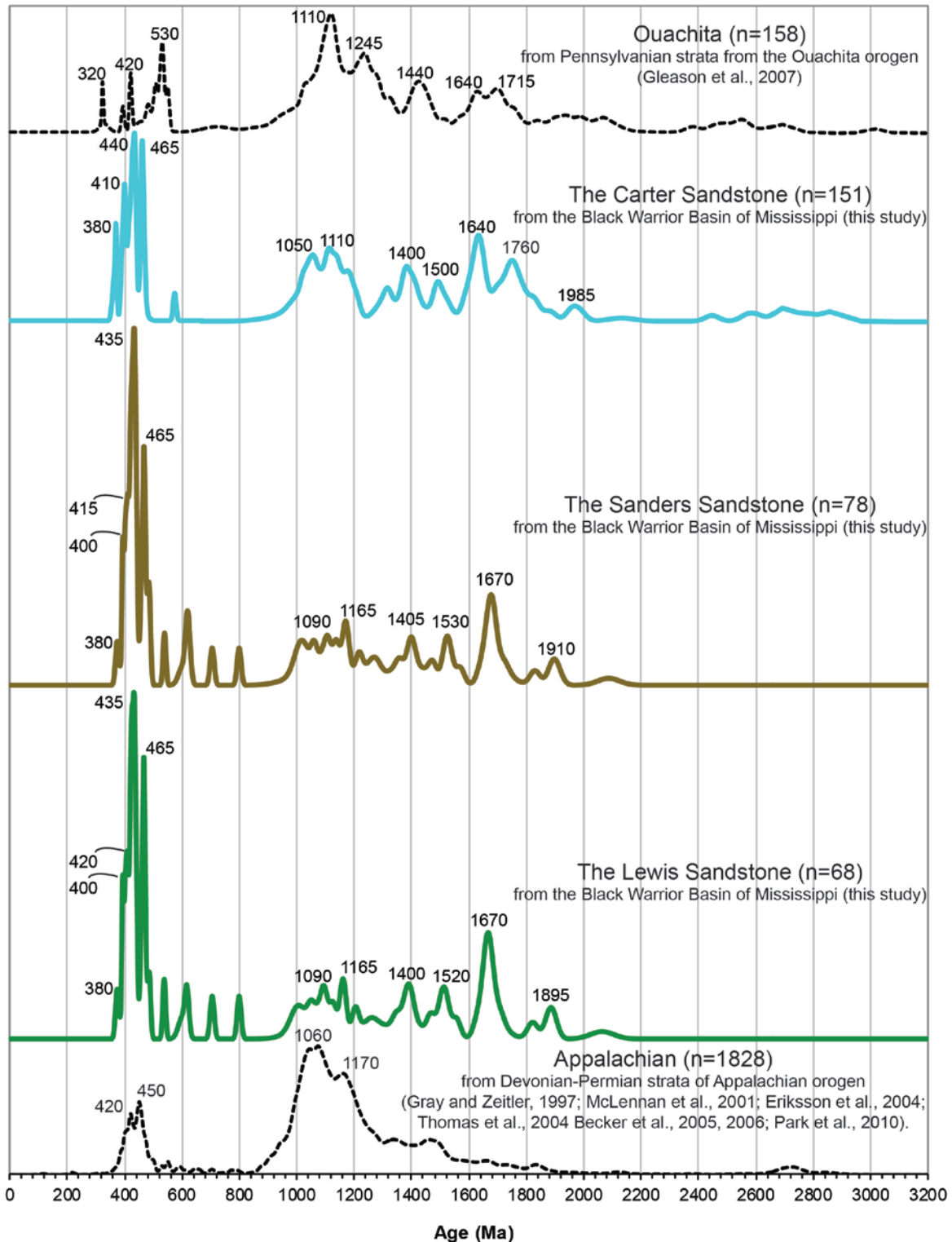
Figure 26. U-Pb detrital zircon geochronology data from Devonian to Permian strata of the Appalachian Orogeny (cited above), and Pennsylvanian strata from the Ouachita Orogeny (cited above) is compared to U-Pb detrital zircon geochronology from the Lewis, Sanders, and Carter samples from this study.

Minor peaks occur between 800-500 Ma (~540, 620, 710, 800 Ma) in the Lewis

and Sanders, and at ~580 Ma in the Carter (Figure 26). This age range of peaks is

small and represented by ~7% of the Lewis and Sanders samples, and ~1% of the

Carter sample. They coincide adequately with multiple 800-500 Ma signals in the

Appalachian dataset (Figure 26). Park et al. (2010) attributed the 700-500 Ma grains to

recycled Pan African/Brasiliano zircons in the Acadian clastic wedge. Rodinian rifting

also took place between 800 and 550 Ma (Aleinikoff et al., 1995; Hoffman, 1999).

Thomas (2004) discussed the substantial volume of sediment delivered to the

Appalachian foreland basin as a result of rifting. These 800-500 Ma age ranges are well

represented within the Dahlonega terrane (western Gondwana) and have been reported

within recycled sediments in the Appalachian foreland (Park et al., 2010). Although the

signals are minor, the 800-500 Ma populations (Figure 26) potentially help endorse the

connection between the Lewis, Sanders, and Carter to the Appalachian region. While

there is no evidence supporting that the origin of these ages are from Gondwanan

terranes, it is likely that they are of Appalachian origin given the strong evidence of

recycled detritus from the Taconic and Acadian clastic wedges within the BWb.

As discussed earlier, Grenville-age populations (1350-900 Ma) are common in

geochronologic data and are also present in the Appalachian datasets. There are also

prominent peaks in the Lewis, Sanders, and Carter sandstones between 1500-1300 Ma

(peaks at ~1400, 1405, 1500, 1520, 1530 Ma) (Figure 26). These age ranges are often

attributed to the Granite-Rhyolite province of the midcontinent region (Van Schmus et

al., 1996). Park et al. (2010) discussed the presence of the Granite-Rhyolite signatures

within the Appalachian foreland and their presence in the Taconic clastic wedge.

Eriksson et al. (2004) proposed that Mesoproterozoic zircons are from a weathered Granite-Rhyolite and/or Grenville Province and recycled into the Appalachian foreland basin and passive margin region.

The Lewis and Sanders samples display large peaks at ~1670 Ma (Figure 26). This population provides the third largest group in terms of number of raw grains (13-14%) from the Mazatzal time period (1700-1600 Ma). The Carter sample also has grains of Mazatzal age (peak at ~1640 Ma); however, it has an even greater number of grains with ages similar to the Yavapai province (1800-1700 Ma; peak at ~1760 Ma) than the other BWb samples. Additionally, Cambrian passive margin quartzarenites in the Appalachian foreland also have significant populations from the late Paleoproterozoic (1800-1300 Ma) (Eriksson et al., 2004), which may account for the 1800-1300 signatures in the BWb dataset.

Minor signatures appear from 2000-1800 Ma in the Appalachian dataset (Figure 26). These 2000-1800 Ma signatures appear in the Appalachian foreland strata and are interpreted to represent recycled detritus from the midcontinent orogens (Park et al., 2010) or from Gondwanan terranes (Thomas, 2004). This influence is very minor within the BWb samples. Ages of ~2900-2400 Ma are present in the Carter and Appalachian datasets. The Archean zircons in the Carter sandstone in this study are thought to be from the Superior Province and are recycled from either the midcontinent region or from the Appalachian foreland similar to interpretations by Eriksson et al. (2004).

5.2 Model One: Previous Interpretations for a Northern Sediment Source

A northern source provenance model was supported by petrographic data and/or subsurface mapping (Swann, 1964; Welch, 1978; Cleaves and Broussard, 1980;

Cleaves, 1983; Bearden, 1985; Cleaves and Bat, 1988; Stapor and Cleaves, 1992; Ettensohn and Pashin, 1993; Pashin and Rindsberg, 1993). Shepard (1979) declared that mean grain size in Mississippian sand bodies increased to the northwest. Cleaves (1983) reported monocrystalline quartz and chert fragments, lacking proof of orogenic provenance within Mississippian sandstones. Similarly, Cleaves and Bat (1988) agreed that the composition of these sandstones indicated a cratonic source from the midcontinent interior. The percentage of metamorphic rock fragments, muscovite, and polycrystalline quartz is too low to be from an orogenic source (Cleaves and Bat, 1988). In a related study, Hughes and Meylan (1988) determined that Chesterian age sandstones (i.e., Lewis, Evans, Sanders, Rea, and Carter sandstones) plot as quartzarenites on the Folk (1980) sandstone classification and these plot very similar to results from the BWb data (Figure 9). Hughes and Meylan (1988) concluded a northern, probably cratonic interior sandstone provenance, was responsible for the Chesterian sandstones of the BWb.

In a review of subsurface mapping explanations that are in favor of a northern sedimentary source, Swann (1964) detailed that similarities in facies and cyclic sequences in the Illinois basin fit the model that the Michigan River supplied sediment from the north. Later, Cleaves and Broussard (1980) and Cleaves (1983) provided subsurface mapping and facies patterns to detail that Chesterian-age sandstones in the BWb have a northern provenance from a likely cratonic interior source.

While the petrographic results from this study are analogous to that of previous northern-source-proposing authors, there are complications that exist with their model. Mack et al. (1981) suggest that connecting Mississippian sands between the Illinois and

BWb is unreliable because of post-Mississippian erosion. There are several other issues, unrelated to BWb sedimentation, that are problematic for a source directly from the Illinois basin. The St. Peter Sandstone (the youngest pre-Mississippian sand body in the Illinois Basin) is a thick Ordovician quartzarenite, but in order for the St. Peter Sandstone to contribute sediment, all strata above it (a thick Silurian and Devonian section of carbonates) would need to be eroded first. The lack of carbonate grains in the BWb samples make this an unlikely scenario. Additionally, the St. Peter Sandstone was deposited during the Tippecanoe transgression (Sloss, 1963; Shaw and Schrieber, 1991; Meyers and Peters, 2011) and sedimentation and shoreline migration trends were to the northeast at that time (with respect to the present day midcontinent) (Dott et al., 1986; Shaw and Schrieber, 1991; Runkel, 1992, 1994; Runkel et al., 2007). Furthermore, in a study assessing provenance of pre-Silurian quartzarenites of the midcontinent region, Konstantinou et al. (2014) found that all samples have 2800-2550 Ma age grains representative of the Archean Superior Province (Whitmeyer and Karlstrom, 2007). The lack of major influence of the Archean Superior Province in the Lewis and Sanders samples makes the midcontinent/northern source model questionable. However, the mapping interpretations of sand bodies in the subsurface of the BWb (Cleaves and Broussard, 1980; Cleaves, 1983; Cleaves and Bat, 1988; Stapor and Cleaves, 1992; Ettensohn and Pashin, 1993) seem valid and provide justification to the idea of deposition from the north. The current study agrees with the mapping interpretations of these authors; however, geochronologic results suggest that the dominant origin of these sediments is from the Appalachian region rather than the Illinois Basin or the Ozark Dome.

5.3 Model Two: Previous Interpretations for a Proximal but Controversial

Sediment Source from the Ouachita Orogenic Belt

Similar to northern sediment source interpretations, studies utilizing petrography

and subsurface mapping have been used to support the idea that the Ouachita orogenic

belt was the dominant sediment source (Thomas 1972, 1974; Thomas and Mack, 1982;

Mack et al., 1983; Nix, 1991; Thomas, 2011). Mack et al. (1981) report late

Mississippian formations comprised of sedimentary, metamorphic, and volcanic-derived

grains. The majority of sandstones are classified as lithic arenites, except the Hartselle

Sandstone which is categorized as a quartzarenite, indicative of a recycled orogenic

source on the Dickinson et al. (1983) ternary diagram. Mack et al. (1981) argue the

Hartselle could not have come from a northern source like the Illinois basin, as

sandstones in that basin are generally classified as sublitharenites. Although the

Hartselle Sandstone plots in the continental block provenance on the QFL diagram,

Mack (1984) suggests the mature composition of the Hartselle is due to weathering,

marine re-working, and a humid environment which combined to diminish grains

indicative of what would be present in an Ouachita source.

Data from the Hartselle Sandstone petrography (Mack et al., 1981) is plotted with

sandstones from this study on a Folk (1980) diagram (Figure 9). There are clear

similarities between the sandstones from this study (Lewis, Sanders, Evans, and Carter)

and Hartselle data from Mack et al. (1981). Thus, the Hartselle Sandstone may not be a

product of Ouachita-derived sediments. Rather, all these sandstones are likely from a

recycled source. Point counting results from this study show the Mississippian sands

range from quartzarenites to sublitharenites. There is an absence of feldspars, lithics,

and an overall indication of a first-cycle sediment sourcing in the samples. The explanation of reworking and weathering of sediments (Mack et al., 1981) is plausible and significant alteration through mechanical attrition and chemical diagenesis as a result of long distance transport and weathering would produce these mature sandstones. However, an Ouachita belt dominant source would mean that these Mississippian sands would be deposited in a syndepostional manner and due to the proximity to the Ouachita belt there might not be enough time for this degree of weathering and reworking to create such a mature character.

Mack et al. (1981) also state that later Mississippian sandstones, specifically the Parkwood Formation, are lithic arenites containing metamorphics and unstable polycrystalline quartz, suggestive of a metamorphic terrane. In contrast to the explanations of Thomas and Mack (1980) and Mack et al. (1981), Cleaves (1983) notes that the previous author's petrographic studies of the Parkwood Formation focused on sandstones from outcrop of the folded Appalachian region where polycrystalline quartz and metamorphic fragments dominate compared to the basin center. Cleaves (1983) argues that the petrography of the Chesterian age sandstones proximal to the northern shelf of the basin are dissimilar from those samples in the folded Appalachian outcrops. The results of this study agree with the interpretations of Cleaves (1983). Petrographic analysis of Parkwood samples in other parts of the basin, rather than the folded region, should yield results more similar to the subsurface Carter Sandstone (Parkwood Formation) composition from this study (Figures 9-11).

Thomas (1972, 1974) suggests that the thickness of Mississippian sand bodies increases towards the southwest based on subsurface mapping interpretations. Thomas

(1972) notices a trend of eastward regression in distributary lobes, in addition to coarser sediment in the west for the Mississippian-Pennsylvanian clastic facies of northeastern Mississippi. Thomas (1988) summarizes available evidence for northeastward-prograding deltaic systems and integrates the observations into tectonic models for basin subsidence and subsurface geometry. An overall southwestward thickening of the Mississippian-Pennsylvanian succession and facies patterns from paleogeographic reconstructions favor the explanation of arc-continent collision supplying sediment from the southwest of the basin. However, Welch (1972) argues that the subsurface mapping by Thomas (1972) was in an area that is heavily faulted, which has proven to be problematic for correlating and assessing thickness and geometry trends of Mississippian sand bodies. Thus, Welch (1972) suggests that significant uncertainties exist in any interpretation. While contradictory, the present study is not able to refute the interpretations from subsurface mapping more proximal to the Ouachita belt due to the fact that the data in this study was collected from a single area and may not be representative of the entire basin.

The somewhat surprising lack of Alleghanian grains in Appalachian sediment has been explained as a "lag time" (Gehrels et al., 2011). Appalachian synorogenic wedges lack sediment from the most recent orogeny because substantial erosional unroofing is required to supply significant volumes of sediment into the system (Thomas, 2004; 2011). The Ouachita orogen likely behaved similarly and it remains very possible that in Mississippian time the only sediment that would be derived from the Ouachita thrust belt would be recycled sediment from Laurentian sources like the Appalachian orogen. Unfortunately, no definitive ages of sediment from the Ouachita orogen have been

documented in this region. These limitations make it impossible to estimate the influence of Ouachita-derived sediments on the Mississippian sand bodies in the BWb. Datasets from Upper Triassic sandstones (Chinle-Dockum fluvial system on the High Plains and the Auld Lang Syne Group in the Great Basin) depict what is reported to be a dominantly Ouachita provenance (Dickinson et al., 2010). There is too large of a difference in time of deposition between the Triassic and the Mississippian datasets for comparison. However, Pennsylvanian data (n=158) that has an inferred source from the Ouachita orogen (Gleason et al., 2007) is used for comparison against the Mississippian BWb samples (Figure 26).

The Ouachita dataset contains many similarities to the BWb data in terms of prominent age peaks (Figure 26). The most important difference is the lack of a representation from the Acadian and Taconic orogens in the Ouachita dataset. Gleason et al. (2007) discussed that ~400 Ma zircons have been rare in proximal Ouachita accumulations and attributed their small populations (2% of the Pennsylvanian dataset) to the Yucatan basement. The Taconic orogen (490-440 Ma) signal is minor in the Ouachita dataset (peak at ~485 Ma) (Figure 26), which has been attributed to an Appalachian source (Gleason et al., 2007). The Taconic orogen is represented by only 2 zircon grains in the Ouachita suite (1% of Ouachita sample), whereas the BWb Taconic-age representation was much larger (15% of the Lewis and Sanders, and 10% of the Carter Sandstone). This lack of Taconic signature has also been noted in the Pennsylvanian age Jackfork Sandstone (zircon ages fell between 1.0-3.5 Ga) within the Ouachita assemblage (Gleason et al., 2001).

The influence of the Yucatan-Maya terrane in Ouachita-derived sediment has been well documented by various authors (Weber et al., 2006, 2008; Soreghan and Soreghan, 2013). Neoproterozoic (specifically, 650-600 Ma) grains with a feldspar-rich mineralogy would be expected in abundance if the Ouachita is a dominant source (Soreghan and Soreghan, 2013). However, the Yucatan-Maya terrane was not exposed until the Pennsylvanian-Permian time (Weber et al., 2006, 2008; Soreghan and Soreghan, 2013). Therefore, using accreted Mexican terranes as an indicator for Ouachita provenance during the Mississippian time is not an option and it is apparent that differentiating between an Appalachian and Ouachita source within the BWb solely using U-Pb detrital zircon age signatures is difficult due to the potential presence of recycled Appalachian grains within the Ouachita region (Soreghan and Soreghan, 2013).

5.4 A New Model: Deposition from the North of Recycled Appalachian Foreland Sediment

Petrographic results in this study reveal that the Mississippian sandstones in the BWb are from a recycled orogenic or cratonic interior source and can be classified as quartzarenites to sublitharenites (Figures 9-11). It is expected that Ouachita-derived sediment would have a greater abundance of sedimentary lithic fragments, as seen within the Blaylock Sandstone from the Ouachita assemblage, due to the original deposition in an accretionary prism (Lowe, 1985; Gleason et al., 2001). The Lewis, Evans, Sanders, and Carter sandstones are quartz-rich sands that have been sorted, well-rounded, and are indicative of multiple recycling events and long term transport in a not-so-proximal depositional system. The Ouachita source is thought to be too proximal

to provide sediment that would depict this degree of transport and reworking. Additionally, the lack of strong Taconic and Acadian age signatures within Pennsylvanian strata of Ouachita-derived sediment (the Blaylock Sandstone from Gleason et al., 2001; the Haymond Formation from Gleason et al., 2007) indicates that the Appalachian region has had a greater influence on BWb sedimentation.

The notion of sediment traveling from the northeast down to the BWb is not new; a southwestward-prograding clastic wedge called the Pennington-Pottsville clastic wedge has been identified for the late Mississippian to Pennsylvanian strata in Alabama (Mack et al., 1981, 1983). This clastic wedge merges with the Floyd-Pride Mountain-Hartselle-Parkwood-Pottsville wedge in Alabama (Mack et al., 1983). Additionally, Graham et al. (1976) and Gleason et al. (1994) hypothesize that Carboniferous sediment derived from the southern Appalachians was recycled and delivered to the Ouachita embayment in a transportation route through the BWb. Based on Neodymium isotopic data, Gleason et al. (1994) postulate that multiple Carboniferous foreland and interior basins within the Appalachian-Ouachita region may be filled with sediment from the Appalachian province along a transport path to the Ouachita region. Tectonic recycling and long distance sediment transport may have been responsible for moving Appalachian derived sediment of Late Ordovician-Early Silurian age to the Ouachita region in early Paleozoic time (Gleason et al., 1994). Patchett et al. (1999) also used Neodymium isotopic data to illustrate that massive river systems supplied Taconic-age orogenic sediment from the Appalachian system to most regions of the North American craton, and sediment was transported from the Appalachians southwestward towards the BWb. Furthermore, Eriksson et al. (2004) discuss the extent and relevance of

multiple recycling events in the Appalachian Basin using U-Pb detrital zircon data. There have not been any subsurface mapping interpretations in literature that support the idea of the Chesterian age sediment traveling across the carbonate shelf in Alabama and being deposited to form the Lewis, Evans, Sanders, and Carter sandstones on the Mississippi side of the BWb. However, U-Pb detrital zircon geochronology age data from this study along with the maturity and character of these sandstones support a model of recycled sediment with an Appalachian foreland origin.

The K-S data comparison (Table 11) from the geochronology results suggests that the Carter is from a different source; however, we attribute that to the larger influence of Yavapai and Archean grains. The associations between two or more zircon populations may not always be properly revealed by sole use of K-S statistical comparison (Dickinson et al., 2010). Visual comparison of the detrital zircon age signatures (Figure 15) reveals that the proportions of grains derived from a terrane, represented by different magnitudes are different. Strictly using statistical analysis ignores the assumption that erosional unroofing of a sedimentary basin may be producing different proportions of these signatures due to multiple recycling events from one sedimentary source.

The importance of river systems dominating the Mississippian time and transporting sediment from the Appalachians westward across the continental United States has been supported by detrital zircon geochronology data (Gehrels et al., 2011). Detrital zircon grains with ages between 480 and 380 Ma have been transported westward through major river systems across the North American craton, from the central and southern Appalachians to the Grand Canyon (Gehrels et al., 2011). Data in

the current study shows a similar dominant age distribution. The current study did not incorporate subsurface mapping and thus is not able to propose that fluvial systems were also responsible for transporting Appalachian sediment (principal population ~465-380 Ma) southwest across the carbonate shelf to the BWb from the Appalachian foreland. This study proposes that recycling of sediment from the Appalachian foreland westward and then southward into the BWb is the most plausible scenario (Figure 27). Thus, the mapping interpretations from various authors (Cleaves and Broussard, 1980; Cleaves, 1983; Cleaves and Bat, 1988; Stapor and Cleaves, 1992; Ettensohn and Pashin, 1993) that portray deposition from the north of the BWb remain valid.

The proposed model (Figure 27) contradicts the idea of progradational deltas from a proximal source like the Ouachita orogenic belt to the southwest (Mack et al., 1981; Thomas, 1974, 1988) and includes an extended longitudinal sediment delivery system of distances >1000km. Long distance transport of sediment provides a viable explanation for the mature character of the Mississippian sandstones. This study recognizes that data collected from other parts of the basin may portray a different scenario. It is not within the scope of this study to assess the limit of the proposed delta front prograding from the southwest (Mack et al., 1981; Thomas, 1974, 1988) and the data from this study is only able to indicate that the extent of the proposed delta front from the Ouachita is not confirmed within the study area. Additional information from the Ouachita region may help constrain the Ouachita's timing and influence on the BWb sedimentation.
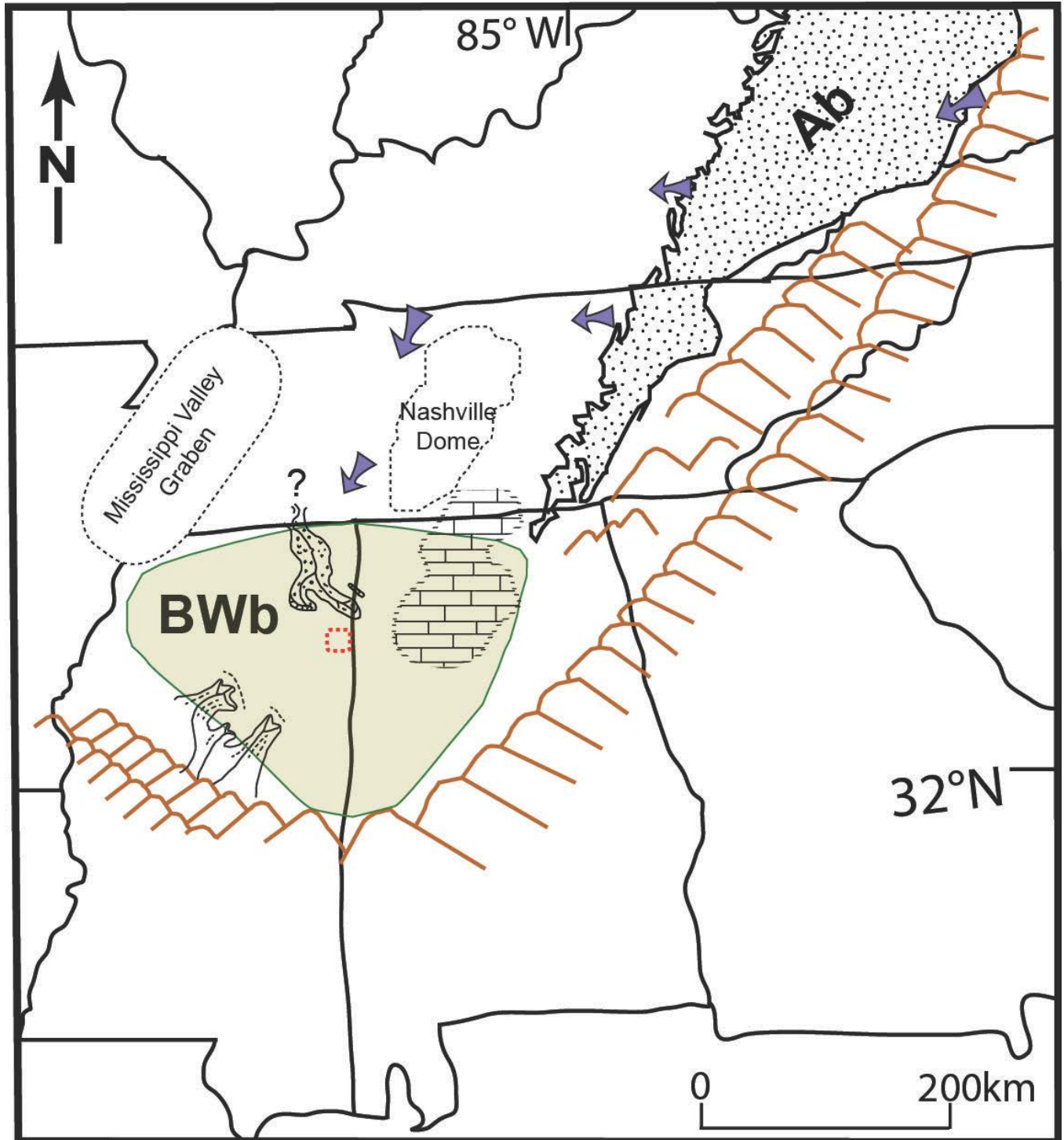
Figure 27. Suggested model proposing sedimentation during Chesterian time in the Black Warrior Basin (BWb) of Mississippi. Study area is dotted red box and purple arrows display suggested route of transport of recycled sediment from the Appalachian foreland basin (Ab). Deltas from the southwest are those previously proposed by multiple authors (Mack et al., 1981; Thomas, 1974, 1988). Regional geology was modified from multiple authors (Cleaves et al., 1980; Harry and Londono, 2004; Park et al., 2010; Thomas, 2010).

6. CONCLUSIONS

1. U-Pb detrital zircon geochronology results conclude that major age peaks in the Lewis, Sanders, and Carter sandstones are representative of the Acadian, Taconic, and Grenville Orogenies, with influence from an 1800-1600 Ma source terrane (recycled Yavapai-Mazatzal from the Appalachian foreland or a peri-Gondwanan terrane).

2. Incorporation of data other than U-Pb detrital zircon geochronology must be used for assessing Mississippian age sand bodies since the unique Ouachita signature (accreted Mexican terranes) is not present until Pennsylvanian time

3. The lack of lithic sedimentary fragments within Mississippian BWb samples indicate the Ouachita was not the dominant source within this study area

4. Point counting and U-Pb detrital zircon geochronology results indicate mature sediment likely recycled from the Appalachian foreland basin.

5. Conceivably, fluvial systems recycled sediment from the Appalachian region westward, and then transported sediment southwestward into the BWb.

6. The Ouachita orogen remains a possible source for BWb sedimentation due to its proximity but point counting results from this study suggest that these sandstones are quartzarenites to sublitharenites and thus are too mature for this to be a syndepositional system in Mississippian time.

References

Aleinikoff, J.N., Horton, J.W., Jr., Drake, A.A., Jr., Fanning, C.M., 2002. SHRIMP and conventional U-Pb ages of Ordovician granites and tonalites in the central Appalachian Piedmont; implications for Paleozoic tectonic events. American Journal of Science 302, 50-75.

Bat, D.T., A subsurface facies analysis of the distribution, depositional environments, and diagenetic overprint of the Evans and Lewis Sandstone units in northern Mississippi and northwestern Alabama.

Beard, R.H., Meylan, M.A., 1987. Petrology and hydrocarbon reservoir potential of subsurface Pottsville (Pennsylvanian) sandstones, Black Warrior Basin, Mississippi. Transactions - Gulf Coast Association of Geological Societies 37, 11-24.

Bearden, B.L., 1985. Petroleum trapping mechanisms in the Carter Sandstone (Upper Mississippian) in the Black Warrior Basin of Alabama. Oil and Gas Report (Tuscaloosa, Ala.) 9.

Bearden, B.L., Mancini, E.A., 1985. Petroleum geology of Carter Sandstone (Upper Mississippian), Black Warrior Basin, Alabama. AAPG Bulletin 69, 361-377.

Becker, T.P., Thomas, W.A., Samson, S.D., Gehrels, G.E., 2005. Detrital zircon evidence of Laurentian crustal dominance in the Lower Pennsylvanian deposits of the Alleghanian clastic wedge in eastern North America. Sedimentary Geology 182, 59-86.

Berger, S., Cochrane, D., Simons, K., Savov, I., Ryan, J.G., Peterson, V.L., 2001. Insights from rare earth elements into the genesis of the Buck Creek Complex, Clay County, NC. Southeastern Geology 40, 201-212.

Cawood, P.A., Nemchin, A.A., 2001. Paleogeographic development of the East Laurentian margin; constraints from U-Pb dating of detrital zircons in the Newfoundland Appalachians. Geological Society of America Bulletin 113, 1234-1246.

Cleaves, A.W., 1983. Carboniferous terrigenous clastic facies, hydrocarbon producing zones, and sandstone provenance, northern shelf of Black Warrior Basin. AAPG Bulletin 67, 1462-1463.

Cleaves, A.W., Bat, D.T., 1988. Terrigenous clastic facies distribution and sandstone diagenesis, subsurface Lewis and Evans format units (Chesterian), on northern shelf of Black Warrior Basin. AAPG Bulletin 72, 1111.

Cleaves, A.W., Broussard, M.C., 1980. Chester and Pottsville depositional systems, outcrop and subsurface, in the Black Warrior Basin of Mississippi and Alabama. Transactions - Gulf Coast Association of Geological Societies 30, 49-59.

Coler, D.G., Wortman, G.L., Samson, S.D., Hibbard, J.P., Stern, R., 2000. U-Pb geochronologic, Nd isotopic, and geochemical evidence for the correlation of the Chopawamsic and Milton terranes, Piedmont Zone, Southern Appalachian Orogen. Journal of Geology 108, 363-380.

Dalziel, I.W.D., 1991. Pacific margins of Laurentia and East Antarctica-Australia as a conjugate rift pair; evidence and implications for an Eocambrian supercontinent. Geology (Boulder) 19, 598-601.

Dickinson, W.R., 1970. Interpreting detrital modes of graywacke and arkose. Journal of Sedimentary Petrology 40, 695-707.

Dickinson, W.R., Beard, L.S., Brakenridge, G.R., Erjavec, J.L., Ferguson, R.C., Inman, K.F., Knepp, R.A., Lindberg, F.A., Ryberg, P.T., 1983. Provenance of North American Phanerozoic sandstones in relation to tectonic setting. Geological Society of America Bulletin 94, 222-235.

Dickinson, W.R., Gehrels, G.E., 2003. U-Pb ages of detrital zircons from Permian and Jurassic eolian sandstones of the Colorado Plateau, USA; paleogeographic implications. Sedimentary Geology 163, 29-66.

Dickinson, W.R., Gehrels, G.E., 2009. U-Pb ages of detrital zircons in Jurassic eolian and associated sandstones of the Colorado Plateau: Evidence for transcontinental dispersal and intraregional recycling of sediment. Bulletin of the Geological Society of America 121, 408-433.

Dickinson, W.R., Gehrels, G.E., Stern, R.J., 2010. Late Triassic Texas uplift preceding Jurassic opening of the Gulf of Mexico; evidence from U-Pb ages of detrital zircons. Geosphere 6, 641-662.

Dickinson, W.R., Lawton, T.F., 2003. Sequential intercontinental suturing as the ultimate control for Pennsylvanian ancestral Rocky Mountains deformation. Geology (Boulder) 31, 609-612.

Dorsch, J., Bambach, R.K., Driese, S.G., 1994. Basin-rebound origin for the "Tuscarora unconformity" in southwestern Virginia and its bearing on the nature of the Taconic Orogeny. American Journal of Science 294, 237-255.

Dott, R.H., Jr., Byers, C.W., Fielder, G.W., Stenzel, S.R., Winfree, K.E., 1986. Aeolian to marine transition in Cambro-Ordovician cratonic sheet sandstones of the northern Mississippi Valley, U.S.A. Sedimentology 33, 345-367.

Drake, A.A., Jr., Sinha, A.K., Laird, J., Guy, R.E., 1989. The Taconic Orogen. Geol. Soc. Am., Boulder, CO, Boulder, CO, United States (USA).

Ehrlich, R., 1965. The geologic evolution of the black warrior detrital basin (Alabama). Unpub. Ph.D. Thesis, Louisiana State University, Baton Rouge, LA, United States (USA), 64 p.

Eriksson, K.A., Campbell, I.H., Palin, J.M., Allen, C.M., 2003. Predominance of Grenvillian magmatism recorded in detrital zircons from modern Appalachian rivers. Journal of Geology 111, 707-717.

Eriksson, K.A., Campbell, I.H., Palin, J.M., Allen, C.M., Bock, B., 2004. Evidence for multiple recycling in Neoproterozoic through Pennsylvanian sedimentary rocks of the central Appalachian Basin. Journal of Geology 112, 261-276.

Ettensohn, F.R., Pashin, J.C., 1993. Mississippian stratigraphy of the Black Warrior Basin and adjacent parts of the Appalachian Basin; evidence for flexural interaction between two foreland basins. Guidebook for the Annual Field Trip of the Alabama Geological Society 30, 29-40.

Eusden, J.D., Jr., 2000. Acadian tectonics as viewed from Mt. Washington, New Hampshire. Abstracts with Programs - Geological Society of America 32, 15-16.

Folk, R.L., 1980. Petrology of sedimentary rocks. Hemphill Publ. Co., Austin, TX, Austin, TX, United States (USA), 184 pp.

Gazzi, P., 1967. Le arenarie del flysch sopracretaceo dell'Appennino modenese; correlazioni con il flysch di Monghidoro. Mineralogica et Petrographica Acta 12, 69-97.

Gazzi, P., Zuffa, G.G., Gandolfi, G., Paganelli, L., 1973. Provenienza e dispersione litoranea delle sabbie delle spiagge adriatiche fra le foci dell'Isonzo e del Foglia; inquadramento regionale. Memorie della Societa Geologica Italiana 12, 1-37.

Gehrels, G., Valencia, V., Pullen, A., 2006. Detrital zircon geochronology by laser-ablation multicollector ICPMS at the Arizona Laserchron Center. The Paleontological Society Papers 12, 67-76.

Gehrels, G., Valencia, V., Ruiz, J. 2008. Enhanced precision, accuracy, efficiency, and spatial resolution of U-Pb ages by laser ablation-multicollector inductively coupled plasma-mass spectrometry. Geochemistry, Geophysics, Geosystems 9, 1-13.

Gehrels, G.E., Blakey, R., Karlstrom, K.E., Timmons, J.M., Dickinson, B., Pecha, M., 2011. Detrital zircon U-Pb geochronology of Paleozoic strata in the Grand Canyon, Arizona. Lithosphere 3, 183-200.

Gleason, J.D., Gehrels, G.E., Dickinson, W.R., Patchett, P.J., Kring, D.A., 2007. Laurentian sources for detrital zircon grains in turbidite and deltaic sandstones of the Pennsylvanian Haymond Formation, Marathon assemblage, West Texas, U.S.A. Journal of Sedimentary Research 77, 888-900.

Gleason, J.D., Patchett, P.J., Dickinson, W.R., Ruiz, J., 1994. Nd isotopes link Ouachita turbidites to Appalachian sources. Geology (Boulder) 22, 347-350.

Gleason, J.D., Patchett, P.J., Dickinson, W.R., Ruiz, J., 1995. Nd isotopic constraints on sediment sources of the Ouachita-Marathon fold belt. Geological Society of America Bulletin 107, 1192-1210.

Gleason, J.D., Gehrels, G.E., Finney, S.C., 2001. Tectonic Recycling in the Paleozoic Ouachita Assemblage from U-Pb Detrital Zircon Studies. American Geophysical Union Spring Meeting

Graham, S.A., Ingersoll, R.V., Dickinson, W.R., 1976. Common provenance for lithic grains in Carboniferous sandstones from Ouachita Mountains and Black Warrior Basin. Journal of Sedimentary Petrology 46, 620-632.

Gray, M.B., Zeitler, P.K., 1997. Comparison of clastic wedge provenance in the Appalachian foreland using U/Pb ages of detrital zircons. Tectonics 16, 151-160.

Guynn, J., Gehrels, G., 2010. Comparison of detrital zircon age distributions using the K-S test. University of Arizona online dataset, www.geo.arizona.edu/alc

Harry, D., Londono, J., 2004. Structure and evolution of the central Gulf of Mexico continental margin and coastal plain, southeast United States. Bulletin of the Geological Society of America 116, 188-199.

Hatch, J.R., Pawlewicz, M.J., 2007. Introduction to the assessment of undiscovered oil and gas resources of the Black Warrior Basin Province of Alabama and Mississippi. U.S.Geological Survey Digital Data Series.

Hietpas, J., Samson, S., Moecher, D., Chakraborty, S., 2011. Enhancing tectonic and provenance information from detrital zircon studies; assessing terrane-scale sampling and grain-scale characterization. Journal of the Geological Society of London 168, 309-318.

Higginbotham, D.R., 1986. Regional stratigraphy, environments of deposition, and tectonic framework of Mississippian clastic rocks between the Tuscumbia and Bangor limestones in the Black Warrior Basin of Alabama and Mississippi. Transactions - Gulf Coast Association of Geological Societies 36, 161-169.

Hoffman, P.F., 1989. Precambrian geology and tectonic history of North America. Geol. Soc. Am., Boulder, CO, Boulder, CO, United States (USA).

Hughes, S.B., Meylan, M.A., 1988. Petrology and hydrocarbon reservoir potential of Mississippian (Chesterian) sandstones, Black Warrior Basin, Mississippi. Transactions - Gulf Coast Association of Geological Societies 38, 167-176.

Ingersoll, R.V., Fullard, T.F., Ford, R.L., Grimm, J.P., Pickle, J.D., Sares, S.W., 1984. The effect of grain size on detrital modes; a test of the Gazzi-Dickinson point-counting method. Journal of Sedimentary Petrology 54, 103-116.

Karabinos, P., Samson, S.D., Hepburn, J.C., Stoll, H.M., 1998. Taconian Orogeny in the New England Appalachians; collision between Laurentia and the Shelburne Falls Arc. Geology (Boulder) 26, 215-218.

Kidd, C., 2008. Subsurface characterization and sequence stratigraphy of late Mississippian strata in the Black Warrior Basin, Alabama and Mississippi. University of Kentucky Master's Theses. Paper 561

Konstantinou, A., Wirth, K.R., Vervoort, J.D., Malone, D.H., Davidson, C., Craddock, J.P., 2014. Provenance of quartz arenites of the early Paleozoic Midcontinent region, USA. Journal of Geology 122, 201-216.

Kugler, R.L., Pashin, J.C., 1992. Reservoir heterogeneity in Carter Sandstone, North Blowhorn Creek oil unit and vicinity, Black Warrior Basin, Alabama, United States (USA).

Lowe, D.R., 1985. Ouachita trough: Part of a Cambrian failed rift system, Geology 13, 790-793.

Ludwig, K.R., 2008. Isoplot 3.60. Berkeley Geochronology Center. Special Publication 4, 77 p.

Mack, G.H., 1984. Exceptions to the relationship between plate tectonics and sandstone composition. Journal of Sedimentary Petrology 54, 212-220.

Mack, G.H., James, W.C., Thomas, W.A., 1981. Orogenic provenance of Mississippian sandstones associated with Southern Appalachian-Ouachita Orogen. AAPG Bulletin 65, 1444-1456.

Mack, G.H., Thomas, W.A., Horsey, C.A., 1983. Composition of Carboniferous sandstones and tectonic framework of southern Appalachian-Ouachita orogen. Journal of Sedimentary Petrology 53, 931-946.

McBride, E.F., 1987. Diagenesis of the Maxon Sandstone (Early Cretaceous), Marathon region, Texas; a diagenetic quartzarenite. Journal of Sedimentary Petrology 57, 98-107.

McClellan, E.A., Miller, C.F., 2000. Ordovician age confirmed for the Hillabee Greenstone, Talladega Belt, southernmost Appalachians. Abstracts with Programs - Geological Society of America 32, 61.

McLennan, S.M., Bock, B., Compston, W., Hemming, S.R., McDaniel, D.K., 2001. Detrital zircon geochronology of Taconian and Acadian foreland sedimentary rocks in New England. Journal of Sedimentary Research 71, 305-317.

Mellen, F.F., 1947. Black Warrior Basin, Alabama and Mississippi. Bulletin of the American Association of Petroleum Geologists 31, 1801-1816.

Meyers, S.R., Peters, S.E., 2011. A 56 million year rhythm in North American sedimentation during the Phanerozoic. Earth and Planetary Science Letters 303, 174-180.

Miller, C.F., Hatcher, R.D., Jr., Ayers, J.C., Coath, C.D., Harrison, T.M., 2000. Age and zircon inheritance of eastern Blue Ridge plutons, southwestern North Carolina and northeastern Georgia, with implications for magma history and evolution of the Southern Appalachian Orogen. American Journal of Science 300, 142-172.

Milliken, K.L., 1988. Loss of provenance information through subsurface diagenesis in Plio-Pleistocene sandstones, northern Gulf of Mexico. Journal of Sedimentary Petrology 58, 992-1002.

Moores, E.M., 1991. Southwest U.S.-East Antarctic (SWEAT) connection; a hypothesis. Geology (Boulder) 19, 425-428.

Mueller, P.A., Heatherington, A.L., Wooden, J.L., Shuster, R.D., Nutman, A.P., Williams, I.S., 1994. Precambrian zircons from the Florida basement; a Gondwanan connection. Geology (Boulder) 22, 119-122.

Murphy, J.B., Pisarevsky, S.A., Nance, R.D., Keppie, J.D., 2003. Neoproterozoic-early Paleozoic evolution of peri-Gondwanan terranes and implications for Laurentia-Gondwana connections. Abstracts with Programs - Geological Society of America 35, 17.

Nance, R.D., Thompson, M.D., 1996. Avalonian and related peri-Gondwanan terranes of the Circum-North Atlantic; an introduction. Special Paper - Geological Society of America 304, 1-7.

Nix, M.A., Facies and facies relationships of the lower part of the Parkwood Formation in the Black Warrior Basin of Mississippi and Alabama.

Opdyke, N.D., Jones, D.S., MacFadden, B.J., Smith, D.L., Mueller, P.A., Shuster, R.D., 1987. Florida as an exotic terrane; paleomagnetic and geochronologic investigation of lower Paleozoic rocks from the subsurface of Florida. Geology (Boulder) 15, 900-903.

Osberg, P.H., Tull, J.F., Robinson, P., Hon, R., Butler, J.R., 1989. The Acadian Orogen. Geol. Soc. Am., Boulder, CO, Boulder, CO, United States (USA).

Ostrom, M.E., 1970. Sedimentation cycles in the lower paleozoic rocks of western wisconsin. Information Circular - Wisconsin, Geological and Natural History Survey, 10-34.

Ostrom, M.E., Odom, I.E., 1978. Stratigraphic relationships of lower Paleozoic rocks of Wisconsin. Field Trip Guide Book (Madison), 3-22.

Pashin, J.C., Rindsberg, A.K., 1993. Tectonic and Paleotopographic control of basal chesterian sedimentation in the Black Warrio Basin of Alabama, Transactions – Gulf Coast Association of Geological Societies 43, 291-304.

Patchett, P.J., Ross, G.M., Gleason, J.D., 1999. Continental drainage in North America during the Phanerozoic from Nd isotopes. Science 283, 671-673.

Plas, L.v.d., Tobi, A.C., 1965. A chart for judging the reliability of point counting results. American Journal of Science 263, 87-90.

Press, W.H., Teukolsky, S.A., Vetterling, W.T., Flannery, B.P., 2007. Numerical recipes; the art of scientific computing. Cambridge University Press, New York, NY, New York, NY, United States (USA), 1235 pp.

Runkel, A.C., 1992. Deposition of the Upper Cambrian Jordan Sandstone, Upper Mississippi Valley region. Abstracts with Programs - Geological Society of America 24, 350.

Runkel, A.C., 1994. Deposition of the Uppermost Cambrian (Croixan) Jordan Sandstone, and the nature of the Cambrian-Ordovician boundary in the Upper Mississippi Valley. Geological Society of America Bulletin 106, 492-506.

Runkel, A.C., Miller, J.F., McKay, R.M., Palmer, A.R., Taylor, J.F., 2007. High-resolution sequence stratigraphy of lower Paleozoic sheet sandstones in central North America; the role of special conditions of cratonic interiors in development of stratal architecture. Geological Society of America Bulletin 119, 860-881.

Runkel, A.C., Tipping, R.G., Miller, J.F., 1998. Field trip #4; Stratigraphy and hydrogeology of Paleozoic rocks of southeastern Minnesota. Proceedings and Abstracts - Institute on Lake Superior Geology.Meeting 44, Part 2, 103-130.

Sevigny, J.H., Hanson, G.N., 1993. Orogenic evolution of the New England Appalachians of southwestern Connecticut; with Suppl. Data 9330. Geological Society of America Bulletin 105, 1591-1605.

Shaw, H.F., Wasserburg, G.J., 1984. Isotopic constraints on the origin of Appalachian mafic complexes. American Journal of Science 284, 319-349.

Shaw, T.H., Schreiber, B.C., 1991. Lithostratigraphy and depositional environments of the Ancell Group in central Illinois; a Middle Ordovician carbonate-siliciclastic transition. SEPM Core Workshop 15, 309-351.

Shepard, B.K., Petrography and environments of deposition of the Carter Sandstone (Mississippian) in the Black Warrior Basin of Alabama and Mississippi.

Sinha, A.K., Hanan, B.B., Wayne, D.M., 1997. Igneous and metamorphic U-Pb zircon ages from the Baltimore mafic complex, Maryland Piedmont. Memoir - Geological Society of America 191, 275-286.

Sloss, L.L., 1963. Sequences in the cratonic interior of North America. Geological Society of America Bulletin 74, 93-113.

Soreghan, G.S., Soreghan, M.J., 2013. Tracing clastic delivery to the Permian Delaware Basin, U.S.A.; implications for paleogeography and circulation in westernmost equatorial Pangea. Journal of Sedimentary Research 83, 786-802.

Spell, T.L., Norrell, G.T., 1990. The Ropes Creek assemblage; petrology, geochemistry, and tectonic setting of an ophiolitic thrust sheet in the Southern Appalachians. American Journal of Science 290, 811-842.

Stacey, J.S., Kramers, J.D., 1975. Approximation of terrestrial lead isotope evolution by a two-stage model. Earth and Planetary Science Letters 26, 207-221.

Stapor, F.W., Cleaves, A.W., 1992. Mississippian (Chesterian) sequence stratigraphy in the Black Warrior Basin; Pride Mountain Formatoin (lowstand wedge) and Hartselle Sandstone (transgressive systems tract). AAPG Bulletin 76.9, 683-695.

Swann, D.H., 1964. Late Mississippian rhythmic sediments of Mississippi Valley. Bulletin of the American Association of Petroleum Geologists 48, 637-658.

Thiel, G.A., 1935. Sedimentary and petrographic analysis of the Saint Peter sandstone. Geological Society of America Bulletin 46, 559-614.

Thomas, W.A., 1972. Regional Paleozoic Stratigraphy in Mississippi Between Ouachita and Appalachian Mountains. The American Association of Petroleum Geologists Bulletin 56, 81-106.

Thomas, W.A., 1974. Converging clastic wedges in the Mississippian of Alabama. Special Paper - Geological Society of America, 187-207.

Thomas, W.A., 1976. Evolution of Ouachita-Appalachian continental margin. Journal of Geology 84, 323-342.

Thomas, W.A., 1977. Evolution of Appalachian-Ouachita salients and recesses from reentrants and promontories in the continental margin. American Journal of Science 277, 1233-1278.

Thomas, W.A., 1985. The Appalachian-Ouachita connection; Paleozoic orogenic belt at the southern margin of North America. Annual Review of Earth and Planetary Sciences 13, 175-199.

Thomas, W.A., 1988. The Black Warrior Basin. Geol. Soc. Am., Denver, CO, Denver, CO, United States (USA).

Thomas, W.A., 1989. The Appalachian-Ouachita Orogen beneath the Gulf Coastal Plain between the outcrops in the Appalachian and Ouachita Mountains. Geol. Soc. Am., Boulder, CO, Boulder, CO, United States (USA).

Thomas, W.A., 1991. The Appalachian-Ouachita rifted margin of southeastern North America. Geological Society of America Bulletin 103, 415-431.

Thomas, W.A., 1995. Diachronous thrust loading and fault partitioning of the Black Warrior foreland basin within the Alabama recess of the late Paleozoic Appalachian-Ouachita thrust belt. Special Publication - Society for Sedimentary Geology 52, 111-126.

Thomas, W.A., 2004. Genetic relationship of rift-stage crustal structure, terrane accretion, and foreland tectonics along the Southern Appalachian-Ouachita Orogen. Journal of Geodynamics 37, 549-563.

Thomas, W.A., 2010. Interactions between the Southern Appalachian-Ouachita orogenic belt and basement faults in the orogenic footwall and foreland. Memoir - Geological Society of America 206, 897-916.

Thomas, W.A., 2011. Detrital-zircon geochronology and sedimentary provenance. Lithosphere 3, 304-308.

Thomas, W.A., Gleason, J.D., Patchett, P.J., Dickinson, W.R., Ruiz, J., 1995. Nd isotopes link Ouachita turbidites to Appalachian sources; discussion and reply. Geology (Boulder) 23, 93-95.

Thomas, W.A., Gleason, J.D., Patchett, P.J., Dickinson, W.R., Ruiz, J., 1997. Nd isotopic constraints on sediment sources of the Ouachita-Marathon fold belt; alternative interpretation and reply. Geological Society of America Bulletin 109, 779-787.

Thomas, W.A., Mack, G.H., 1980. Barrier-island and shelf-bar sedimentation, Mississippian Hartselle Sandstone, northern Alabama. Geol. Soc. Am., Southeast. Sect., United States (USA).

Thomas, W.A., Mack, G.H., 1982. Paleogeographic relationship of a Mississippian barrier-island and shelf-bar system (Hartselle Sandstone) in Alabama to the Appalachian-Ouachita orogenic belt. Geological Society of America Bulletin 93, 6-19.

Tucker, R.D., Robinson, P., 1990. Age and setting of the Bronson Hill magmatic arc; a re-evaluation based on U-Pb zircon ages in southern New England. Geological Society of America Bulletin 102, 1404-1419.

Van Schmus, W.R., Bickford, M.E., Turek, A., 1996. Proterozoic geology of the east-central Midcontinent basement. Special Paper - Geological Society of America 308, 7-32.

Viele, G.W., Thomas, W.A., 1989. Tectonic synthesis of the Ouachita orogenic belt. Geol. Soc. Am., Boulder, CO, Boulder, CO, United States (USA).

Welch, S.W., 1978. Mississippian rocks of the Black Warrior Basin. Miss. Geol. Soc., Jackson, MS, Jackson, MS, United States (USA), 79 pp.

Weber, B., Schaaf, P., Valencia, V.A., Iriondo, A., Ortega-Gutierrez, F., 2006. Provenance ages of late Paleozoic sandstones (Santa Rosa Formation) from the Maya Block, SE Mexico: implications on the tectonic evolution of western Pangea: Revista Mexicana de Ciencias Geologicas 23, 262-276.

Weber, B., Valencia, V.A., Schaaf, P., Pompa-Mera, V., Ruiz, J., 2008, Significance of provenance ages from the Chiapas Massif Complex (southeastern Mexico): redefining the Paleozoic basement of the Maya Block and its evolution in a peri-Gondwanan realm: Journal of Geology 116, 619-639.

Whitmeyer, S.J., Karlstrom, K.E., 2007. Tectonic model for the Proterozoic growth of North America. Geosphere 3, 220-259.

APPENDICES

Appendix I- General information about the conventional core used for thin sections

Well Operator	Lease Name	API #	County	Depth (Feet)	Formation	Thin Section ID
PLACID OIL CO	CALDWELL 28-10 #1	23-087-20048	Lowndes			
				4772.5	Carter	C3
				4782	Carter	C5
				4802.5	Carter	C7
				4804	Carter	C8
				4804.5	Carter	C9
				4807	Carter	C10
				4809	Carter	C11
				4812	Carter	C12
				4813	Carter	C13
				4817	Carter	C14
PRUET & HUGHES CO.	FORD 4-14 #1	23-087-20007	Lowndes			
				5363	Carter	F1
				5368	Carter	F2
				5375	Carter	F3
				5387	Carter	F4
				5404	Carter	F5
PRUET PRODUCTION CO	COLEMAN ETAL 36-5 #1	23-095-20379	Monroe			
				5376	Lewis	L1
				5380	Lewis	L3
				5382	Lewis	L4
				5385	Lewis	L5
				5388	Lewis	L6
				5394	Lewis	L7
PRUET PRODUCTION CO	FIELDS UNIT 35-7 #1	23-095-20206	Monroe			
				5388	Lewis	A1
PRUET & HUGHES CO.	DALRYMPLE UN 21-9 #1	23-095-20063	Monroe	2466	Evans	D1
				2467	Evans	D2
				2468	Evans	D3
				2470	Evans	D4
				2471	Evans	D5
				2472.5	Evans	D6
				2474	Evans	D7
				2476	Evans	D8
				2477	Evans	D9
				2479	Evans	D10

Appendix I (continued)

Well Operator	Lease Name	API #	County	Depth (Feet)	Formation	Thin Section ID
MICHIGAN OIL COMPANY	MALONE 25-1	23-087-20123	Lowndes			
				4945	Sanders	M1
				4948	Sanders	M3
				4951	Sanders	M5
				4955	Sanders	M7
				4956	Sanders	M8
				4957	Sanders	M9
				4959	Sanders	M10
				4960	Sanders	M11
				4962	Sanders	M13
				4978	Sanders	M14
				4980	Sanders	M16
				4982	Sanders	M18
SOHIO PETROLEUM CO	OWEN #1	23-087-20025	Lowndes			
				5432	Sanders	O1
				5437	Sanders	O2
				5451	Sanders	O3

Appendix II- U-Pb Detrital Zircon Geochronology Data

BW1						Isotope ratios						Apparent ages (Ma)							
Analysis	U	206Pb	U/Th	206Pb*	±	207Pb*	±	206Pb*	±	error	206Pb*	±	207Pb*	±	206Pb*	±	Best age	±	Conc
	(ppm)	204Pb		207Pb*	(%)	235U*	(%)	238U	(%)	corr.	238U*	(Ma)	235U	(Ma)	207Pb*	(Ma)	(Ma)	(Ma)	(%)
BW-1-49	118	3646	1.1	20.9380	7.7	0.3934	7.9	0.0597	1.7	0.22	374.0	6.3	336.8	22.7	87.4	183.7	374.0	6.3	NA
BW-1-59	576	22580	0.9	17.6076	1.1	0.4924	1.4	0.0629	0.8	0.59	393.1	3.2	406.6	4.7	483.6	25.3	393.1	3.2	NA
BW-1-42	143	6107	0.9	20.3593	5.2	0.4301	5.5	0.0635	1.7	0.31	396.9	6.6	363.2	16.8	153.5	122.1	396.9	6.6	NA
BW-1-22	258	15754	0.9	18.6673	2.6	0.4766	2.8	0.0645	0.9	0.32	403.1	3.4	395.8	9.0	353.0	59.0	403.1	3.4	114.2
BW-1-75	1324	23288	1.9	17.9384	0.8	0.4976	2.3	0.0647	2.1	0.94	404.4	8.4	410.1	7.7	442.3	17.9	404.4	8.4	91.4
BW-1-25	147	13228	1.4	19.2247	4.7	0.4714	4.9	0.0657	1.3	0.27	410.4	5.3	392.2	15.9	286.1	107.9	410.4	5.3	143.4
BW-1-99	237	10057	1.4	19.1726	3.4	0.4741	3.5	0.0659	0.9	0.25	411.6	3.5	394.0	11.3	292.3	76.7	411.6	3.5	140.8
BW-1-69	162	10274	4.9	18.3526	4.4	0.5063	4.6	0.0674	1.1	0.24	420.4	4.5	416.0	15.5	391.3	99.2	420.4	4.5	107.5
BW-1-73	179	6725	1.0	19.9302	4.3	0.4684	4.5	0.0677	1.2	0.26	422.3	4.8	390.1	14.5	203.1	100.3	422.3	4.8	207.9
BW-1-46	283	7756	0.7	18.1140	3.0	0.5168	3.2	0.0679	1.0	0.32	423.5	4.1	423.0	10.9	420.5	66.8	423.5	4.1	100.7
BW-1-35	275	9591	7.0	19.0743	3.8	0.4961	4.0	0.0686	1.1	0.28	427.9	4.6	409.0	13.4	304.1	87.0	427.9	4.6	140.7
BW-1-27	157	5535	1.0	18.9544	4.8	0.5003	4.9	0.0688	0.9	0.19	428.8	3.9	411.9	16.4	318.4	108.4	428.8	3.9	134.7
BW-1-72	268	11423	1.3	18.5272	2.9	0.5177	3.0	0.0696	0.7	0.24	433.5	3.0	423.6	10.5	370.0	66.3	433.5	3.0	117.2
BW-1-29	302	9508	0.8	17.9080	3.2	0.5369	3.5	0.0697	1.4	0.39	434.5	5.7	436.4	12.5	446.0	72.0	434.5	5.7	97.4
BW-1-1	67	9463	0.9	16.6538	8.9	0.5774	9.3	0.0697	2.7	0.29	434.6	11.3	462.8	34.6	605.2	192.9	434.6	11.3	71.8
BW-1-95	156	8397	0.9	18.7784	4.2	0.5137	4.4	0.0700	1.2	0.26	435.9	4.9	420.9	15.1	339.6	95.9	435.9	4.9	128.4
BW-1-24	319	9933	1.6	18.2897	2.5	0.5287	2.8	0.0701	1.2	0.44	436.9	5.2	430.9	10.0	399.0	57.1	436.9	5.2	109.5
BW-1-56	199	12412	0.5	18.0315	2.8	0.5427	2.9	0.0710	0.9	0.30	442.0	3.8	440.2	10.5	430.7	62.6	442.0	3.8	102.6
BW-1-71	466	15359	1.1	17.7921	1.3	0.5698	1.5	0.0735	0.8	0.51	457.3	3.5	457.9	5.7	460.4	29.3	457.3	3.5	99.3
BW-1-53	253	7875	1.5	18.0399	2.5	0.5712	2.7	0.0747	1.0	0.36	464.6	4.4	458.8	9.9	429.7	55.5	464.6	4.4	108.1
BW-1-86	80	3689	1.1	19.3414	8.9	0.5377	9.0	0.0754	1.7	0.19	468.7	7.9	436.9	32.1	272.3	203.6	468.7	7.9	172.2
BW-1-7	187	8854	1.1	18.6308	3.8	0.5585	3.9	0.0755	0.9	0.24	469.0	4.2	450.5	14.3	357.4	86.5	469.0	4.2	131.2
BW-1-82	339	26962	1.5	17.4758	1.8	0.5954	2.0	0.0755	0.8	0.42	469.0	3.8	474.3	7.7	500.1	40.4	469.0	3.8	93.8
BW-1-19	84	4109	2.0	18.2811	7.9	0.5714	8.1	0.0758	1.8	0.22	470.8	8.1	458.9	30.1	400.0	178.1	470.8	8.1	117.7
BW-1-79	102	11401	0.8	19.3864	5.7	0.5573	5.8	0.0784	1.2	0.21	486.3	5.8	449.8	21.2	267.0	131.0	486.3	5.8	182.2
BW-1-70	379	2715	0.6	16.8290	2.0	0.7133	2.2	0.0871	1.0	0.44	538.1	4.9	546.7	9.2	582.6	42.7	538.1	4.9	92.4
BW-1-90	64	2283	1.0	16.5446	7.6	0.8144	8.0	0.0977	2.5	0.31	601.0	14.3	604.9	36.7	619.4	165.1	601.0	14.3	97.0
BW-1-21	134	10887	0.7	17.4315	4.2	0.7956	4.4	0.1006	1.3	0.30	617.9	7.7	594.4	19.7	505.7	92.2	617.9	7.7	122.2
BW-1-74	276	9695	1.7	15.9712	1.4	0.9985	1.6	0.1157	0.7	0.45	705.5	4.8	703.0	8.1	695.1	30.5	705.5	4.8	101.5
BW-1-2	109	6359	1.8	15.7492	3.2	1.1555	3.4	0.1320	1.0	0.31	799.2	7.8	779.8	18.4	724.8	68.1	799.2	7.8	110.3
BW-1-66	165	18349	1.9	13.8335	1.2	1.6579	1.6	0.1663	1.1	0.67	991.9	9.9	992.6	10.2	994.1	24.3	994.1	24.3	99.8
BW-1-39	164	15795	2.1	13.7170	1.1	1.7577	1.4	0.1749	0.8	0.60	1038.8	8.0	1030.0	9.0	1011.2	22.7	1011.2	22.7	102.7
BW-1-34	65	14442	2.9	13.5763	2.7	1.8081	2.8	0.1780	1.0	0.34	1056.2	9.4	1048.4	18.6	1032.1	54.1	1032.1	54.1	102.3
BW-1-17	72	5665	1.0	13.5551	3.0	1.8617	3.2	0.1830	1.0	0.30	1083.5	9.6	1067.6	21.0	1035.2	61.3	1035.2	61.3	104.7
BW-1-92	279	20313	1.1	13.4545	0.7	1.8697	1.0	0.1825	0.7	0.69	1080.4	6.6	1070.4	6.4	1050.3	14.2	1050.3	14.2	102.9
BW-1-33	214	45541	1.7	13.2484	0.8	1.8568	1.0	0.1784	0.6	0.59	1058.3	5.8	1065.8	6.6	1081.3	16.2	1081.3	16.2	97.9
BW-1-15	394	28961	1.1	13.1501	0.6	1.9248	1.2	0.1836	1.1	0.87	1086.5	10.2	1089.7	7.8	1096.2	11.5	1096.2	11.5	99.1
BW-1-9	145	10366	1.9	13.0004	1.7	2.0413	1.9	0.1925	0.7	0.35	1134.7	6.8	1129.4	12.6	1119.1	34.6	1119.1	34.6	101.4
BW-1-45	279	28123	1.5	12.9516	0.6	2.0072	1.0	0.1885	0.8	0.78	1113.5	8.4	1117.9	7.1	1126.6	12.9	1126.6	12.9	98.8
BW-1-100	356	37414	3.3	12.7277	0.5	2.0468	0.9	0.1889	0.7	0.84	1115.6	7.4	1131.2	5.9	1161.3	9.2	1161.3	9.2	96.1
BW-1-3	294	33035	3.1	12.7207	0.5	2.0954	0.9	0.1933	0.7	0.77	1139.3	7.0	1147.3	6.0	1162.4	10.9	1162.4	10.9	98.0
BW-1-18	310	23201	2.5	12.4541	0.6	2.0903	0.9	0.1888	0.6	0.73	1114.9	6.3	1145.6	5.8	1204.2	11.5	1204.2	11.5	92.6
BW-1-58	126	8634	2.3	12.2793	1.6	2.3204	1.7	0.2067	0.7	0.40	1211.0	7.5	1218.6	12.1	1232.1	30.5	1232.1	30.5	98.3
BW-1-98	149	12460	1.4	12.0802	1.2	2.3798	1.7	0.2085	1.1	0.69	1220.9	12.7	1236.6	11.9	1264.1	23.6	1264.1	23.6	96.6
BW-1-36	106	8043	2.0	11.7951	1.4	2.4209	1.7	0.2071	0.9	0.51	1213.4	9.6	1248.8	12.1	1310.5	28.0	1310.5	28.0	92.6
BW-1-89	126	25082	2.3	11.5603	0.8	2.7724	1.2	0.2324	0.8	0.70	1347.3	9.9	1348.1	8.7	1349.4	16.1	1349.4	16.1	99.8
BW-1-20	239	24096	1.6	11.3682	0.5	2.8453	0.9	0.2346	0.8	0.85	1358.6	9.7	1367.6	7.0	1381.7	9.6	1381.7	9.6	98.3
BW-1-51	92	16244	1.6	11.3015	1.6	2.9833	3.1	0.2445	2.6	0.85	1410.2	33.1	1403.4	23.4	1393.0	31.2	1393.0	31.2	101.2
BW-1-96	327	33174	2.5	11.2753	0.4	2.9291	0.8	0.2395	0.7	0.86	1384.3	9.1	1389.5	6.4	1397.4	8.3	1397.4	8.3	99.1
BW-1-83	106	5880	0.9	11.1568	1.6	3.0830	1.8	0.2495	0.9	0.51	1435.7	12.0	1428.5	14.1	1417.7	30.4	1417.7	30.4	101.3
BW-1-97	251	41146	2.1	10.8663	0.4	3.2404	0.7	0.2554	0.6	0.82	1466.1	7.7	1466.9	5.5	1467.9	7.7	1467.9	7.7	99.9
BW-1-57	122	12042	2.0	10.6807	1.1	3.4583	1.1	0.2679	0.7	0.68	1530.1	10.0	1517.8	8.5	1500.6	15.0	1500.6	15.0	102.0
BW-1-14	166	22474	2.3	10.5970	0.7	3.4030	1.0	0.2615	0.8	0.73	1497.7	10.0	1505.1	8.0	1515.4	13.1	1515.4	13.1	98.8
BW-1-44	227	22708	1.8	10.5741	0.6	3.3775	1.0	0.2590	0.9	0.83	1484.9	11.3	1499.2	8.1	1519.5	10.9	1519.5	10.9	97.7
BW-1-60	170	21287	1.8	10.3669	0.7	3.6321	1.2	0.2731	1.0	0.83	1556.5	13.5	1556.6	9.4	1556.7	12.3	1556.7	12.3	100.0
BW-1-55	197	24012	2.8	9.9674	0.5	3.8564	0.9	0.2788	0.7	0.82	1585.2	10.4	1604.6	7.3	1630.1	9.7	1630.1	9.7	97.2
BW-1-93	184	29396	5.4	9.8209	0.4	4.0310	1.0	0.2871	0.9	0.90	1627.1	12.3	1640.5	7.8	1657.6	7.8	1657.6	7.8	98.2
BW-1-12	173	14778	3.1	9.8073	0.8	3.8318	1.8	0.2726	1.6	0.89	1553.8	21.9	1599.5	14.3	1660.2	14.9	1660.2	14.9	93.6
BW-1-78	216	37006	9.5	9.7908	0.5	4.0836	0.8	0.2900	0.7	0.83	1641.4	10.1	1651.0	6.8	1663.3	8.5	1663.3	8.5	98.7
BW-1-38	106	11829	1.0	9.7483	0.9	4.2015	1.4	0.2971	1.1	0.76	1676.7	15.8	1674.3	11.6	1671.3	17.0	1671.3	17.0	100.3
BW-1-88	428	55762	1.1	9.7419	0.7	3.9892	0.7	0.2819	0.2	0.96	1600.7	10.0	1632.0	6.0	1672.5	3.9	1672.5	3.9	95.7
BW-1-62	155	28318	0.8	9.7181	0.6	4.1481	1.4	0.2924	1.2	0.89	1653.4	17.8	1663.8	11.2	1677.1	11.6	1677.1	11.6	98.6
BW-1-40	112	12273	1.3	9.5581	0.9	4.2847	1.3	0.2970	0.9	0.68	1676.5	12.8	1690.4	10.5	1707.7	17.3	1707.7	17.3	98.2
BW-1-11	40	5767	1.1	9.5222	1.9	4.3733	2.2	0.3020	1.2	0.52	1701.3	17.2	1707.3	18.5	1714.6	35.3	1714.6	35.3	99.2
BW-1-85	217	25168	1.8	8.9761	0.3	4.8898	0.7	0.3183	0.6	0.85	1781.6	8.6	1800.5	5.5	1822.5	6.3	1822.5	6.3	97.8
BW-1-47	83	15148	0.9	8.6917	0.9	5.4460	1.4	0.3433	1.0	0.74	1902.6	17.0	1892.1	11.9	1880.7	16.7	1880.7	16.7	101.2
BW-1-28	87	14257	2.7	8.6326	0.7	5.6012	1.5	0.3507	1.4	0.89	1937.9	23.0	1916.3	13.3	1893.0	12.7	1893.0	12.7	102.4
BW-1-13	23	4007	1.9	7.8419	2.4	6.5918	2.7	0.3749	1.4	0.50	2052.4	23.9	2058.2	24.2	2064.1	41.9	2064.1	41.9	99.4

BW2					Isotope ratios						Apparent ages (Ma)						Best age	±	Conc
Analysis	U	206Pb	U/Th	206Pb*	±	207Pb*	±	206Pb*	±	error	206Pb*	±	207Pb*	±	206Pb*	±			
	(ppm)	204Pb		207Pb*	(%)	235U*	(%)	238U	(%)	corr.	238U*	(Ma)	235U	(Ma)	207Pb*	(Ma)	(Ma)	(Ma)	(%)
BW-2-49	117	5833	1.1	20.2218	7.0	0.4079	7.3	0.0598	1.7	0.24	374.6	6.3	347.4	21.3	169.3	164.7	374.6	6.3	NA
BW-2-59	573	36128	0.9	17.4540	1.0	0.4968	1.3	0.0629	0.8	0.63	393.2	3.2	409.5	4.5	502.8	22.6	393.2	3.2	NA
BW-2-42	142	9771	0.9	19.9232	4.9	0.4398	5.2	0.0636	1.7	0.33	397.2	6.6	370.1	16.1	203.9	113.5	397.2	6.6	NA
BW-2-22	257	25206	0.9	18.4733	2.5	0.4817	2.7	0.0645	0.9	0.33	403.2	3.5	399.2	8.8	376.5	56.6	403.2	3.5	107.1
BW-2-75	1316	37261	1.9	17.7865	0.7	0.5018	2.3	0.0647	2.1	0.95	404.4	8.4	412.9	7.7	461.1	16.2	404.4	8.4	87.7
BW-2-25	146	21165	1.4	18.9965	4.6	0.4772	4.8	0.0657	1.3	0.28	410.4	5.3	396.1	15.7	313.4	105.1	410.4	5.3	131.0
BW-2-99	235	16091	1.4	18.9218	3.1	0.4809	3.2	0.0660	0.9	0.27	412.0	3.5	398.7	10.7	322.3	70.9	412.0	3.5	127.8
BW-2-91	52	2863	1.1	19.7063	9.9	0.4686	10.3	0.0670	3.0	0.29	417.9	12.1	390.2	33.5	229.3	229.1	417.9	12.1	182.3
BW-2-4	41	1175	1.0	20.2772	18.8	0.4571	19.3	0.0672	4.1	0.21	419.4	16.6	382.2	61.4	162.9	443.4	419.4	16.6	257.5
BW-2-69	161	16438	4.9	18.0866	4.3	0.5140	4.4	0.0674	1.1	0.25	420.6	4.5	421.1	15.3	423.9	95.7	420.6	4.5	99.2
BW-2-73	178	10759	1.0	19.5228	4.0	0.4786	4.1	0.0678	1.2	0.28	422.6	4.8	397.1	13.6	250.8	91.4	422.6	4.8	168.5
BW-2-46	281	12410	0.7	17.8255	2.5	0.5255	2.7	0.0679	1.0	0.37	423.7	4.1	428.8	9.6	456.3	56.4	423.7	4.1	92.9
BW-2-35	273	15345	7.0	18.8120	3.7	0.5031	3.8	0.0686	1.1	0.29	428.0	4.6	413.8	13.0	335.5	83.1	428.0	4.6	127.6
BW-2-27	156	8856	1.0	18.5300	4.2	0.5122	4.3	0.0688	0.9	0.22	429.2	3.9	420.0	14.8	369.6	94.3	429.2	3.9	116.1
BW-2-72	266	18278	1.3	18.2749	2.8	0.5250	2.9	0.0696	0.7	0.24	433.7	3.0	428.5	10.2	400.8	63.3	433.7	3.0	108.2
BW-2-29	300	15213	0.8	17.6605	3.0	0.5446	3.3	0.0698	1.4	0.41	434.7	5.7	441.4	11.9	476.9	67.0	434.7	5.7	91.1
BW-2-1	67	15140	0.9	16.4502	8.8	0.5847	9.2	0.0698	2.7	0.29	434.7	11.3	467.5	34.5	631.8	189.9	434.7	11.3	68.8
BW-2-95	155	13436	0.9	18.5148	4.0	0.5213	4.2	0.0700	1.1	0.28	436.2	4.9	426.0	14.5	371.5	90.1	436.2	4.9	117.4
BW-2-24	318	15893	1.6	18.0350	2.3	0.5364	2.6	0.0702	1.2	0.47	437.1	5.2	436.0	9.3	430.3	51.7	437.1	5.2	101.6
BW-2-84	91	1723	1.9	19.6287	11.5	0.4929	11.6	0.0702	1.7	0.14	437.2	7.1	406.9	39.0	238.4	266.1	437.2	7.1	183.4
BW-2-56	198	19859	0.5	17.8090	2.7	0.5497	2.8	0.0710	0.9	0.32	442.2	3.8	444.8	10.1	458.4	59.2	442.2	3.8	96.5
BW-2-71	463	24575	1.1	17.5946	1.2	0.5763	1.4	0.0735	0.8	0.54	457.4	3.5	462.0	5.4	485.1	26.7	457.4	3.5	94.3
BW-2-53	252	12600	1.5	17.7510	2.2	0.5808	2.4	0.0748	1.0	0.40	464.9	4.4	465.0	9.0	465.6	49.0	464.9	4.4	99.8
BW-2-82	337	43140	1.5	17.3555	1.8	0.5994	2.0	0.0755	0.8	0.43	468.9	3.8	476.9	7.5	515.3	39.4	468.9	3.8	91.0
BW-2-7	186	14167	1.1	18.3501	3.6	0.5672	3.8	0.0755	0.9	0.25	469.2	4.2	456.2	13.8	391.6	81.8	469.2	4.2	119.8
BW-2-86	80	5903	1.1	18.7423	8.1	0.5557	8.3	0.0755	1.7	0.21	469.4	7.9	448.7	30.0	343.9	183.1	469.4	7.9	136.5
BW-2-19	83	6575	2.0	17.7737	7.5	0.5885	7.7	0.0759	1.8	0.23	471.4	8.1	469.9	29.1	462.8	167.3	471.4	8.1	101.9
BW-2-87	83	6095	0.9	19.6125	6.1	0.5474	6.3	0.0779	1.5	0.24	483.3	7.0	443.3	22.7	240.3	141.6	483.3	7.0	201.1
BW-2-79	102	18242	0.8	19.1412	5.6	0.5646	5.7	0.0784	1.2	0.22	486.5	5.8	454.5	20.9	296.1	127.2	486.5	5.8	164.3
BW-2-70	377	4344	0.6	16.1978	1.5	0.7427	1.8	0.0872	1.0	0.54	539.2	4.9	564.0	7.7	665.0	32.1	539.2	4.9	81.1
BW-2-90	64	3653	1.0	15.8690	6.8	0.8512	7.3	0.0980	2.5	0.34	602.5	14.4	625.3	33.9	708.8	145.3	602.5	14.4	85.0
BW-2-21	133	17419	0.7	17.2120	4.1	0.8061	4.3	0.1006	1.3	0.30	618.1	7.7	600.2	19.5	533.5	89.9	618.1	7.7	115.8
BW-2-41	91	1431	0.9	17.9281	5.8	0.7805	5.9	0.1015	1.4	0.23	623.1	8.1	585.7	26.5	443.5	128.7	623.1	8.1	140.5
BW-2-74	274	15512	1.7	15.7616	1.2	1.0122	1.4	0.1157	0.7	0.51	705.8	4.8	710.0	7.1	723.2	25.4	705.8	4.8	97.6
BW-2-2	108	10175	1.8	15.4968	3.0	1.1750	3.2	0.1321	0.6	0.32	799.6	7.8	789.0	17.5	759.0	63.6	799.6	7.8	105.4
BW-2-80	131	4805	0.9	13.8762	2.7	1.7343	2.8	0.1745	0.7	0.26	1037.1	6.9	1021.3	18.0	987.8	55.1	987.8	55.1	105.0
BW-2-66	164	29358	1.9	13.7240	1.1	1.6712	1.5	0.1663	1.1	0.70	991.9	9.9	997.6	9.8	1010.2	22.5	1010.2	22.5	98.2
BW-2-65	179	36172	2.6	13.7131	1.2	1.7827	1.4	0.1773	0.9	0.59	1052.2	8.3	1039.2	9.4	1011.8	23.5	1011.8	23.5	104.0
BW-2-39	163	25272	2.1	13.6079	1.1	1.7719	1.3	0.1749	0.8	0.62	1038.9	8.0	1035.2	8.7	1027.4	21.4	1027.4	21.4	101.1
BW-2-34	65	23107	2.9	13.4688	2.6	1.8226	2.8	0.1780	1.0	0.35	1056.3	9.4	1053.6	18.2	1048.2	52.5	1048.2	52.5	100.8
BW-2-92	278	32501	1.1	13.3838	0.6	1.8792	0.9	0.1824	0.7	0.76	1080.2	6.6	1073.8	5.8	1060.9	11.6	1060.9	11.6	101.8
BW-2-17	72	9064	1.0	13.3344	2.5	1.8940	2.7	0.1832	1.0	0.36	1084.3	9.6	1079.0	17.8	1068.4	50.2	1068.4	50.2	101.5
BW-2-33	213	72866	1.7	13.1886	0.8	1.8648	1.0	0.1784	0.6	0.60	1058.1	5.8	1068.7	6.5	1090.4	15.8	1090.4	15.8	97.0
BW-2-15	391	46338	1.1	13.0710	0.5	1.9362	1.1	0.1836	1.0	0.89	1086.4	10.2	1093.7	7.6	1108.3	10.2	1108.3	10.2	98.0
BW-2-45	277	44997	1.5	12.8782	0.6	2.0184	1.0	0.1885	0.8	0.81	1113.4	8.4	1121.7	6.9	1138.0	12.0	1138.0	12.0	97.8
BW-2-9	144	16585	1.9	12.8680	1.5	2.0629	1.6	0.1925	0.7	0.39	1135.0	6.8	1136.6	11.3	1139.5	30.1	1139.5	30.1	99.6
BW-2-61	97	23675	2.1	12.7792	1.9	2.1983	2.0	0.2037	0.6	0.32	1195.4	7.0	1180.5	13.7	1153.3	36.9	1153.3	36.9	103.7
BW-2-100	354	59863	3.3	12.6707	0.4	2.0571	0.8	0.1890	0.7	0.85	1116.2	7.4	1134.7	5.8	1170.2	8.8	1170.2	8.8	95.4
BW-2-3	292	52857	3.1	12.6577	0.5	2.1055	0.8	0.1933	0.7	0.80	1139.2	7.0	1150.6	5.8	1172.2	10.1	1172.2	10.1	97.2
BW-2-18	308	37121	2.5	12.3710	0.5	2.1043	0.8	0.1888	0.6	0.76	1114.9	6.3	1150.2	5.6	1217.4	10.3	1217.4	10.3	91.6
BW-2-76	53	13841	1.6	12.2996	2.7	2.4602	2.9	0.2195	1.1	0.37	1279.1	12.3	1260.4	20.7	1228.8	52.2	1228.8	52.2	104.1
BW-2-94	18	3477	1.8	12.2134	8.8	2.4875	9.1	0.2203	2.4	0.26	1283.7	27.8	1268.4	65.9	1242.6	172.0	1242.6	172.0	103.3
BW-2-58	125	13814	2.3	12.1342	1.2	2.3493	1.4	0.2068	0.7	0.48	1211.5	7.5	1227.3	10.0	1255.3	24.0	1255.3	24.0	96.5
BW-2-98	148	19936	1.4	11.9963	1.0	2.3973	1.5	0.2086	1.1	0.75	1221.2	12.7	1241.8	10.9	1277.6	19.8	1277.6	19.8	95.6
BW-2-36	105	12869	2.1	11.6701	1.3	2.4479	1.5	0.2072	0.8	0.56	1213.8	9.6	1256.8	11.1	1331.2	24.7	1331.2	24.7	91.2
BW-2-89	126	40131	2.3	11.5027	1.1	2.7859	1.1	0.2324	0.8	0.71	1347.1	9.9	1351.8	8.6	1359.1	15.5	1359.1	15.5	99.1
BW-2-20	238	38554	1.6	11.2954	0.4	2.8636	0.9	0.2346	0.8	0.87	1358.5	9.7	1372.4	6.8	1394.0	8.5	1394.0	8.5	97.5
BW-2-96	325	53078	2.5	11.2346	0.4	2.9397	0.8	0.2395	0.7	0.88	1384.3	9.1	1392.2	6.3	1404.4	7.6	1404.4	7.6	98.6
BW-2-51	92	25990	1.6	11.2246	1.4	3.0039	3.1	0.2445	2.6	0.86	1410.3	33.1	1408.6	23.3	1406.1	30.3	1406.1	30.3	100.3
BW-2-83	106	9409	0.9	11.0077	1.3	3.1269	1.6	0.2496	0.9	0.59	1436.6	12.0	1439.3	12.1	1443.4	24.3	1443.4	24.3	99.5
BW-2-97	250	65833	2.1	10.8315	0.4	3.2507	0.7	0.2554	0.6	0.84	1466.1	7.7	1469.4	5.4	1474.0	7.2	1474.0	7.2	99.5
BW-2-57	121	19268	2.0	10.5843	0.7	3.4907	1.0	0.2680	0.7	0.72	1530.4	10.0	1525.1	8.1	1517.7	13.5	1517.7	13.5	100.8
BW-2-14	165	35959	2.1	10.5329	0.7	3.4236	1.0	0.2615	0.7	0.75	1497.7	10.0	1509.8	7.9	1526.9	12.4	1526.9	12.4	98.1
BW-2-44	225	36332	1.8	10.5145	1.0	3.3964	1.0	0.2590	0.9	0.86	1484.8	11.3	1503.6	7.8	1530.2	9.7	1530.2	9.7	97.0
BW-2-60	169	34059	1.8	10.2944	0.6	3.6578	1.2	0.2731	1.0	0.84	1556.5	13.5	1562.2	9.2	1569.9	11.6	1569.9	11.6	99.1
BW-2-55	196	38420	2.8	9.9019	0.5	3.8819	0.9	0.2788	0.7	0.85	1585.2	10.4	1609.9	7.1	1642.4	8.7	1642.4	8.7	96.5
BW-2-93	182	47034	5.4	9.7785	0.4	4.0487	0.9	0.2871	0.9	0.91	1627.2	12.3	1644.0	7.7	1665.6	7.3	1665.6	7.3	97.7
BW-2-78	214	59210	9.5	9.7431	0.7	4.1029	0.8	0.2899	0.7	0.81	1641.2	10.0	1654.9	6.7	1672.3	8.0	1672.3	8.0	98.1
BW-2-12	172	23645	3.1	9.7329	0.7	3.8615	1.7	0.2726	1.6	0.91	1553.9	21.9	1605.7	14.1	1674.3	13.6	1674.3	13.6	92.8
BW-2-88	426	89220	1.1	9.7068	0.2	4.0026	0.7	0.2818	0.7	0.96	1600.3	10.0	1634.7	6.0	1679.2	3.7	1679.2	3.7	95.3
BW-2-38	106	18927	1.0	9.6741	0.8	4.2344	1.4	0.2971	1.2	0.79	1676.9	15.8	1680.7	11.2	1685.5	15.6	1685.5	15.6	99.5
BW-2-62	154	45309	0.8	9.6574	0.6	4.1740	1.4	0.2924	1.2	0.90	1653.3	17.8	1668.9	11.2	1688.6	11.2	1688.6	11.2	97.9
BW-2-40	111	19636	1.3	9.4883	0.9	4.3168	1.2	0.2971	0.9	0.71	1676.7	12.8	1696.6	10.0	1721.2	15.7	1721.2	15.7	97.4
BW-2-11	39	9228	1.1	9.4083	1.7	4.4294	2.1	0.3022	1.2	0.56	1702.4	17.3	1717.8	17.0	1736.7	31.2	1736.7	31.2	98.0
BW-2-85	216	40269	1.8	8.9355	0.3	4.9113	0.6	0.3183	0.6	0.88	1781.3	8.6	1804.2	5.3	1830.7	5.5	1830.7	5.5	97.3
BW-2-47	83	24237	0.9	8.6385	0.9	5.4797	1.3	0.3433	1.0	0.77	1902.6	17.0	1897.4	11.5	1891.7	15.4	1891.7	15.4	100.6
BW-2-28	86	22812	2.7	8.5732	0.6	5.6403	1.5	0.3507	1.4	0.90	1937.9	23.0	1922.3	13.1	1905.4	11.7	1905.4	11.7	101.7
BW-2-13	23	6411	1.9	7.7366	2.2	6.6889	2.6	0.3753	1.4	0.53	2054.4	24.0	2071.2	22.9	2087.9	38.7	2087.9	38.7	98.4

84

BW3						Isotope ratios						Apparent ages (Ma)							
Analysis	U	206Pb/204Pb	U/Th	206Pb*/207Pb*	±	207Pb*/235U*	±	206Pb*/238U	±	error corr.	206Pb*/238U*	±	207Pb*/235U	±	206Pb*/207Pb*	±	Best age	±	Conc
	(ppm)				(%)		(%)		(%)		(Ma)	(Ma)	(Ma)	(Ma)	(Ma)	(Ma)	(Ma)	(Ma)	(%)
bw3 0-100 30um-74	704	457	1.3	17.9028	7.9	0.3744	8.6	0.0486	3.4	0.39	306.0	10.2	322.9	23.8	446.7	176.3	306.0	10.2	NA
bw3 0-100 30um-13	458	609	1.2	19.9064	9.6	0.3371	10.1	0.0487	3.1	0.31	306.3	9.4	294.9	25.8	205.9	223.1	306.3	9.4	NA
bw3 0-100 30um-30	313	1054	1.0	15.8178	8.2	0.5117	8.8	0.0587	3.1	0.37	367.7	11.5	419.6	30.3	715.6	174.3	367.7	11.5	NA
bw3 101-200 30um-76	243	4860	0.9	19.2247	3.7	0.4325	3.8	0.0603	0.9	0.24	377.5	3.3	365.0	11.8	286.1	85.6	377.5	3.3	NA
bw3 0-100 30um-34	158	9437	1.5	19.8747	5.2	0.4196	5.3	0.0605	1.0	0.19	378.5	3.7	355.7	15.9	209.6	120.7	378.5	3.7	NA
bw3 101-200 30um-24	100	3774	0.7	18.7494	6.6	0.4677	6.7	0.0636	1.1	0.17	397.5	4.4	389.6	21.7	343.1	149.9	397.5	4.4	NA
bw3 0-100 30um-58	73	4610	0.7	20.1058	8.7	0.4403	8.9	0.0642	1.6	0.18	401.2	6.2	370.5	27.5	182.7	203.5	401.2	6.2	219.6
bw3 101-200 30um-49	229	10128	1.3	19.0111	3.3	0.4706	3.4	0.0649	0.6	0.18	405.3	2.4	391.6	11.0	311.6	75.9	405.3	2.4	130.1
bw3 0-100 30um-64	75	4617	1.0	20.3922	6.7	0.4390	6.9	0.0649	1.6	0.24	405.5	6.4	369.6	21.3	149.7	156.8	405.5	6.4	271.0
bw3 0-100 30um-59	144	6820	1.6	19.3328	4.9	0.4661	5.0	0.0654	0.9	0.18	408.1	3.6	388.5	16.2	273.3	112.9	408.1	3.6	149.3
bw3 0-100 30um-90	328	20782	0.6	18.1681	2.1	0.4966	2.2	0.0654	0.7	0.31	408.6	2.8	409.4	7.6	413.9	47.6	408.6	2.8	98.7
bw3 0-100 30um-83	316	4457	1.8	18.1379	2.3	0.5070	2.5	0.0667	1.2	0.46	416.2	4.7	416.4	8.7	417.6	50.6	416.2	4.7	99.7
bw3 101-200 30um-78	369	1724	1.1	18.7000	2.3	0.4984	2.5	0.0676	0.8	0.34	421.7	3.5	410.6	8.4	349.1	52.7	421.7	3.5	120.8
bw3 0-100 30um-54	82	4773	1.0	20.4231	6.9	0.4610	7.1	0.0683	1.4	0.20	425.8	5.9	385.0	22.7	146.1	162.6	425.8	5.9	291.4
bw3 0-100 30um-6	84	6312	0.8	18.9977	5.9	0.4972	6.0	0.0685	1.3	0.22	427.1	5.4	409.8	20.4	313.2	134.3	427.1	5.4	136.4
bw3 0-100 30um-49	60	4148	1.3	20.0789	8.9	0.4729	9.0	0.0689	1.5	0.16	429.3	6.1	393.2	29.3	185.8	206.6	429.3	6.1	231.1
bw3 0-100 30um-66	714	14182	1.5	17.5500	1.6	0.5450	1.7	0.0694	1.0	0.30	432.4	2.1	441.7	6.1	490.8	35.8	432.4	2.1	88.1
bw3 101-200 30um-93	368	2874	1.1	18.7427	4.1	0.5122	4.1	0.0696	0.5	0.13	433.9	2.2	419.9	14.2	343.9	93.0	433.9	2.2	126.2
bw3 101-200 30um-73	55	3091	1.2	21.0684	10.3	0.4580	10.5	0.0700	1.9	0.18	436.1	7.9	382.9	33.4	72.7	245.4	436.1	7.9	600.0
bw3 101-200 30um-58	203	9612	1.1	18.2449	3.0	0.5307	3.0	0.0702	0.6	0.20	437.5	2.5	432.3	10.6	404.5	66.4	437.5	2.5	108.2
bw3 0-100 30um-10	99	5527	0.7	20.4728	6.3	0.4769	6.6	0.0708	1.8	0.27	441.0	7.5	395.9	21.5	140.4	148.2	441.0	7.5	314.0
bw3 101-200 30um-30	180	8316	0.5	18.9091	4.3	0.5163	4.3	0.0708	0.8	0.15	441.0	2.8	422.7	14.9	323.9	96.7	441.0	2.8	136.2
bw3 0-100 30um-5	173	11078	1.1	18.7553	3.3	0.5224	3.3	0.0711	0.8	0.23	442.5	3.4	426.7	11.7	342.4	73.6	442.5	3.4	129.3
bw3 0-100 30um-15	154	13095	0.5	19.3335	4.0	0.5082	4.1	0.0713	0.9	0.22	443.7	3.9	417.2	14.1	273.2	92.3	443.7	3.9	162.4
bw3 101-200 30um-7	73	16991	1.5	18.1210	7.5	0.5435	7.6	0.0714	1.5	0.20	444.8	6.4	440.7	27.3	419.7	167.2	444.8	6.4	106.0
bw3 101-200 30um-29	101	4709	1.6	20.0557	6.5	0.5111	6.8	0.0743	1.8	0.27	462.2	8.0	419.2	23.3	188.5	152.4	462.2	8.0	245.2
bw3 101-200 30um-32	140	1513	5.0	19.9909	6.2	0.5145	6.3	0.0746	0.8	0.13	463.8	3.6	421.5	21.6	196.1	144.4	463.8	3.6	236.6
bw3 101-200 30um-14	121	5553	0.8	18.9918	5.3	0.5447	5.4	0.0750	0.9	0.16	466.4	3.9	441.5	19.3	313.9	121.0	466.4	3.9	148.6
bw3 101-200 30um-100	157	5304	1.2	19.4001	4.7	0.5334	4.8	0.0750	0.6	0.13	466.5	2.9	434.0	16.9	265.3	108.8	466.5	2.9	175.8
bw3 101-200 30um-47	130	5165	0.7	19.4882	6.2	0.5313	6.3	0.0751	0.6	0.09	466.8	2.7	432.7	22.1	254.9	143.8	466.8	2.7	183.1
bw3 101-200 30um-89	41	1237	1.4	23.6909	15.4	0.4407	15.6	0.0757	2.7	0.18	470.5	12.5	370.7	48.5	-213.9	387.7	470.5	12.5	NA
bw3 0-100 30um-99	58	19999	0.9	19.2094	7.5	0.5437	7.7	0.0757	1.4	0.19	470.7	6.5	440.9	27.4	287.9	172.3	470.7	6.5	163.5
bw3 101-200 30um-66	157	4887	1.0	18.7216	4.1	0.5614	4.2	0.0762	0.7	0.17	473.6	3.2	452.4	15.2	346.4	93.1	473.6	3.2	136.7
bw3 0-100 30um-7	125	7697	0.7	17.4693	3.5	0.7369	3.6	0.0934	0.9	0.26	575.4	5.1	560.6	15.5	500.9	76.6	575.4	5.1	114.9
bw3 0-100 30um-85	85	9823	2.6	14.3405	2.8	1.5274	2.9	0.1589	0.8	0.27	950.5	6.9	941.5	18.0	920.5	58.1	920.5	58.1	103.3
bw3 0-100 30um-75	90	12663	0.8	14.0033	2.4	1.5766	2.5	0.1601	0.8	0.32	957.4	7.3	961.0	15.7	969.2	48.6	969.2	48.6	98.8
bw3 0-100 30um-55	133	26028	3.6	13.8057	1.4	1.6646	1.5	0.1667	0.5	0.30	993.8	5.0	995.1	9.5	998.1	28.4	998.1	28.4	99.3
bw3 0-100 30um-36	122	21094	6.3	13.7950	1.4	1.7394	1.6	0.1740	0.6	0.40	1034.3	6.0	1023.3	10.2	999.7	29.3	999.7	29.3	103.5
bw3 0-100 30um-92	88	25270	3.1	13.7175	2.3	1.7790	2.4	0.1770	0.6	0.27	1050.5	6.2	1037.8	15.5	1011.1	46.7	1011.1	46.7	103.9
bw3 101-200 30um-31	108	27851	2.6	13.6651	1.8	1.7633	1.9	0.1748	0.6	0.30	1038.3	5.5	1032.1	12.2	1018.9	36.4	1018.9	36.4	101.9
bw3 0-100 30um-82	65	8398	1.2	13.6506	3.1	1.7923	3.2	0.1774	0.7	0.23	1053.0	7.2	1042.7	20.9	1021.0	63.1	1021.0	63.1	103.1
bw3 101-200 30um-88	609	56365	1.4	13.6394	0.3	1.7864	0.5	0.1767	0.4	0.76	1049.0	3.8	1040.5	3.3	1022.7	6.7	1022.7	6.7	102.6
bw3 0-100 30um-71	118	25481	2.9	13.5631	1.4	1.8051	1.6	0.1776	0.7	0.43	1053.7	6.7	1047.3	10.4	1034.1	29.0	1034.1	29.0	101.9
bw3 101-200 30um-26	597	31731	5.6	13.5108	0.4	1.7015	0.8	0.1667	0.7	0.85	994.1	6.3	1009.1	5.1	1041.9	8.5	1041.9	8.5	95.4
bw3 0-100 30um-27	129	20968	1.3	13.4515	1.4	1.8277	1.6	0.1783	0.8	0.47	1057.7	7.4	1055.4	10.6	1050.8	28.7	1050.8	28.7	100.7
bw3 101-200 30um-83	133	21040	1.7	13.4183	1.3	1.7973	1.5	0.1749	0.8	0.51	1039.1	7.2	1044.5	9.7	1055.7	25.7	1055.7	25.7	98.4
bw3 101-200 30um-1	165	12155	1.7	13.4006	1.4	1.8109	1.5	0.1760	0.4	0.30	1045.1	4.3	1049.4	9.8	1058.4	28.7	1058.4	28.7	98.7
bw3 101-200 30um-5	400	32447	1.9	13.3969	0.5	1.8319	0.5	0.1780	0.3	0.51	1056.0	2.6	1056.9	3.5	1058.9	9.2	1058.9	9.2	99.7
bw3 0-100 30um-16	121	19579	1.7	13.3484	1.4	1.7762	1.6	0.1720	0.9	0.52	1022.9	8.1	1036.8	10.6	1066.3	28.0	1066.3	28.0	95.9
bw3 101-200 30um-72	206	14997	0.5	13.2997	1.1	1.7455	1.4	0.1684	0.8	0.62	1003.1	7.8	1025.5	8.7	1073.6	21.2	1073.6	21.2	93.4
bw3 101-200 30um-25	128	29455	3.5	13.2804	1.2	1.9159	1.3	0.1845	0.6	0.48	1091.7	6.5	1086.6	9.0	1076.5	23.7	1076.5	23.7	101.4
bw3 101-200 30um-12	103	27739	1.2	13.2078	2.0	1.9280	2.0	0.1847	0.5	0.24	1092.5	4.9	1090.9	13.6	1087.5	39.4	1087.5	39.4	100.5
bw3 0-100 30um-24	119	45844	2.9	13.1930	1.3	1.9090	1.5	0.1827	0.8	0.50	1081.5	7.5	1084.2	10.0	1089.8	26.0	1089.8	26.0	99.2
bw3 0-100 30um-67	629	2287	10.5	13.1314	1.8	1.7075	2.1	0.1626	1.1	0.51	971.3	9.7	1011.3	13.6	1099.1	36.5	1099.1	36.5	88.4
bw3 0-100 30um-80	69	21051	1.9	13.0988	2.6	1.9522	2.7	0.1855	0.8	0.30	1096.7	8.2	1099.2	18.0	1104.1	51.1	1104.1	51.1	99.3
bw3 0-100 30um-82	35	10637	1.8	13.0728	6.2	1.9081	6.3	0.1809	1.1	0.17	1072.0	10.4	1083.9	41.8	1108.0	123.6	1108.0	123.6	96.7
bw3 0-100 30um-37	233	49529	2.4	13.0721	0.6	1.9706	0.8	0.1868	0.5	0.63	1104.2	5.3	1105.5	5.6	1108.1	12.9	1108.1	12.9	99.6
bw3 0-100 30um-57	142	13699	2.5	13.0601	1.1	2.0039	1.4	0.1898	0.9	0.62	1120.3	9.2	1116.8	9.7	1110.0	22.3	1110.0	22.3	100.9
bw3 101-200 30um-60	370	34467	0.6	13.0532	0.5	1.9619	0.8	0.1857	0.5	0.71	1098.2	5.5	1102.5	5.2	1111.0	10.8	1111.0	10.8	98.8
bw3 101-200 30um-95	191	28919	1.3	12.9668	0.8	2.0175	1.0	0.1897	0.6	0.61	1119.9	6.3	1121.4	6.8	1124.3	15.9	1124.3	15.9	99.6
bw3 101-200 30um-81	99	15169	1.7	12.9625	1.6	1.9256	1.8	0.1810	0.9	0.48	1072.6	7.1	1090.0	11.8	1125.0	32.0	1125.0	32.0	95.3
bw3 101-200 30um-74	165	14455	1.5	12.9256	1.1	2.0424	1.2	0.1915	0.5	0.40	1129.3	5.1	1129.8	8.4	1130.6	22.4	1130.6	22.4	99.9
bw3 101-200 30um-67	266	25230	2.4	12.9232	0.8	1.8336	1.3	0.1719	1.0	0.77	1022.3	9.2	1057.6	8.3	1131.0	16.2	1131.0	16.2	90.4
bw3 101-200 30um-23	393	33832	2.0	12.8626	0.5	2.0354	0.6	0.1899	0.3	0.49	1120.7	3.0	1127.4	4.0	1140.4	10.1	1140.4	10.1	98.3
bw3 101-200 30um-20	109	14446	2.0	12.7602	1.4	2.1533	1.5	0.1993	0.6	0.38	1171.5	6.2	1166.1	10.4	1156.2	27.4	1156.2	27.4	101.3
bw3 0-100 30um-1	120	24798	1.6	12.7306	1.3	2.1683	1.4	0.2002	0.5	0.36	1176.4	5.4	1170.9	9.5	1160.8	25.3	1160.8	25.3	101.3
bw3 101-200 30um-56	176	18148	2.5	12.7190	0.8	2.0478	1.3	0.1889	1.0	0.77	1115.4	10.3	1131.5	9.0	1162.6	16.7	1162.6	16.7	95.9
bw3 101-200 30um-46	113	20861	1.6	12.7174	1.4	2.1512	1.5	0.1984	0.5	0.35	1166.8	5.6	1165.5	10.5	1162.9	28.2	1162.9	28.2	100.3
bw3 101-200 30um-3	169	15824	2.3	12.7169	1.1	2.1185	1.2	0.1954	0.5	0.40	1150.5	5.1	1154.8	8.3	1163.0	22.0	1163.0	22.0	98.9
bw3 0-100 30um-17	58	9034	1.8	12.7123	2.4	2.1623	2.7	0.1994	1.1	0.41	1171.9	11.6	1169.0	18.5	1163.7	48.3	1163.7	48.3	100.7
bw3 0-100 30um-48	161	27408	2.4	12.5914	0.8	2.2150	1.0	0.2023	0.6	0.63	1187.6	6.6	1185.8	6.8	1182.6	14.9	1182.6	14.9	100.4
bw3 101-200 30um-98	288	22973	1.6	12.5806	0.6	2.0892	1.1	0.1906	0.9	0.81	1124.8	8.8	1145.3	7.3	1184.3	12.2	1184.3	12.2	95.0
bw3 0-100 30um-3	677	2837	1.2	12.4692	0.8	1.8118	2.8	0.1639	2.6	0.95	978.2	23.8	1049.7	18.0	1201.9	16.7	1201.9	16.7	81.4
bw3 0-100 30um-38	215	34133	2.3	12.4171	0.7	2.2448	0.9	0.2022	0.7	0.72	1186.9	7.2	1195.2	6.6	1210.1	12.8	1210.1	12.8	98.1

(BW3 continued)						Isotope ratios						Apparent ages (Ma)							
Analysis	U	206Pb	U/Th	206Pb*	±	207Pb*	±	206Pb*	±	error	206Pb*	±	207Pb*	±	206Pb*	±	Best age	±	Conc
	(ppm)	204Pb		207Pb*	(%)	235U*	(%)	238U	(%)	corr.	238U*	(Ma)	235U	(Ma)	207Pb*	(Ma)	(Ma)	(Ma)	(%)
bw3 0-100 30um-56	123	17591	3.4	11.9248	1.3	2.4183	1.7	0.2092	1.0	0.59	1224.3	10.9	1248.1	11.9	1289.3	26.0	1289.3	26.0	95.0
bw3 0-100 30um-77	57	8626	1.0	11.9067	2.0	2.5215	2.3	0.2177	1.0	0.43	1269.9	11.3	1278.2	16.5	1292.2	39.8	1292.2	39.8	98.3
bw3 101-200 30um-28	91	9156	1.8	11.8327	1.4	2.4978	1.8	0.2144	1.1	0.60	1252.0	12.0	1271.4	12.8	1304.3	27.5	1304.3	27.5	96.0
bw3 101-200 30um-40	114	14897	2.0	11.8135	1.2	2.6565	1.3	0.2276	0.5	0.41	1321.9	6.5	1316.4	9.9	1307.5	23.8	1307.5	23.8	101.1
bw3 0-100 30um-86	208	35327	1.9	11.7558	0.6	2.5189	1.0	0.2148	0.8	0.79	1254.1	8.9	1277.5	7.2	1317.0	11.8	1317.0	11.8	95.2
bw3 101-200 30um-37	125	25066	1.5	11.6986	0.8	2.6755	1.0	0.2270	0.6	0.57	1318.8	7.0	1321.7	7.5	1326.4	16.2	1326.4	16.2	99.4
bw3 101-200 30um-57	209	17453	1.1	11.5307	0.8	2.7274	0.9	0.2281	0.4	0.44	1324.5	4.5	1336.0	6.4	1354.4	15.0	1354.4	15.0	97.8
bw3 0-100 30um-89	142	31874	1.8	11.4052	0.7	2.9291	1.0	0.2423	0.7	0.68	1398.6	8.3	1389.5	7.3	1375.5	13.6	1375.5	13.6	101.7
bw3 0-100 30um-4	312	7354	1.7	11.3942	0.5	2.7698	0.8	0.2289	0.7	0.79	1328.7	8.0	1347.4	6.3	1377.3	10.1	1377.3	10.1	96.5
bw3 0-100 30um-69	112	21884	1.3	11.3770	1.5	2.9835	1.4	0.2462	0.9	0.65	1418.8	11.1	1403.4	10.3	1380.2	19.8	1380.2	19.8	102.8
bw3 101-200 30um-25	185	16370	2.0	11.3637	0.7	2.9179	0.8	0.2405	0.4	0.45	1389.2	4.6	1386.6	6.1	1382.5	13.9	1382.5	13.9	100.5
bw3 0-100 30um-40	233	32167	1.5	11.2480	0.5	2.9132	0.9	0.2377	0.7	0.79	1374.5	8.6	1385.3	6.6	1402.1	10.3	1402.1	10.3	98.0
bw3 101-200 30um-16	122	9431	2.1	11.2363	1.0	2.9387	1.2	0.2395	0.6	0.55	1384.0	8.1	1391.9	9.0	1404.1	19.0	1404.1	19.0	98.6
bw3 101-200 30um-18	68	17111	2.2	11.2343	1.6	2.9095	1.7	0.2371	0.6	0.38	1371.4	7.8	1384.4	12.7	1404.4	29.7	1404.4	29.7	97.6
bw3 0-100 30um-23	168	2964	1.8	11.2076	1.5	2.4078	2.2	0.1957	1.5	0.71	1152.3	16.1	1244.9	15.5	1409.0	29.2	1409.0	29.2	81.8
bw3 101-200 30um-71	212	4423	0.9	11.1832	0.9	2.6661	3.0	0.2162	2.8	0.96	1262.0	32.5	1319.1	21.9	1413.2	16.5	1413.2	16.5	89.3
bw3 0-100 30um-84	70	14929	2.1	11.1674	1.8	2.6675	2.7	0.2160	2.0	0.74	1260.9	23.0	1319.5	20.0	1415.9	34.7	1415.9	34.7	89.1
bw3 101-200 30um-38	79	12720	2.3	10.9853	1.5	3.2740	1.6	0.2608	0.6	0.36	1494.2	7.8	1474.9	12.5	1447.2	28.5	1447.2	28.5	103.2
bw3 101-200 30um-87	144	26659	2.8	10.7611	0.7	3.3322	0.9	0.2601	0.5	0.56	1490.2	6.6	1488.6	7.0	1486.4	14.0	1486.4	14.0	100.3
bw3 101-200 30um-11	165	5362	1.0	10.7315	0.8	3.3561	1.1	0.2612	0.8	0.69	1496.1	10.3	1494.2	8.8	1491.6	15.5	1491.6	15.5	100.3
bw3 101-200 30um-8	80	7518	0.9	10.7263	1.5	3.0894	1.7	0.2403	0.8	0.48	1388.4	10.5	1430.1	13.4	1492.5	28.9	1492.5	28.9	93.0
bw3 0-100 30um-98	757	34145	1.5	10.7101	0.3	3.1890	0.8	0.2477	0.7	0.94	1426.7	9.4	1454.5	6.0	1495.4	4.9	1495.4	4.9	95.4
bw3 101-200 30um-52	68	13010	1.5	10.6846	1.7	3.2369	2.0	0.2508	1.0	0.52	1442.8	13.5	1466.0	15.7	1499.9	32.6	1499.9	32.6	96.2
bw3 0-100 30um-100	145	59693	2.3	10.5698	0.8	3.4863	1.0	0.2673	0.6	0.63	1526.9	8.4	1524.1	7.7	1520.3	14.2	1520.3	14.2	100.4
bw3 0-100 30um-88	82	19108	1.8	10.4962	1.1	3.4430	1.3	0.2621	0.7	0.52	1500.6	8.9	1514.3	10.2	1533.5	20.8	1533.5	20.8	97.9
bw3 101-200 30um-22	234	4246	1.0	10.2074	0.7	3.5322	0.7	0.2615	0.7	0.76	1497.5	6.9	1534.5	5.4	1585.8	8.3	1585.8	8.3	94.4
bw3 101-200 30um-69	106	25805	1.1	10.1251	0.9	3.8502	1.3	0.2827	0.9	0.73	1605.1	13.1	1603.3	10.1	1600.9	16.0	1600.9	16.0	100.3
bw3 101-200 30um-97	66	13060	0.7	10.0544	1.4	3.8523	1.5	0.2809	0.7	0.44	1596.0	9.5	1603.7	12.3	1614.0	25.4	1614.0	25.4	98.9
bw3 0-100 30um-35	148	25537	0.8	10.0347	0.6	3.9520	0.9	0.2876	0.7	0.74	1629.6	10.0	1624.4	7.6	1617.6	11.8	1617.6	11.8	100.7
bw3 0-100 30um-39	220	998	1.3	10.0209	1.5	3.4054	1.8	0.2475	1.0	0.57	1425.6	13.2	1505.6	14.2	1620.2	27.7	1620.2	27.7	88.0
bw3 101-200 30um-13	50	16826	2.9	10.0153	1.5	4.0714	1.7	0.2957	0.7	0.39	1670.1	9.6	1648.6	13.6	1621.2	28.7	1621.2	28.7	103.0
bw3 0-100 30um-78	55	18955	0.8	10.0151	1.4	3.9195	1.6	0.2847	0.8	0.51	1615.0	11.9	1617.7	13.1	1621.3	25.8	1621.3	25.8	99.6
bw3 0-100 30um-73	37	13541	0.6	10.0048	2.0	4.0194	2.2	0.2917	0.8	0.39	1649.8	12.4	1638.1	17.6	1623.2	37.1	1623.2	37.1	101.6
bw3 101-200 30um-17	227	27066	1.6	9.9820	0.4	3.5425	0.8	0.2565	0.7	0.87	1471.7	9.0	1536.8	6.3	1627.4	7.4	1627.4	7.4	90.4
bw3 101-200 30um-18	171	28214	1.3	9.9627	0.9	3.5169	0.9	0.2541	0.7	0.77	1459.7	9.0	1531.0	7.1	1631.0	10.8	1631.0	10.8	89.5
bw3 101-200 30um-99	85	18771	1.2	9.9541	0.8	4.1064	1.1	0.2965	0.7	0.66	1673.7	10.7	1655.6	9.0	1632.6	15.4	1632.6	15.4	102.5
bw3 0-100 30um-81	318	24167	1.2	9.9442	0.4	3.3169	2.3	0.2392	2.3	0.98	1382.7	28.3	1485.0	18.1	1634.5	8.0	1634.5	8.0	84.6
bw3 0-100 30um-63	107	27847	1.4	9.9078	0.8	4.1483	0.9	0.2981	0.4	0.46	1681.8	6.0	1663.9	7.3	1641.3	14.7	1641.3	14.7	102.5
bw3 0-100 30um-32	110	26609	0.7	9.9041	0.6	3.8727	1.0	0.2782	0.6	0.62	1582.2	8.5	1608.0	7.8	1642.0	14.1	1642.0	14.1	96.4
bw3 0-100 30um-29	144	23453	1.4	9.8992	0.6	4.2588	0.9	0.3058	0.7	0.80	1719.8	11.2	1685.4	7.6	1642.9	10.2	1642.9	10.2	104.7
bw3 101-200 30um-4	141	26291	1.5	9.8341	0.6	4.1530	0.9	0.2962	0.6	0.65	1672.5	8.2	1664.8	7.0	1655.1	12.0	1655.1	12.0	101.0
bw3 0-100 30um-22	69	56009	0.8	9.7960	0.9	4.2955	1.2	0.3052	0.8	0.67	1716.9	12.0	1692.5	9.7	1662.3	16.1	1662.3	16.1	103.3
bw3 0-100 30um-76	107	47126	1.1	9.6635	0.7	4.2800	0.9	0.3000	0.7	0.70	1691.1	9.9	1689.5	7.8	1687.5	12.4	1687.5	12.4	100.2
bw3 0-100 30um-9	169	48218	2.1	9.6081	0.5	4.1160	0.8	0.2868	0.6	0.79	1625.6	8.8	1657.5	6.3	1698.1	8.7	1698.1	8.7	95.7
bw3 0-100 30um-72	74	19037	1.0	9.6061	1.0	4.4352	1.1	0.3090	0.5	0.49	1735.8	8.2	1718.9	9.1	1698.5	17.6	1698.5	17.6	102.2
bw3 0-100 30um-94	151	48007	1.0	9.5270	0.5	4.4739	0.7	0.3091	0.5	0.71	1736.4	7.4	1726.1	5.6	1713.7	8.7	1713.7	8.7	101.3
bw3 0-100 30um-79	283	8780	1.2	9.4546	1.5	3.7289	1.9	0.2557	1.2	0.62	1467.8	15.4	1577.6	15.1	1727.7	27.3	1727.7	27.3	85.0
bw3 101-200 30um-79	77	18115	1.1	9.4506	0.9	4.5015	1.1	0.3085	0.5	0.48	1733.5	7.9	1731.3	9.0	1728.5	17.4	1728.5	17.4	100.3
bw3 0-100 30um-52	514	68449	3.2	9.4449	0.2	4.4005	0.5	0.3014	0.5	0.94	1698.4	7.2	1712.4	4.2	1729.6	3.3	1729.6	3.3	98.2
bw3 0-100 30um-60	258	66485	1.8	9.3949	0.3	4.6681	0.5	0.3181	0.5	0.88	1780.3	7.3	1761.5	4.5	1739.3	4.7	1739.3	4.7	102.4
bw3 0-100 30um-33	124	40843	1.0	9.3665	0.5	4.5460	0.8	0.3088	0.6	0.74	1734.9	9.1	1739.4	6.8	1744.9	10.1	1744.9	10.1	99.4
bw3 0-100 30um-43	258	64784	2.9	9.3204	0.3	4.5756	0.7	0.3093	0.6	0.92	1737.2	9.4	1744.8	5.6	1753.9	4.7	1753.9	4.7	99.1
bw3 101-200 30um-42	119	16429	1.5	9.3137	0.7	4.5684	0.8	0.3086	0.4	0.53	1733.8	6.4	1743.5	6.6	1755.2	12.3	1755.2	12.3	98.8
bw3 0-100 30um-2	90	39884	1.0	9.2993	0.9	4.8422	1.2	0.3266	0.9	0.70	1821.8	13.8	1792.3	10.4	1758.0	16.2	1758.0	16.2	103.6
bw3 101-200 30um-9	319	56258	1.1	9.2945	0.2	4.4820	0.5	0.3021	0.4	0.89	1701.9	6.3	1727.7	3.9	1759.0	4.0	1759.0	4.0	96.8
bw3 101-200 30um-55	86	11828	3.3	9.2078	0.8	4.9212	0.5	0.3286	0.5	0.49	1831.8	7.4	1805.9	8.1	1776.1	15.2	1776.1	15.2	103.1
bw3 0-100 30um-87	51	22014	1.4	9.1921	1.3	4.6667	1.6	0.3111	0.9	0.57	1746.2	14.1	1761.3	13.4	1779.2	24.0	1779.2	24.0	98.1
bw3 101-200 30um-21	109	20593	1.5	9.1774	0.7	4.8478	0.8	0.3227	0.4	0.47	1802.8	6.0	1793.2	6.8	1782.1	13.1	1782.1	13.1	101.2
bw3 0-100 30um-65	185	54123	3.1	9.1215	0.3	4.8401	0.6	0.3202	0.5	0.85	1790.7	8.5	1791.9	5.4	1793.3	6.2	1793.3	6.2	99.9
bw3 101-200 30um-53	54	10556	0.7	9.0145	1.2	5.1174	1.2	0.3346	1.0	0.65	1860.5	16.0	1839.0	13.0	1814.7	21.3	1814.7	21.3	102.5
bw3 101-200 30um-6	155	15823	1.8	8.9701	0.5	4.9213	0.6	0.3202	0.4	0.64	1790.6	6.4	1805.9	5.4	1823.7	9.0	1823.7	9.0	98.2
bw3 0-100 30um-31	112	33981	1.5	8.9263	0.5	4.9763	1.1	0.3222	1.0	0.91	1800.3	16.3	1815.3	9.7	1832.6	8.5	1832.6	8.5	98.2
bw3 0-100 30um-42	38	27802	0.7	8.7891	1.6	5.2640	1.8	0.3356	0.8	0.45	1865.2	13.0	1863.0	15.3	1860.6	29.0	1860.6	29.0	100.3
bw3 101-200 30um-51	48	9274	1.0	8.6642	1.2	5.4881	1.3	0.3449	0.6	0.45	1910.0	9.6	1898.7	11.1	1886.4	20.8	1886.4	20.8	101.3
bw3 101-200 30um-62	189	6846	4.3	8.3491	0.8	5.2894	0.9	0.3203	0.4	0.45	1791.2	6.0	1867.2	7.3	1952.8	13.7	1952.8	13.7	91.7
bw3 101-200 30um-80	61	26709	0.5	8.2694	0.9	5.9584	1.0	0.3574	0.5	0.49	1969.6	8.2	1969.8	8.6	1969.9	15.4	1969.9	15.4	100.0
bw3 101-200 30um-10	136	19293	1.9	8.1638	0.4	6.1532	0.5	0.3643	0.3	0.59	2002.7	5.4	1997.8	4.7	1992.8	7.7	1992.8	7.7	100.5
bw3 0-100 30um-45	15	7715	5.6	7.5404	2.6	7.5471	2.8	0.4127	1.1	0.39	2227.4	20.7	2178.6	25.0	2132.9	44.9	2132.9	44.9	104.4
bw3 0-100 30um-44	43	17163	0.7	6.2818	0.6	10.0448	1.0	0.4576	0.8	0.80	2429.1	15.8	2438.9	9.1	2447.1	10.1	2447.1	10.1	99.3
bw3 101-200 30um-75	124	29328	1.4	5.8407	0.2	11.4308	0.6	0.4842	0.6	0.92	2545.6	12.3	2558.9	5.9	2569.5	4.0	2569.5	4.0	99.1
bw3 0-100 30um-70	36	15107	1.2	5.7172	0.6	11.6037	1.0	0.4812	0.8	0.78	2532.3	16.6	2573.0	9.5	2605.2	10.6	2605.2	10.6	97.2
bw3 0-100 30um-21	166	40769	0.8	5.4733	0.2	11.6345	1.2	0.4618	1.2	0.99	2447.7	24.4	2575.4	11.3	2677.6	3.1	2677.6	3.1	91.4
bw3 0-100 30um-46	118	42095	0.7	5.4158	0.2	12.8758	0.6	0.5057	0.5	0.94	2638.5	11.7	2670.6	5.4	2695.0	3.3	2695.0	3.3	97.9
bw3 101-200 30um-2	302	21878	10.1	5.3625	0.2	11.0490	0.5	0.4297	0.4	0.92	2304.5	8.6	2527.3	4.5	2711.3	3.0	2711.3	3.0	85.0
bw3 101-200 30um-86	55	26448	0.6	5.2299	0.4	14.2970	0.9	0.5423	0.8	0.89	2793.1	17.7	2769.6	8.3	2752.6	6.6	2752.6	6.6	101.5
bw3 0-100 30um-95	143	80318	1.3	5.1179	0.2	14.0890	0.4	0.5230	0.3	0.89	2711.7	7.3	2755.7	3.5	2788.1	2.7	2788.1	2.7	97.3
bw3 101-200 30um-61	125	44949	0.9	4.9356	0.2	15.2524	0.6	0.5460	0.6	0.93	2808.4	13.0	2831.1	5.9	2847.3	3.8	2847.3	3.8	98.6
bw3 101-200 30um-33	30	10223	1.5	4.9019	0.9	14.2263	1.6	0.5058	1.3	0.82	2638.5	27.5	2764.9	14.7	2858.5	14.6	2858.5	14.6	92.3
bw3 0-100 30um-28	424	94540	14.2	4.7447	0.1	15.4304	0.6	0.5310	0.6	0.98	2745.6	12.9	2842.2	5.6	2911.4	1.8	2911.4	1.8	94.3

Notes for data tables:

1. 1. Analyses with >20% uncertainty (1-sigma) in 206Pb/238U age are not included.
2. Analyses with >20% uncertainty (1-sigma) in 206Pb/207Pb age are not included, unless 206Pb/238U age is <500 Ma.
3. Best age is determined from 206Pb/238U age for analyses with 206Pb/238U age <1000 Ma and from 206Pb/207Pb age for analyses with 206Pb/238Uage > 1000 Ma.
4. Concordance is based on 206Pb/238U age / 206Pb/207Pb age. Value is not reported for 206Pb/238U ages <500 Ma because of large uncertainty in 206Pb/207Pb age.
5. Analyses with 206Pb/238U age > 500 Ma and with >20% discordance (<80% concordance) are not included.
6. Analyses with 206Pb/238U age > 500 Ma and with >5% reverse discordance (<105% concordance) are not included.
7. All uncertainties are reported at the 1-sigma level, and include only measurement errors.
8. Systematic errors are as follows (at 2-sigma level): [sample 1: 2.5% (206Pb/238U) & 1.4% (206Pb/207Pb)] These values are reported on cells U1 and W1 of NUagecalc.
9. Analyses conducted by LA-MC-ICPMS, as described by Gehrels et al. (2008).
10. U concentration and U/Th are calibrated relative to Sri Lanka zircon standard and are accurate to ~20%.
11. Common Pb correction is from measured 204Pb with common Pb composition interpreted from Stacey and Kramers (1975).
12. Common Pb composition assigned uncertainties of 1.5 for 206Pb/204Pb, 0.3 for 207Pb/204Pb, and 2.0 for 208Pb/204Pb.
13. U/Pb and 206Pb/207Pb fractionation is calibrated relative to fragments of a large Sri Lanka zircon of 563.5 ± 3.2 Ma (2-sigma).
14. U decay constants and composition as follows: 238U = 9.8485 x 10-10, 235U = 1.55125 x 10-10, 238U/235U = 137.88.
15. Weighted mean and concordia plots determined with Isoplot (Ludwig, 2008).

VITA

Personal Background	Patrick Michael O'Connor Fort Worth, Texas Born April 21, 1989, South Euclid, Ohio Son of Michael and Lisa O'Connor
Education	Bachelors of Science in Environmental Geology, 2012 Ohio University, Athens, Ohio Masters of Science in Geology, 2015 Texas Christian University, Fort Worth, Texas
Experience	Mudlogger, March, 2012 - June, 2013 Weatherford International, Midland, Texas Geoscience Intern, Summer 2014 Hunt Oil Company, Dallas, Texas
Professional Memberships	American Association of Petroleum Geologists Dallas Geological Society Fort Worth Geological Society Geological Society of America

ABSTRACT

PROVENANCE AND SEDIMENT DISPERSAL OF MISSISSIPPIAN SANDSTONES IN THE BLACK WARRIOR BASIN, NE MISSISSIPPI

Patrick Michael O'Connor, M.S., 2015
School of Geology, Energy and the Environment
Texas Christian University

Thesis Advisor: Dr. Xiangyang Xie
Committee Members: Dr. Helge Alsleben and Dr. John Holbrook

The Black Warrior Basin is one of several Carboniferous foreland basins along the Ouachita belt in the southern midcontinent region. Mapping the distribution of siliciclastic rocks and building a depositional model in the Black Warrior Basin is challenging because of the complex tectonic history, lack of outcrops, and sandstone maturity. This study focuses on documenting the provenance and proposing potential sediment dispersal patterns for Mississippian sandstones. Data for this study includes conventional core from seven wells, and forty-seven thin sections from the Mississippian sandstones in northeastern counties of Mississippi (Monroe and Lowndes). Uranium-lead detrital zircon geochronology along with sandstone point counting is used together to determine sediment sources of these sand bodies and identify depositional systems. Two competing models exist to explain the sediment sources. The first model suggests that siliciclastic sediment was sourced from a prograding deltaic system southwest of the basin; the second model argues that these sand bodies were from a cratonic interior provenance northwest of the basin. Modal mineral analysis results display that sublitharenites to mature quartzarenites dominate this section and are mainly derived from intracratonic sources. However, detrital zircon geochronology results of three sandstones (Lewis, Sanders, and Carter Sandstones) suggest that provenance of these Mississippian sand bodies include Acadian and Taconic orogenic sources from the northeast, along with Proterozoic basement influence.